

Production of Ultracold Lithium

Triplet Dimers by

STIRAP

A thesis submitted to the
University of Stuttgart

in collaboration with the

University of British Columbia

for the degree of
Master of Sciences

presented by

DENIS UHLAND

Prof. Tilman Pfau, examiner
Prof. Joerg Wrachtrup, co-examiner
Prof. Kirk W. Madison, supervisor

April 30, 2018

Statement of Authorship

I declare that I completed this thesis on my own and that information which has been directly or indirectly taken from other sources has been noted as such. Neither this nor a similar work has been presented to an examination committee.

Stuttgart, April 30, 2018

.....

Summary

The goal of this thesis is to create deeply bound Feshbach molecules in the lowest lying triplet molecular state by STIRAP. To achieve this one has to think about which initial quantum states we can populate and to which quantum state we can transfer. Starting from the initial state $|i\rangle$ we need to find a suitable excited state. In the excited molecular potential $c(1^1\Sigma_g^+)$ (named as $|e\rangle$) we found the vibrational state $v' = 20$ via scanning the probe laser frequency over resonance. The natural linewidth of the $|i\rangle \rightarrow |e\rangle$ transition is around 7.2 MHz at $\nu_p^0 = 366861.25$ GHz. The lifetime of our Feshbach molecules in the optical dipole trap (ODT) is around 1273 μs and shows a Rabi frequency $\Omega_1 \approx 28$ kHz for $P_p = 80$ μW . To find the ground state we set the probe laser fix on the single color resonance frequency while scanning with the Stokes laser over the $|e\rangle \rightarrow |g\rangle$ resonance transition frequency. Here, we found all transitions between the $v'' = 0$ and $v'' = 9$ state for the $a(1^3\Sigma_u^+)$ triplet molecular potential. To measure the Rabi frequency of the $|e\rangle \rightarrow |g\rangle$ transition we split the excited state. This is the so-called Autler-Townes splitting which is related to the Rabi frequency of the Stokes field Ω_2 . As an example we show the splitting for the $v'' = 0$ vibrational state in the $a(1^3\Sigma_u^+)$ molecular potential. The splitting shows $\Omega_2 = 14.11$ MHz for a probe power of $P_p = 300$ μW and a Stokes power of $P_s = 10$ mW. Additionally, the dark state spectroscopy showed a revival peak at the two photon resonance.

With this preparation we successfully measured a population revival peak via STIRAP (Stimulated Raman Adiabatic Passage). However, lifetime measurements of the Feshbach molecules in the lowest triplet molecule potential $a(1^3\Sigma_u^+)$ showed, that the $v'' = 9$ state has with $\tau = 2949.17$ μs a longer lifetime than the lower in energy lying $v'' = 0$ state with $\tau = 1585.36$ μs . The lifetime of the $v'' = 6$ lies with $\tau = 2813.61$ μs in between.

Contents

Titel	a
Summary	c
Contents	g
1. Introduction	1
2. Experimental Setup	5
2.1. ${}^6\text{Li}$ Properties	5
2.2. Lithium Light	7
2.3. PA light	9
2.4. Experimental Trap Setup	11
3. Preparation of Cold ${}^6\text{Li}$ Atoms	13
3.1. Zeeman Slower and MOT	13
3.2. Evaporative Cooling in an Optical Dipole Trap	16
4. Ultracold ${}^6\text{Li}_2$ Feshbach Molecules	19
4.1. Basic Idea of a Feshbach Resonance	19
4.2. State Preparation - Towards a Hyperfine Mixture $ 12\rangle$	24
4.3. Feshbach resonances in ${}^6\text{Li}$	28
4.4. Experimental realization of Feshbach Molecules	30
4.5. Quantum Numbers and Selection Rules of the ${}^6\text{Li}_2$ Bound Molecular State	33
4.5.1. Hund's Coupling Case (a)	33
4.5.2. Hund's Coupling Case (b)	34
4.5.3. State Selection and Preparation for Photoassociation	35
5. Photoassociation and Spectroscopy of Ultracold ${}^2\text{Li}_6$ Molecules	37
5.1. Single Color Spectroscopy	40
5.2. Two Color Spectroscopy	45
5.3. Autler-Townes Splitting	47
5.4. Dark State Spectroscopy	49
6. STIRAP of Ultracold Feshbach Molecules	53
6.1. Theory behind STIRAP - The 3-Level Model	54
6.2. The Adiabatic Approximation	57
6.3. STIRAP Experiment and Lifetime of Ultracold Feshbach Molecules	58
7. Conclusion & Outlook	63

A. Bibliography	I
Acknowledgement	IX

1. Introduction

The interaction and collision of two particles is one of the most fundamental circumstances described by the laws of physics. Almost all fields in science are designed to study this simple effect. The range reaches from astronomy, where the interacting bodies are massive planets on their orbit and their movement through space and time towards the smallest particle and the study of matter to answer through a more fundamental question 'what's the world made of?'. Physicists are trying to answer this question by starting to ask, 'how does the interaction of these two particles work' and 'which effects can we see under certain conditions'. On a larger interaction scale collisions of two neutron stars causes gravitational waves [1]. On a smaller scale chemical reactions are studied with a possible outcome to understand, control, manipulate or even suppressed this atom-atom interaction. Moreover, studies of solid states showed nitrogen vacancy centers in diamonds which can be observed as a single quantum system and are still one of the most promising candidates regarding single photon sources and quantum computing [2]. Remaining on the atomic scale, where quantum effects play a major role, it is therefore highly interesting to understand how molecules are formed. Compared to atoms, molecules are more complex and interesting in terms of interaction since they possess magnetic and electric dipole moments. Also, the structure of a molecule itself makes it to a more useful candidate concerning the study of fundamental laws of nature [3–5], quantum simulations [6, 7] or many-body quantum dynamics [8, 9]. All of these experiments were operated after cooling down the atoms. One might ask, *why is ultracold ultra-cool?* In this temperature regime it is possible to trap and capture atoms. By implication this gives the possibilities to study a trapped, almost stationary pure quantum system. A highlight in this regime was the creation of the first Bose-Einstein Condensate (BEC) in 1995 with ^{87}Rb [10], Na [11] and ^7Li [12]. Years later degenerated Fermi gases were created with ^{40}K [13] and ^6Li [14]. The study of this Fermi gases shows a wide range of applications. Since Pauli's exclusion principle forbids the occupation of the same quantum state for identical particle, fermionic systems play a major role in the studies about conductivity or neutron stars. In this limit we can consider our gas to be 'dilute since the distance of the particles (~ 100 nm) is much larger than the particle (~ 0.05 nm). Therefore, two-body interactions are major effects. For a low energy limit this interaction range can be described with the scattering length a (in order of tens $a_0 \sim$ several nm). With external fields it is possible to control the interaction strength of the ultracold gas. Here, we can, for example, use a Feshbach resonance which occurs by applying a magnetic field [15]. From here entering the Bardeen-Cooper-Schrieffer (BCS) regime gives us the possibility to study superfluidity [16]. However, other experiments focuses more on the creation of homonuclear molecules such as Cs_2 [17, 18] or Rb_2 [19] or heteronuclear mixtures like $^{87}\text{Rb}^{133}\text{Cs}$ [20] or $^6\text{Li}^{85}\text{Rb}$ [21].

All those experiments underlying the fact of acting in the ultracold regime. *How do we get our samples ultracold?* A simple and well known method is laser cooling [22]. However, due to the complexity of molecules it is common to cool the atoms first creating then the molecules in the ultracold regime. One method to produce such molecules is the Stimulated Raman Adiabatic Passage (in short STIRAP) [23]. Here, Feshbach molecules are transferred into a deeply bound molecular state via photoassociation.

Outline of this Thesis: The goal of this thesis is to present a method how to generate deeply bound ${}^6\text{Li}_2$ molecules via STIRAP. Since most of the setup was already built up, I refer to the thesis of the former PhD students Will Gunton [21] and Mariusz Semczuk [24] who built the apparatus and measured detailed characterizations of the MOT, ODT or other devices used for the experiment. Furthermore, this Master Thesis appears similar to the PhD thesis of Gene Polovy, who was PhD student in the lab of Prof. Kirk W. Madison working on the same experiment. For a more detailed description of this topic the reader is referred to [25]. Chapter 2 gives a brief introduction of the experiment. In Section 2.1 The atomic structure of ${}^6\text{Li}$ is introduced. Then, Section 2.2 gives a short introduction for the requirements of the light for the magneto-optical trap (MOT) and the Zeeman slower. Section 2.3 introduces the photoassociation (PA) light which we are using to transfer the population from the initial state $|i\rangle$ to the ground state $|g\rangle$. This PA lasers must be phase coherent. We achieved developments in phase noise reduction of the laser system which will be published soon [26]. A detailed scheme about the comb lock can be found in [21]. Section 2.4 introduces the setup of of our optical dipole trap (ODT). Chapter 3 gives a brief introduction about how we are going to produce ultracold ${}^6\text{Li}$ atoms by using a MOT and Zeeman slower. Also, evaporative cooling is introduced as well as the high field and zero field imaging. Chapter 4 talks about Feshbach resonances and Feshbach molecules. First, the basic idea is discussed and how this resonance helps us to create Feshbach molecules. Then, we discuss the need of a hyperfine mixture in order to produce Feshbach molecules. Then, the Feshbach resonance for ${}^6\text{Li}_2$ is characterized followed by a discussion about the experimental realization of Feshbach molecules due to 3-body collisions. Due to experiments in the ODT with different imaging techniques we can figure out the binding energy of the molecules and therefore the needed ODT trap depth to create them. The lifetime of ${}^6\text{Li}_2$ Feshbach molecules in the ODT is measured as well. A set of new quantum numbers will be introduced and the selection of the potential for PA will be discussed. Chapter 5 is a step-by-step instruction of how we find the right molecular states to succeed STIRAP. Therefore, we need to characterize the excited state $|e\rangle$ which we use to couple the initial state $|i\rangle$ with the ground state $|g\rangle$ of the deepest lying triplet potential. The coupling strength are extracted by the measured states and via a two-color and dark state measurement we can get an idea of the two photon resonance and the position of the STIRAP revival peak. This is the goal of this thesis. Additionally, we measured the lifetime of the deeply bound molecules in the lowest triplet molecular potential with the result, that the $v'' = 9$ vibronic state is longer lived than the $v'' = 0$ vibronic state. This result was achieved recently and is therefore not completely understood. However, the latest trap frequency measurements of the ODT showed that our molecular gas is actually a molecular BEC.

Further studies are running right now.

2. Experimental Setup

Since most of the setup was already built up, most of the characterization was already done by previous Ph.D. students. The results and discussions can be found in the Ph.D. thesis from Will Gunton and Mariusz Semczuk [21, 24]. However, the following sections give a short overview of the apparatus. We start with a characterization of Lithium atoms, followed by the requirements for laser cooling and the capturing of atoms followed by a short introduction to photoassociation. Beside this work, there was a 'side project' to implement a fast locking laser system for our PA sequence. These results will be published soon [26].

2.1. ${}^6\text{Li}$ Properties

The first stage of our experiment is the creation of an ultracold quantum gas based on the alkali metal ${}^6\text{Li}$. Therefore, understanding the properties of ${}^6\text{Li}$ is fundamental. The structure of ${}^6\text{Li}$ consists of 3 electrons and 3 protons with the configuration [27]

$$1s^2 2s^1 2p^0 \quad (2.1)$$

Since the first excited state of the ground state is a p orbital, an empty p orbital was included in equation 2.1. We can see that ${}^6\text{Li}$ has a single unpaired valence electron in a s orbital. This corresponds to an angular momentum quantum number $l = 0$ and therefore $m_l = 0$. Since we handle just one electron the spin is given by the spin quantum number $s = 1/2$ and $m_s = \pm 1/2$. Combining these two angular momenta leads to the total angular momentum quantum number $j = l + s$ with values from $m_j = |l - s| \leq j \leq (l + s) = -1/2, 1/2$ (in integer steps). Combining this information together the ground state can be written as [27]

$${}^{2s+1}l_j \quad (2.2)$$

which gives us for ${}^6\text{Li}$ a ground state configuration of ${}^2S_{1/2}$. The first excited state of ${}^6\text{Li}$ is a p orbital which can also be seen by the empty p orbital mentioned in equation 2.1. The transition between the ground and excited state, meaning ${}^2S \rightarrow {}^2P$ is called the D line or D transition (see figure 2.2 left).

Due to the interaction of the intrinsic angular momentum of the valence electron and angular momentum of its orbit we can find sub-features of the D line or transition mentioned in figure 2.2. This splitting is the so-called fine structure and exists because of l-s coupling where j is a good quantum number and also represents our new basis. How can this coupling be described? The orbital angular momentum produces a magnetic dipole moment. So does the spin. Classically, this coupling is no more than the interaction of these two dipole moments. The Hamiltonian for this interaction looks similar to equation 2.3 [27].

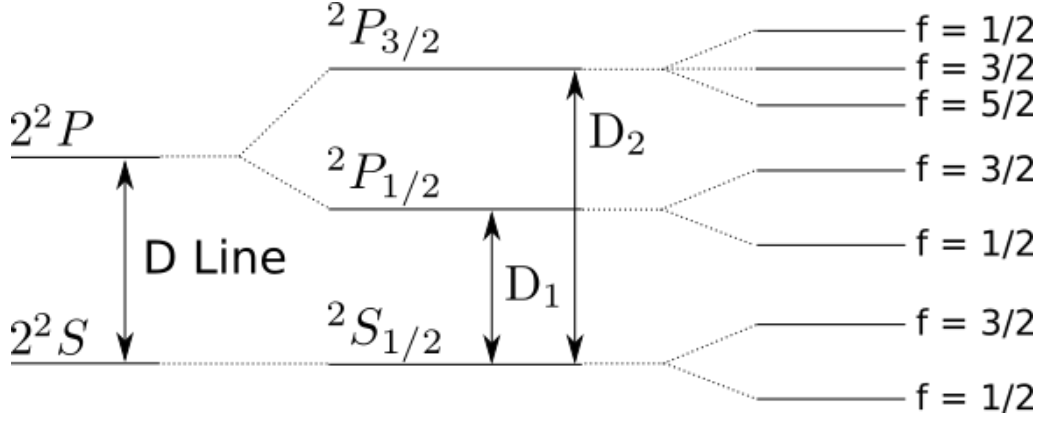


Figure 2.1.: Left: Transition between the ground state 2^2S and excited state 2^2P of ${}^6\text{Li}$. In the ground state the single valence electron with spin $s = 1/2$ is in a s orbital with quantum number $l = 0$. In the excited state the valence electron with $s = 1/2$ jumps into the p orbital with $l = 1$. Middle: Fine structure of the ${}^6\text{Li}$ transition by coupling the spin and the orbital angular momentum s and l . The new states are given in the new basis $j = l + s$ which represents the quantum number for the total angular momentum. The excited state splits into two states since $j = 1/2, 3/2$. The D transition splits into two sub-transitions which are the so-called D_1 and D_2 transitions. Right: Hyperfine structure due to coupling of the angular momentum j with the nuclear spin $i = 1$ for ${}^6\text{Li}$. Taken and adapted from [27].

$$\hat{H} \approx f(r) \hat{L} \cdot \hat{S} \quad (2.3)$$

where \hat{L} and \hat{S} are the operator for the orbital angular momentum and the spin. The function $f(r)$ contains an electric potential which is produced by the inner electrons and the nucleus and which has a radial dependency. Since Hamiltonian 2.3 couples l and s we can find a basis where $j = l + s$ is a good quantum number. The ground state has a total angular momentum of $j = 1/2$. However, for the excited state, the total angular momentum has two possibilities, $j = 1/2, 3/2$. With these results, we can write the excited state as ${}^2P_{1/2}$ and ${}^2P_{3/2}$. In figure 2.2 we used a s and l to create our ground and excited level without taking j into account. Now, since we found two excited states dependent on j we can extend this figure (see figure 2.2 middle).

The difference of the D_1 and D_2 transition is roughly 10 GHz [27]. Since the nucleus interacts with the electron a new quantum number i for the nuclear spin is introduced. For ${}^6\text{Li}$ the nuclear spin is $i = 1$. The idea of coupling the nuclear spin i to the angular momentum j is the same idea as coupling the electron spin s to its orbital momentum l . Therefore, we create a new basis for the total angular momentum $f = j + i$ with values in a range of $|j - i| \leq f \leq (j + i)$. For the ground state ${}^2S_{1/2}$ we find 2 possible quantum numbers $f = 1/2, 3/2$. The splitting between this two hyperfine levels is 228 MHz [27]. For our excited state ${}^2P_{1/2}$ we also find

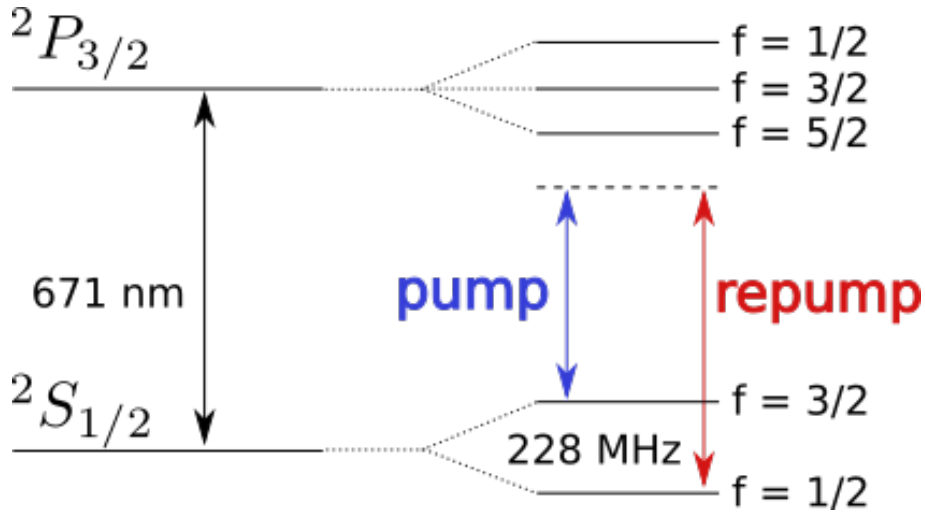


Figure 2.2.: Left: Transition between the ground state $2^2S_{1/2}$ and excited state $2^2P_{3/2}$ of ${}^6\text{Li}$. In the ground state the quantum number for the electronic spin quantum number is $s = 1/2$ and for the orbit momentum $l = 0$. Exciting the ground state the valence electron with $s = 1/2$ jumps into the p orbital with $l = 1$. The separation of the transition is 671 nm and is also known as the D_2 transition [27]. Right: Hyperfine structure of ${}^6\text{Li}$ due to coupling of the electronic spin s with the nuclear spin angular momentum i . For ${}^6\text{Li}$ the nuclear spin is $i = 1$. The total angular momentum is therefore $f = j + i$. Taken and adapted from [27].

2 possible quantum numbers $f = 1/2, 3/2$. However, for the excited state $2^2P_{3/2}$ we find 3 possible quantum numbers $f = 1/2, 3/2, 5/2$ [27]. The hyperfine splitting of the excited state is influenced by the magnetic dipole hyperfine constant and the electric quadrupole hyperfine constant. These hyperfine states are required for laser cooling light as well as for creating Feshbach molecules.

2.2. Lithium Light

The lithium light is generated on a single 'master table'. For our MOT we use the Li D_2 transition, which is the transition between the hyperfine states $f = 3/2 \rightarrow f' = 5/2$ (pump light) and the $f = 1/2 \rightarrow f' = 3/2$ hyperfine transition (repump light). Since the natural linewidth of the pump transition is more than the hyperfine splitting of the $2^2P_{3/2}$, the excitation light excites all three hyperfine levels simultaneously. The excited atom can decay to the $f = 1/2$ ground hyperfine level. Therefore, a repump laser with a similar intensity is needed. In our experiment, a Toptica DL Pro laser (master laser) offers us the required pump and repump light. The output of the master laser after the optical isolators is around 20 mW. From here, this light is either coupled into a 50/50 fiber splitter from Evanescence Optics, seeding an amplifier or lead to our laser lock:

Laser lock: We lock our master laser with absorption spectroscopy while scanning over the D_2 transition of ${}^6\text{Li}$ [28–31]. The laser is locked at a frequency 50 MHz blue detuned of the pump transition. A detailed overview of the beam paths is shown in [24].

Amplification for the experiment: The master light gets amplified by a seeded Mitsubishi ML 101J27 laser diode which is driven at a temperature of 72°C emitting 671 nm. Due to fiber coupling, we seed our homebuilt tapered amplifier (TA) based on an Eagleyard EYP-TPA-0670-00500-2003-CMT02-0000 chip. The output of the homebuilt TA shows around 100 mW and is split to generate the MOT pump and repump beams. For the pump light, we are using a single pass AOM to shift the frequency up by 108 MHz. Then we seed a semiconductor laser amplifier (BoostTA) from Toptica with around 25 mW. After the TA outcoupler, we measure around 200 mW of power. Then a double pass AOM is passed to gives us a frequency which is 45 MHz red detuned of the pump transition. The repump light is directly lead into a second semiconductor laser amplifier (BoostTA) from Toptica seeded with around 25 mW. Then, the frequency is shifted by 40 MHz red of the repump transition due to a double pass AOM. With this setting, we could achieve around 80 mW (or higher) of pump and repump light on the experiment table. However, the Toptica TAs showed some problems lately reducing the outcoupled power of around 40 mW which is still enough to operate the MOT since this power fluctuation does not affect the MOT loading time and steady-state atom number. This and more detailed analysis of the light spectra of the TAs can be seen in [21]. Both beams are coupled into a 50 m long single-mode, polarization-maintaining fiber separately leading to the experiment table.

Zeeman slower and imaging light: The Zeeman slower light is led directly from the fiber splitter to our experiment table due to a 50 m long fiber. There, the light passes a double pass AOM operated with an RF source of 63 MHz using the first negative diffraction order which shifts the laser frequency red of the pump transition by 76 MHz. For slowing the beam, we are using a laser power of around 35 mW. For the absorption imaging, we are using two different setups. The zero field imaging (ZFI) images the atomic cloud with no magnetic field. Therefore, we are using the MOT pump light for imaging. We are using the AOM to detune the laser light on resonance for the $f = 3/2 \rightarrow f' = 5/2$ transition. For a high field image (HFI) where the magnetic field is mostly set to $B = 755$ G the transition is shifted red by around 1 GHz compared to the ZFI transition. Therefore, we are using an offset locked cavity diode laser (ECDL) [24]. This light seeds another slave laser and is led through a double pass AOM. This double pass configuration allows us to shift the frequency by 80 MHz and allows us to image two different ${}^6\text{Li}$ spin states (later mentioned as state $|1\rangle$ and state $|2\rangle$) 2.4.

An overview about how to implement Rubidium into such a system as well as technical details for the vacuum system, the ovens, the MOT and compensation coils is shown in the Ph.D. thesis of Will Gunton and Mariusz Semczuk [21, 24].

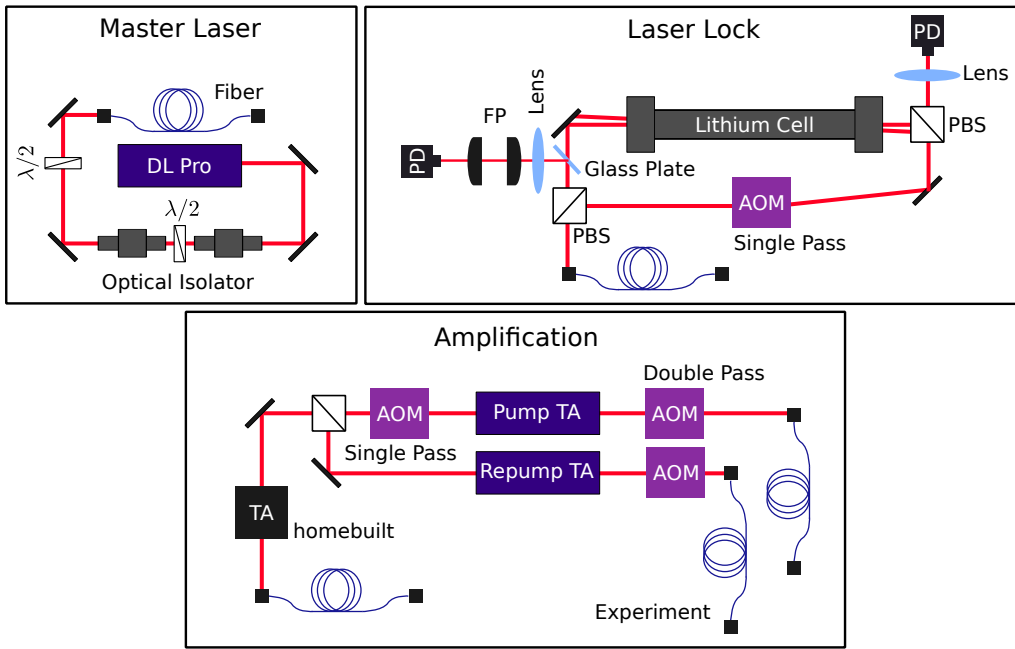


Figure 2.3.: Overview of the master laser table, the laser lock system and the amplification to prepare the laser light for the MOT and the Zeeman slower. A more detailed discussion is given in the section.

2.3. PA light

For the photoassociation experiment (PA) we built a separate laser system. Phase coherence and a narrow linewidth (less than 100 kHz) are crucial for experiments where we transfer the population between different quantum states, for example, dark state spectroscopy and STIRAP. Other requirements are laser and lock stability, a well-defined polarization, high power as well as a widely tunable frequency range. For the probe and Stokes laser we are using two continuous wave Ti:Sapphire 899 ring lasers (TS) manufactured by Coherent. The laser medium of both TS lasers is pumped by a Coherent V18 laser which emits 532 nm. The lasers have a tuning range of 760 nm to 820 nm. With the birefringent filter, the thin and thick etalon we can fine tune the laser frequency. For a detailed discussion about the laser elements, in particular, I refer to [21]. The TS light passes a double pass AOM, labeled as the ratchet AOM. Here, the TS light is frequency shifted. It is important to say that just one of the two TS lasers passes this ratchet AOM. Therefore, only one TS laser is tunable in frequency during an experimental run (mostly this laser is labeled as TS1). The second TS laser surpasses this AOM ratchet lock and emits therefore a fixed frequency. After this stage, the light gets split. One path goes straight to the experiment via a single mode fiber. The second path is for the lock and gets overlapped with the comb light generating a beat note. To lock both TS we are using a femtosecond optical frequency comb. For details, see [21]. Furthermore, we reduced the phase noise with an AOM lock. With this setup we achieved a resolution bandwidth of 300 Hz. The publication is currently in progress [26]. This laser lock

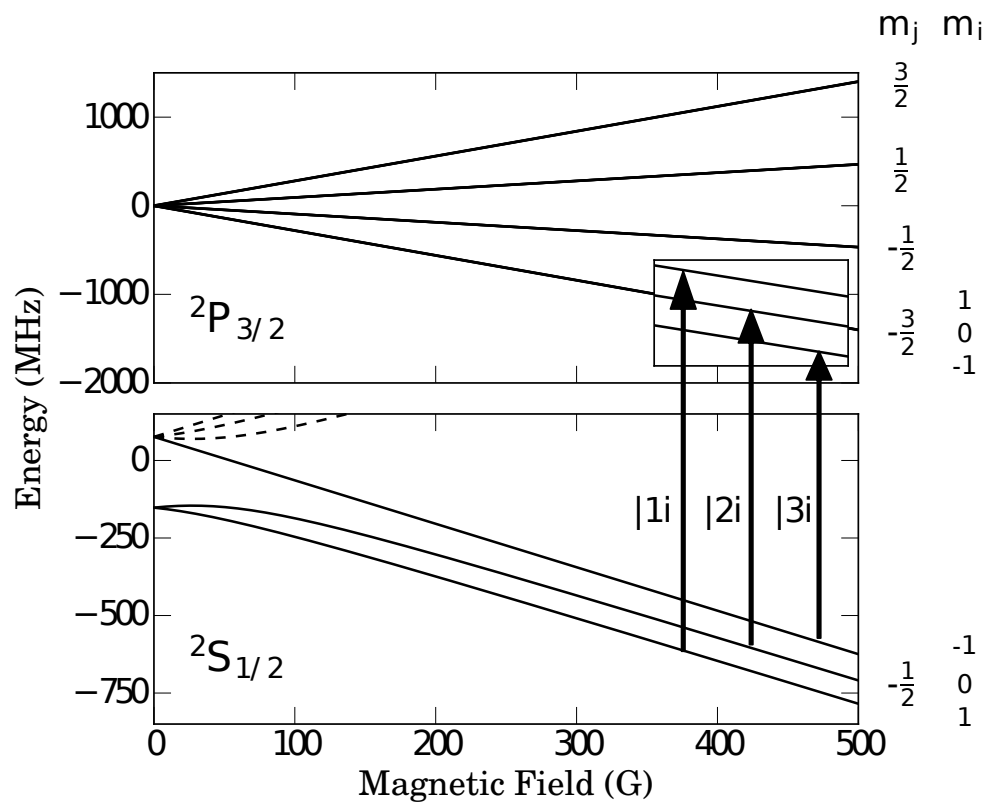


Figure 2.4.: Zeeman levels of the $^2S_{1/2}$ and $^2P_{3/2}$ state. The arrows are representing the transitions used to image the states $|1\rangle$, $|2\rangle$ and $|3\rangle$ for high fields. The splitting of this states is around 1.7 MHz. Figure from [21]

system will also be a major part in the Ph.D. thesis of Gene Polovy [25].

2.4. Experimental Trap Setup

In our experiment we are using two overlapped lasers to apply an optical dipole trap (ODT). A multi-longitudinal mode laser (SPI Lasers, SP-100C-0013, wavelength 1090 nm, linewidth 1 nm) forms the high power trap, which means the evaporation starts at 100 W. The SPI ramps the trap depth exponentially down to 12 W. Here, a transfer to the second, low power trap laser is done. The laser is a single longitudinal mode laser manufactured by IPG Photonics (YLR-20-1064-LP-SF) with a wavelength of 1064 nm and a linewidth of 10 kHz. The IPG evaporates down to a final trapping power of 150 mW (the reason of this value will be explained later). In the experiment both lasers traverse two arms. Each of this arms focuses down on the MOT. The beam waist in the focus for the SPI is $45 \mu\text{m}$ whereas for the IPG it is $35 \mu\text{m}$ [21]. The reason why we first trap with the SPI starting at 100 W is the temperature of the Li atoms in the MOT. Therefore, a deep trap for the transfer from the MOT to the ODT is required [21]. In addition to that, we decided to make our experiment in the IPG since this laser shows a narrower linewidth and is also well polarized. Furthermore, the lowest power setting for the IPG is 200 mW. Therefore, we can tune the trap depth precisely via an AOM from Gooch and Hausego (part number: 97-01672-11) in a single pass configuration. The AOM is driven by 110 MHz RF source and shows an efficiency of roughly 90%. The SPI and IPG are overlapped by a dichroic beam splitter (Semrock LPD01-1064RS-25). This overlap improves the transfer efficiency. For an overview of the setup please see figure 2.5. Other characteristics about the ODT can be read in [21].

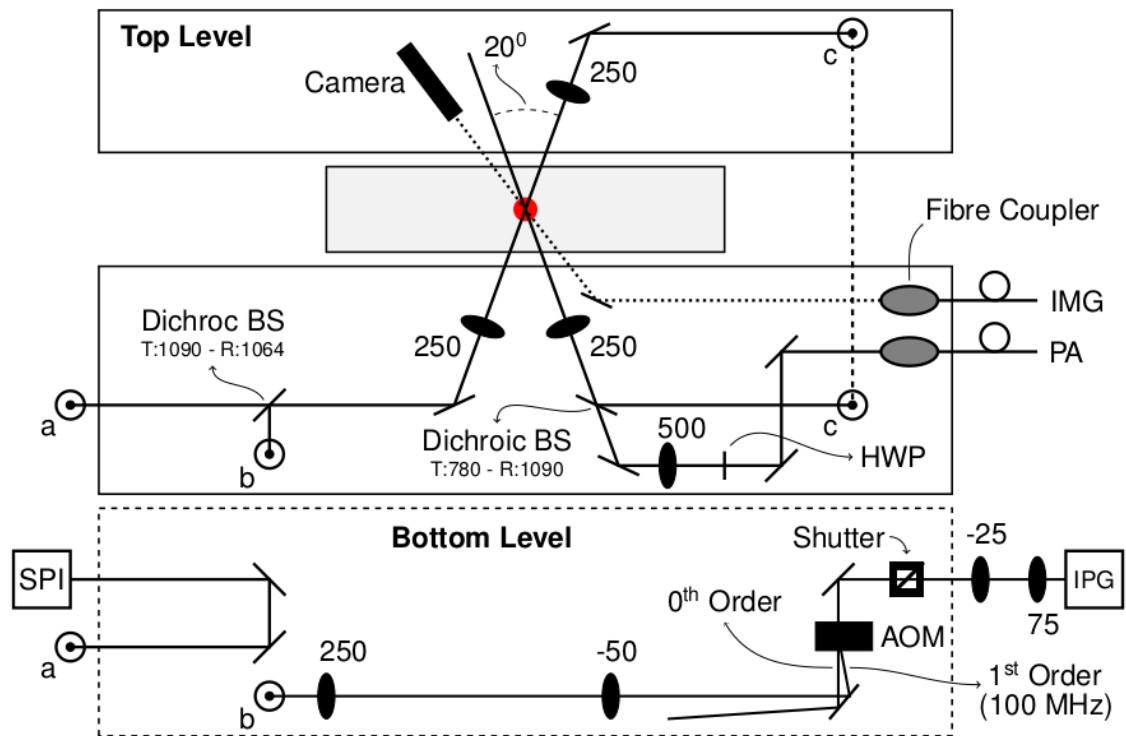


Figure 2.5.: ODT setup. Beam paths are shown for the high power dipole trap (SIP) as well as for the low power dipole trap (IPG). The SPI and IPG are getting overlapped via a dichroic beam splitter. This ensures us a better transfer efficiency. The dashed line by (c) means that the beam path is raised above the experiment. The figure is from [21]

3. Preparation of Cold ${}^6\text{Li}$ Atoms

The basic recipe for our experimental realization is that hot ${}^6\text{Li}$ atoms leave an effusive oven slowed down by a counter-propagating laser beam (Zeeman slower). After slowing down, the atoms are captured by a MOT. This stage of the experiment is where our ultracold quantum gas is generated. However, this is just the beginning of our journey towards creating ultracold Feshbach molecules. After loading into the MOT, the atoms are transferred into an ODT for evaporative cooling. Here, it is also possible to prepare a mixture of different spin states. These steps serve to prepare the sample. The outline of this chapter is to describe the operating principle of the different preparation stages. The magnetic field behavior of the Zeeman slower will be discussed. The full construction of the Zeeman slower can be found in [32]. The next section is a short characterization of the MOT following by a short introduction to evaporative cooling in the ODT.

At the beginning our setup was designed to capture ${}^6\text{Li}$ and ${}^{85}\text{Rb}$ atoms creating a mixture of ${}^6\text{Li} + {}^{85}\text{Rb}$. We set our goal to create ultracold molecules via population transfer into the ground state of a molecular potential. For the first step, we decided to do this with ${}^6\text{Li}$ atoms. Therefore, this thesis focus on the preparation and science for ${}^6\text{Li}$. A full characterization of the Zeeman slower, MOT and ODT was done for ${}^{85}\text{Rb}$. The latest state was to have a ${}^6\text{Li} + {}^{85}\text{Rb}$ mixture captured in a MOT. A full discussion for this mixtures can be found in [21].

3.1. Zeeman Slower and MOT

For a short introduction, we start with an insight into the theory of a Zeeman slower and the hyperfine transition of ${}^6\text{Li}$ which we are using. The Zeeman slower beam is counter-propagated to the hot atoms leaving the effusive oven. This physical slowing effect occurs due to the photon scattering force F_{sc} [21]

$$F_{sc} = \frac{\hbar\omega\gamma}{2mc} \cdot \frac{s}{1 + s + \left(\frac{2\delta}{\gamma}\right)^2} \quad (3.1)$$

where m is the mass of the atom, ω the optical resonance frequency of the Zeeman slower light, γ is the linewidth and s the saturation factor which is the ratio of the laser intensity and the saturation intensity $s = I/I_{sat}$. The detuning of the first light from resonance includes the Doppler effect. The linewidth of an atomic transition is in order of several MHz. When the photon recoil slows these atoms down the resonance condition changes. Therefore, it is necessary to either tune the laser frequency to maintain resonance or use an external magnetic field to move the atomic states back to resonance. The detuning δ of the laser light from the atomic resonance is

$$\delta = \delta_L + \frac{\omega v}{c} - \frac{\mu B}{\hbar} \quad (3.2)$$

This equation explains that the sum of the detuning of the Zeeman slower light δ_L and the Doppler shift (depending on the velocity of the atoms v) can be neglected by the Zeeman shift depending on the magnetic moment μ and its interaction with a magnetic field B . For $\delta = 0$ the atom-light interaction is on resonance. The reduction of the velocity also depends on the length of the Zeeman slower itself. Therefore, the final velocity of the atom is

$$v_f = \sqrt{v_i^2 - 2az} \quad (3.3)$$

where v_i is the initial velocity of the atoms, a a constant deceleration and z the length of the Zeeman slower. To capture atoms leaving the Zeeman slower it is required that the tube length is measured accurately. Otherwise, the slower turns around the propagation of the particles where loading the MOT wouldn't be possible. The field gradient must also ensure an adiabatic slowing condition [32] which causes a challenge when someone wants to slow down multiple species of atoms with the same Zeeman slower [32]. In our experiment, the final magnetic field is produced by the MOT coils. This ensures that the particles get captured in the MOT before blooming effects occur. In general, the design of our Zeeman slower is similar to that of the group of Hackermueller [33]. For a detailed discussion about the magnetic field profile of our Zeeman slower, the MOT coils and loading rates for both, ${}^6\text{Li}$ and ${}^{85}\text{Rb}$, the reader is referred to [21, 24]. Our Zeeman slower uses the Li D_2 transition. In other words we are using the transition $|f = 3/2, m_f = 3/2\rangle \rightarrow |f' = 5/2, m'_f = 5/2\rangle$. The magnetic field is large enough to disrupt the hyperfine cooling of this state, and f is not a good quantum number. Therefore, we rewrite this transition in the basis states of nuclear spin projection m_i and the total orbital angular momentum projection m_j which are $|m_j = 1/2, m_i = 1\rangle \rightarrow |m'_j = 3/2, m'_i = 1\rangle$. For our loading parameters we use a Zeeman slower beam detuning of -76 MHz with respect to the $|f = 3/2, m_f = 3/2\rangle \rightarrow |f' = 5/2, m'_f = 5/2\rangle$ transition at zero field. The beam power is 60 mW. To find the optimal settings for the Li oven temperature one needs to strike a balance between the MOT loading time and the lifetime of the ${}^6\text{Li}$ atoms in the ODT. This measurement was done in [34]. A balance between the MOT loading time and the ODT lifetime was achieved at a temperature of 400 °C. To reach the degeneracy limit of our ultracold gas we need to reduce the temperature of the atoms in the MOT by an additional factor of 10^3 . Therefore, we transfer our atom from the MOT into an ODT. The lifetime of the MOT is three times larger than the lifetime of the ODT due to the trap depth [35]. A detailed discussion of the slowing beam power and MOT loading curve can be found in [21, 24].

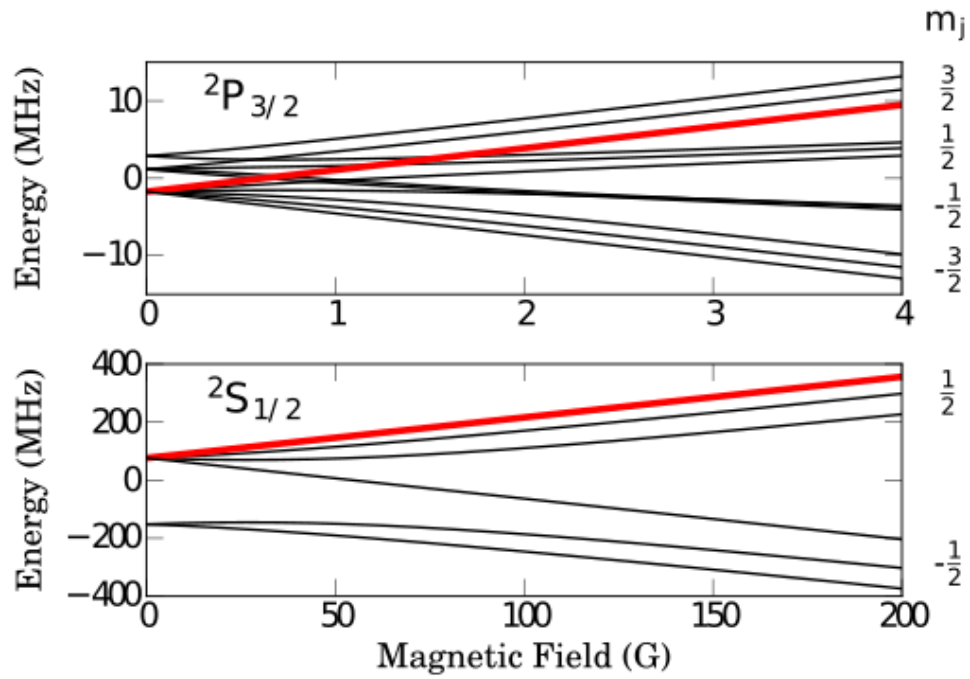


Figure 3.1.: Hyperfine structure of ${}^6\text{Li}$. An external magnetic field is tuned from 0 G to 200 G. For $B = 0$ G the states are $|f = 3/2, m_f = 3/2\rangle$ for the ground state $|g\rangle$ and $|m'_f = 5/2, m'_f = 5/2\rangle$ for the excited state $|e\rangle$. For higher fields the coupling of j and i breaks and the new states are $|m_j = 1/2, m_i = 1\rangle$ and $|m'_j = 3/2, m'_i = 1\rangle$. The picture is from [21].

3.2. Evaporative Cooling in an Optical Dipole Trap

Optical dipole traps (ODT) are often used to confine atoms. The potential of the ODT trap is proportional to the intensity of the beam. The trap depth is given by the induced dipole moment \vec{d} multiplied with the interaction field \vec{E} [36]

$$U_{dip} = \frac{-\vec{d} \cdot \vec{E}}{2} \quad (3.4)$$

Since the beam is far from the atomic resonance it preserves the spin mixture which allows preparing a mixture with a special spin configuration in the ODT. Other external fields can be easily applied to the system. Trapping via an ODT also allows evaporative cooling. With this technique, it is possible to produce degenerate Bose and Fermi gases [37]. For a more detailed overview about ODTs the reader is referred to [36, 38]. To apply evaporative cooling we need to transfer the atoms from the MOT into the SPI induced laser trap [39]. This transfer happens at around 4-5 mK. It is also important to know how efficient the evaporation at the different cooling states is. The evaporation follows the following equation [?]:

$$\frac{N_f}{N_i} = \left(\frac{U_f}{U_i} \right)^{\frac{1}{2} \left(\frac{3}{\eta-3} \right)} \quad (3.5)$$

Here $N_{i/f}$ is the initial/final atom number in the dipole trap, $U_{f/i}$ the initial/final trap depth and $\eta = U/k_B T$ is the ratio of the trap depth and thermal energy of the ensemble. An efficient evaporation is achieved by reaching $\eta = 10$ [37]. The evaporation ramp of the SPI shows an exponential slope from 100 W down to 12 W. Here, we transfer the atoms from the SPI to the IPG. From here, the IPG evaporates exponentially down to a final trapping power of 0.14 W which corresponds to a temperature of 200-300 nK after 2 – 3 s. This temperature was extracted from time of flight measurements. The results can be seen in the Ph.D. thesis from Gene Polovy which is currently in progress [25]. After the evaporation ramp ramps down to 140 mW 40.000 atoms are remaining in the ODT. The whole evaporation sequence takes place at 755 G. The measured evaporation curves are shown the final evaporation stages in the IPG in figure 3.3 for HFI and in figure 3.2 for ZFI. We can see that for the high field case at low final trapping powers the evaporation follows the theoretical value $\eta = 10$. Therefore, we can say that our evaporation is efficient. A more detailed interpretation of this measurement is discussed later.

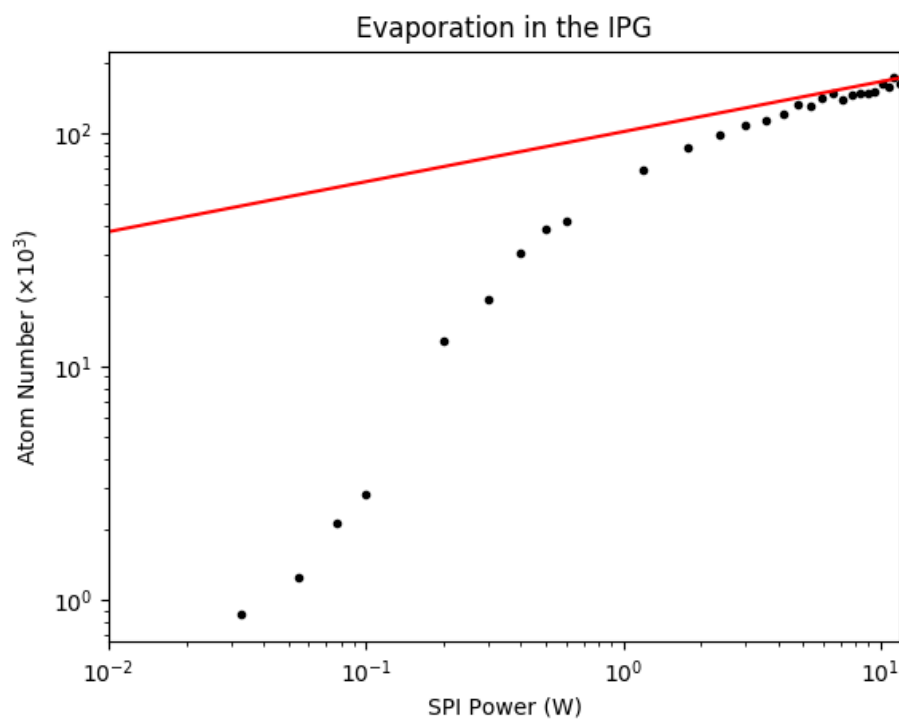


Figure 3.2.: Evaporation in the IPG for zero field imaging (ZFI). At a certain point the atom number is decreasing. The image light for ZFI is not resonant to any transition. The red line is the theoretical value for $\eta = 10$. A detailed discussion is done in the next chapter.

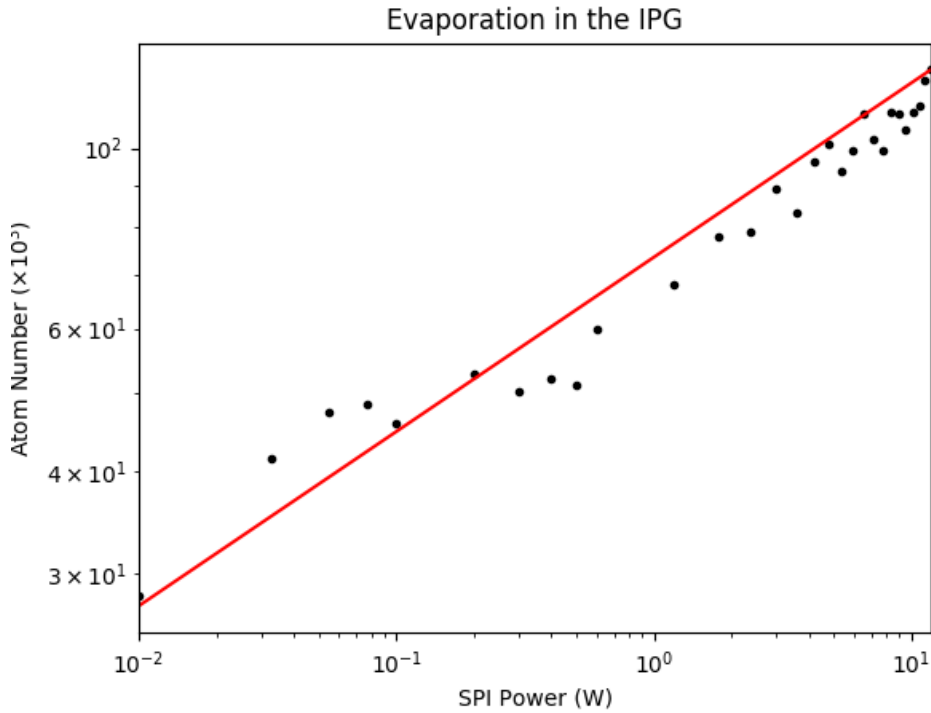


Figure 3.3.: Evaporation in the IPG for high field imaging (HFI) at $B = 755$ G. By turning on the magnetic field the resonance of the image image light is still given due to the hyperfine splitting. Furthermore, the binding energy is small. The molecules break up due to the image process and we detect atoms in the initial state $|i\rangle$. The red line is the theoretical value for $\eta = 10$. A detailed discussion is done in the next chapter.

4. Ultracold ${}^6\text{Li}_2$ Feshbach Molecules

Towards the goal of creating ultracold deeply bound ${}^6\text{Li}_2$ Feshbach molecules one has to ask the questions: *What are Feshbach molecules?* and *How are we going to create them?* This chapter will answer these questions by giving an insight of the nature of Feshbach molecules, its selection rules and the experimental technique used to create them. For a full theoretical background of Feshbach molecules and their collision channels, the reader is referred to section II in 'Feshbach Resonances in Ultracold Gases' by Cheng Chin, Rudolf Grimm, Paul Julienne and Eite Tiesinga [15].

As described in the previous chapter we discussed how to trap our ${}^6\text{Li}$ atoms in a MOT. The next step towards creating Feshbach molecules is loading these atoms into an optical dipole trap (ODT) and evaporative cooling them down to a temperature around 200 nK. During this cooling process, Feshbach molecules are created via 3-body collisions¹.

4.1. Basic Idea of a Feshbach Resonance

The basic idea of a Feshbach resonance is to tune the energy of two colliding atoms into resonance with a bound state of a different molecular potential by tuning the external magnetic field. This was first studied theoretically by Herman Feshbach in the year 1964 [40]. With this technique it is possible to manipulate the interaction strength or/and scattering length of ultracold atoms. For a better understanding of the physics, we start with a simple elastic two-body collision. Two particles (in our case two ${}^6\text{Li}$ atoms) flying towards each other and collide. Depending on the separation of both collision partners, the interaction of the electronic energy is perturbed resulting in an interaction potential represented by the blue potential curve in figure 4.1. The so-called open channel forms the background potential $V_{bg}(R)$. The interaction potential $V_{cc}(R)$, also called the closed channel, is a non-accessible reaction channel above the scattering energy. In other words, the closed channel represents an interaction potential of the same scattered atoms but in a different internal state. This is shown by the green potential curve in figure 4.1 [41].

The closed channel potential $V_{cc}(R)$ contains molecular bound states with energy E_{cc} . If the scattering state of the two colliding atoms in the open channel with energy E equals the energy of a bound state E_{cc} in the closed channel, a Feshbach resonance occurs. One possibility to bring these energies into resonance and couple the two particle scattering state with energy E with an excited molecular bound state can be achieved by optical excitation. However, the optical method shows a

¹The creation of Feshbach molecules via 3-body collisions works well because collisional relaxation of ${}^6\text{Li}_2$ is suppressed.

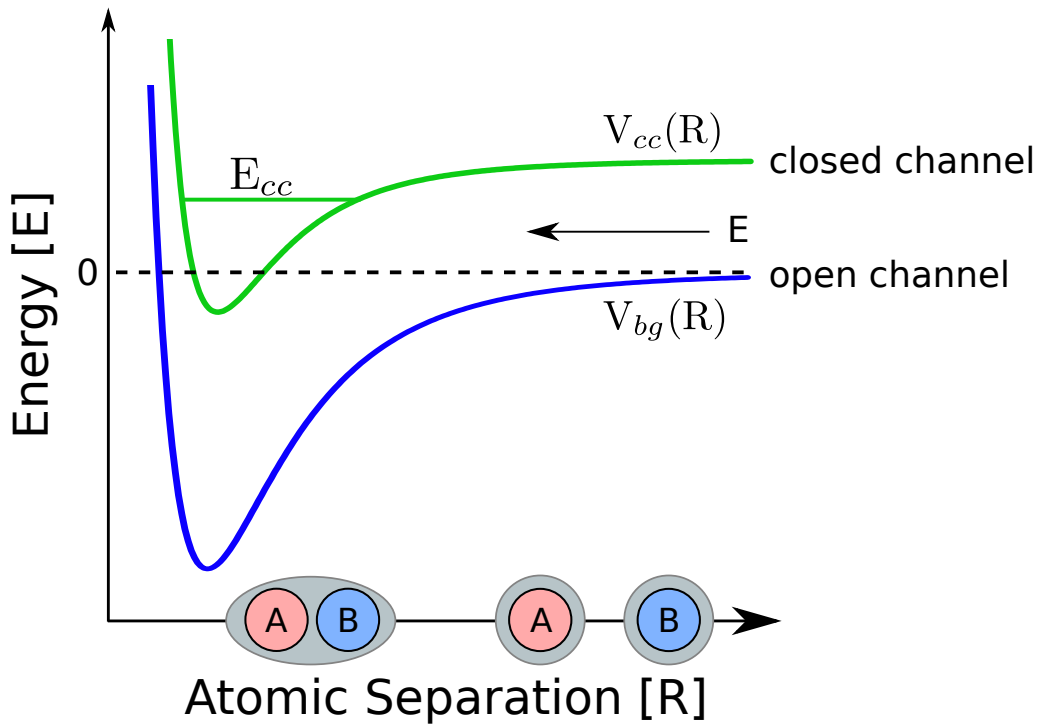


Figure 4.1.: Model for Feshbach resonances. The background potential $V_{bg}(R)$ (also called open channel) is the collision potential of two atoms A and B as a function of their spacial separation R . The separation of both atoms is shown by the cartoon on the x-axis. The second potential $V_{cc}(R)$ is a non-accessible reaction channel which lies above the scattering energy. A Feshbach resonance occurs when the collision energy of two atoms E in the open channel couples to a molecular bound state in the closed channel with energy E_c . The coupling of the states can be evoked by tuning of an external magnetic field which shifts E_c near to the collision energy E . For ultracold gases the collision energy of the colliding atoms is close to 0. Taken and adapted from [15].

collisional loss due to spontaneous emission resulting in a complex scattering length. For a deeper theoretical insight of the influence of resonant light to the scattering length the reader is referred to [42–44]. The second way is to bring the two colliding atoms into resonance with a bound state of the closed channel uses the Zeeman effect. Applying an external magnetic field shifts the weakly bound closed channel state towards the collision energy E of the open channel, and coupling of the states via hyperfine interactions is possible. This method requires that the two channels exhibit a different magnetic moment. Then, tuning the external magnetic field B results into a relative movement of both interaction potentials given by $\Delta E = \Delta\mu B$, respectively [15]. The scattering length $a(B)$ is a function of the magnetic field. Near the Feshbach resonance for s-wave collisions $a(B)$ can be written as shown in equation 4.1. This expression was introduced by Moerdijk *et al.* in the year 1995 [45].

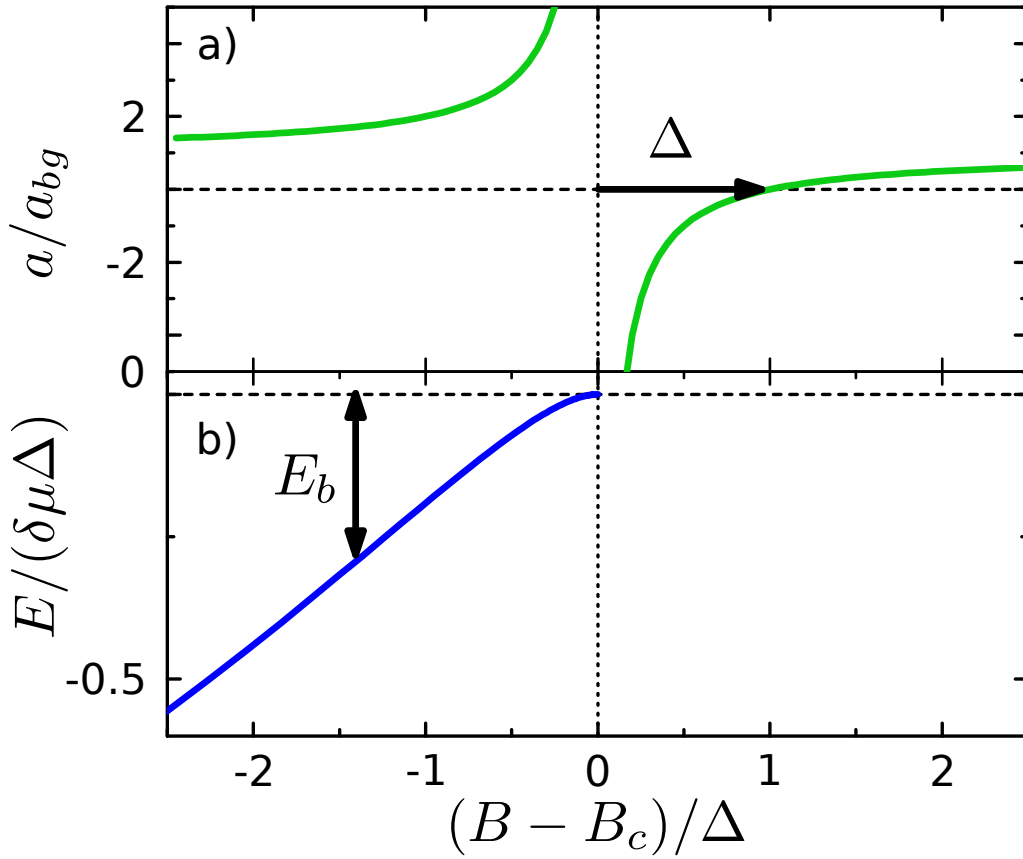


Figure 4.2.: Scattering length and binding energy near a Feshbach resonance. (a) Scattering length $a(B)$ near a Feshbach resonance with resonance width Δ . The equation for the scattering length is shown in 4.1. (b) Molecular state energy near a Feshbach resonance. For a large positive scattering length $a(B)$ a dressed molecular state with binding energy E_b exists. Taken and adapted from [41].

$$a(B) = a_{bg} - a_{bg} \frac{\Delta B}{B - B_0} \quad (4.1)$$

For $B \rightarrow \infty$ the second part of equation 4.1 $\Delta B/(B - B_0)$ goes to zero leading to a scattering length of $a(B) = a_{bg}$. Therefore, a_{bg} can be interpreted as the background scattering length and is independent of external magnetic influences. The distance between the Feshbach resonance B_0 and the zero crossing of the scattering length $a(B)$ is given by ΔB describing the width of the resonance feature. A visualization of the scattering length $a(B)$ is shown in figure 4.2, a).

By tuning the external magnetic field to resonance the open channel mixes with the bound state of the closed channel. Close to the Feshbach resonance B_0 we can obtain a strong scattering length following equation 4.1. Due to this coupling, the energy of these states are modified and they can be interpreted as 'dressed states'. A short calculation can give some insight into this effect. We can simplify the problem into a two-level molecular system. The dependencies of the energy of two molecular diabatic states $E_{1,2}$ and the magnetic field is [41]

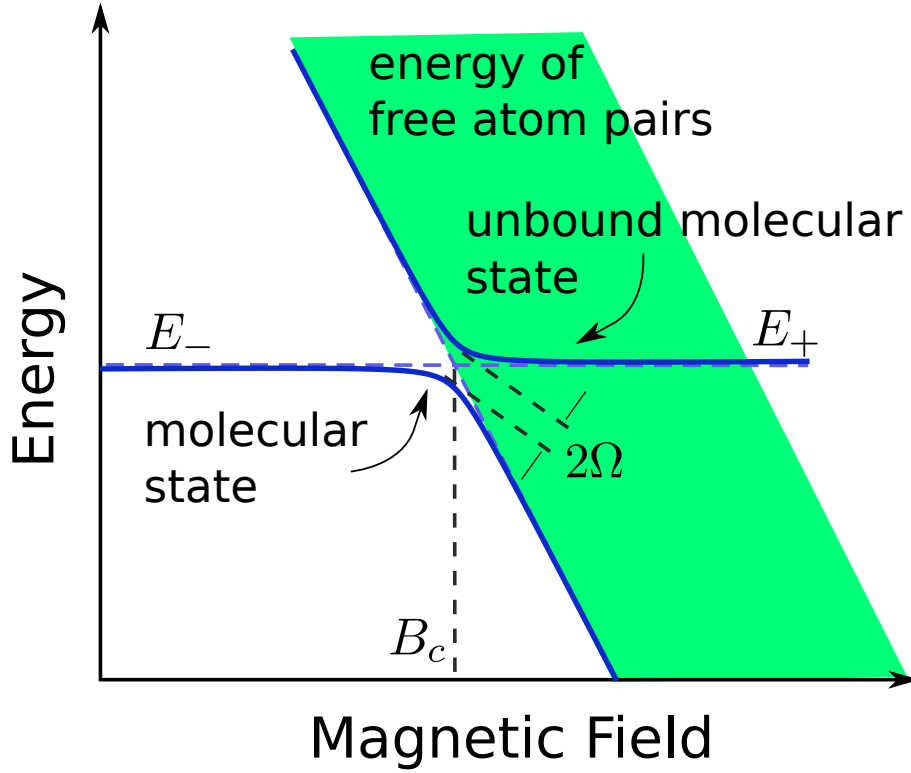


Figure 4.3.: Anti-crossing of the states. Due to coupling a dressed state occurs. Our two colliding atoms are 'sitting' on the edge of the continuum. To create molecules (follow the molecular energy) one has to decrease the magnetic field while crossing the Feshbach resonance adiabatically. Increasing the magnetic field and crossing the Feshbach resonance leads to an embedded bound state in the continuum. This state can not be a stable molecular state. The energy difference at resonance is 2Ω where Ω is the coupling strength of the energy E_+ and E_- .

$$E_{1,2}(B) = \mu_{1,2}(B - B_c) + E_c \quad (4.2)$$

where $\mu_{1,2}$ corresponds to the different magnetic moment of two molecular states labeled as 1 and 2, B_c is the magnetic field and E_c the energy where the bare states cross. The Hamiltonian for this two-level system contains the coupling Ω and the energy E of both states [41].

$$H \sim \begin{bmatrix} E_1 & \Omega \\ \Omega & E_2 + \Delta \end{bmatrix} \quad (4.3)$$

On resonance ($\Delta = 0$) we have the following eigenvalue problem [41]

$$\begin{bmatrix} E_1 & \Omega \\ \Omega & E_2 \end{bmatrix} \begin{bmatrix} \varphi_1 \\ \varphi_2 \end{bmatrix} = E \begin{bmatrix} \varphi_1 \\ \varphi_2 \end{bmatrix} \quad (4.4)$$

The diabatic states are described by $\phi_{1,2}$. The result of this eigenvalue problem is the adiabatic energies E_{\pm} which show an anti-crossing of the bare states [41] near a

Feshbach resonance. This is a so-called dressed state. In other words, the crossing of the energies $E_{1,2}$ of the two states is prevented and get pushed apart due to their interaction. These dressed states have energies E_{\pm} and are sketched in figure 4.3.

$$E_{\pm} = \frac{(E_1 + E_2) \pm \sqrt{(E_1 + E_2)^2 + 4\Omega^2}}{2} \quad (4.5)$$

E_+ is the energy above and E_- below the crossing of the states. The coupling of the dressed states results in an energy difference between E_+ and E_- [41]

$$\Delta E = |E_+ - E_-| = \sqrt{(\mu_1 - \mu_2)^2(B - B_c)^2 + 4\Omega^2} \quad (4.6)$$

On resonance $B = B_c$, where the bare states should cross, the energy difference is 2Ω [41].

Since coupling of two states causes repulsion, it is essential to know from which side the bound state energy E_{cc} approaches the collision energy E . If the weakly bound state energy E_{cc} approaches the collisional energy E from above, the coupling pushes the new dressed colliding state downwards. The interaction is therefore attractive and shows a negative scattering length. On the other hand, if the weakly bound state energy E_{cc} approaches the collisional energy E from below, the coupling pushes the new dressed colliding state upwards. The interaction is repulsive with a positive scattering length. Since there is an anti-crossing of the two channels (see figure 4.3) transforming the free atom state (continuum) into the molecular bound state is possible by slowly changing the magnetic field from above B_c to below B_c where the molecular state is below the continuum. The creation of Feshbach molecules via tuning a magnetic field over a Feshbach resonance were performed in many experiments of several groups [46–50]. To avoid confusion it is important to mention that both energy states are molecular energy states and the different labeling in figure 4.3 was chosen to indicate their asymmetric character respectively. In the regime near the resonance, the dressed molecular states show a binding energy given by equation 4.7.

$$E_b = \frac{\hbar^2}{2m_r a^2} \quad (4.7)$$

where m_r is the reduced mass of the colliding atoms and a the scattering length. The binding energy is dependent to the square of the magnetic field $E_b \sim (B - B_0)^2$ which shows a quadratic behavior for a small detuning near the Feshbach resonance B_0 . In this region the scattering length is large. For a large detuning from resonance, the scattering length is getting smaller and the binding energy E_b shows a linear character. This can be seen in figure 4.1 b). A more detailed description of this two different binding energy regimes is discussed in 'Ultracold Feshbach Molecules' published by Francesca Ferlaino, Steven Knoop and Rudolf Grimm [41].

4.2. State Preparation - Towards a Hyperfine Mixture $|12\rangle$

Using a Feshbach resonance offers the possibility to generate molecules. The fact that ${}^6\text{Li}$ shows a broad Feshbach resonance at a magnetic field of $B \approx 834$ G creates the possibility to study such molecules experimentally. This aspect also makes ${}^6\text{Li}$ atoms important for many-body physics studies as well as for studies of the BEC-BCS crossover [51–53]. Besides sweeping the magnetic field over the Feshbach resonance, Feshbach molecules can be created by 3-body collisions. This process happens naturally during evaporative cooling. Before we can successfully implement evaporative cooling, the ${}^6\text{Li}$ atoms have to be prepared. This chapter represents a step-by-step overview how we create molecules and which atomic states are used.

For the ${}^6\text{Li}$ ground state, as already mentioned in a previous chapter, we can observe two hyperfine states, one for $f = 1/2$ and one for $f = 3/2$, where $\vec{f} = \vec{j} + \vec{i}$ and $\vec{j} = \vec{l} + \vec{s}$. The hyperfine states are separated by 228 MHz [27]. Since $l = 0$ the hyperfine splitting depends on the spin s and nuclei i multiplied by the atomic hyperfine constant $a_{hf} = a_{2S} = 152.2$ MHz [27]. For low magnetic fields ($B < 10$ G), the so-called low field limit, $\vec{i} \cdot \vec{s}$ -coupling occurs and the magnetic field perturbs the interaction Hamiltonian. This perturbation affects the magnetic moment μ_e of the electron and therefore the projection of the spin m_s and the magnetic moment of the nuclei μ_n and the projection m_i . In total the interaction Hamiltonian [54] can be written as shown in equation 4.8

$$H_{int} = \frac{a_{hf}}{\hbar^2} \vec{s} \cdot \vec{i} + \vec{B} \cdot \frac{2\mu_e \vec{s} - \mu_n \vec{i}}{\hbar} \quad (4.8)$$

In the low field limit hyperfine coupling ($\vec{i} \cdot \vec{s}$ -coupling) dominates. The basis of those states can be written as $|f, m_f\rangle$. For high magnetic fields this coupling is disturbed and f is not a good quantum number anymore. Here, the Zeeman splitting is larger than the hyperfine splitting. The new basis is expressed by the decoupled spin quantum number s , its projection m_s , the nuclear quantum number i and its projection m_i written as $|s, m_s\rangle|i, m_i\rangle$. The orbital quantum number can be neglected since $l = 0$ for the ${}^6\text{Li}$ ground state. The eigenstates are therefore linear combinations of both quantum numbers. The spin quantum number has the value $s = 1/2$. Therefore, the projection of the spin quantum number takes the values $m_s = \pm 1/2$. For the projection of the total angular momentum we find the sum of all projection quantum numbers $m_f = m_i + m_l + m_s$. We can rearrange this equation to find an expression of the projection of the nuclear quantum number $m_i = m_f - m_l - m_s$. Please note that for ${}^6\text{Li}$ $m_l = 0$. This leads to six eigenstates labeled from $|1\rangle$ to $|6\rangle$. The eigenstates are visualized in figure 4.8 and summarized in table 4.1. In our experiment we are using the states labeled with $|1\rangle$ and $|2\rangle$. Both of these states have a spin projection of $m_s = -1/2$. These two states are good candidates since inelastic two-body collisions are suppressed due to s-wave collisions and the projection m_f is conserved. However, for high magnetic fields near the Feshbach resonance at $B \approx 834$ G the two-atom scattering state is coupled to a

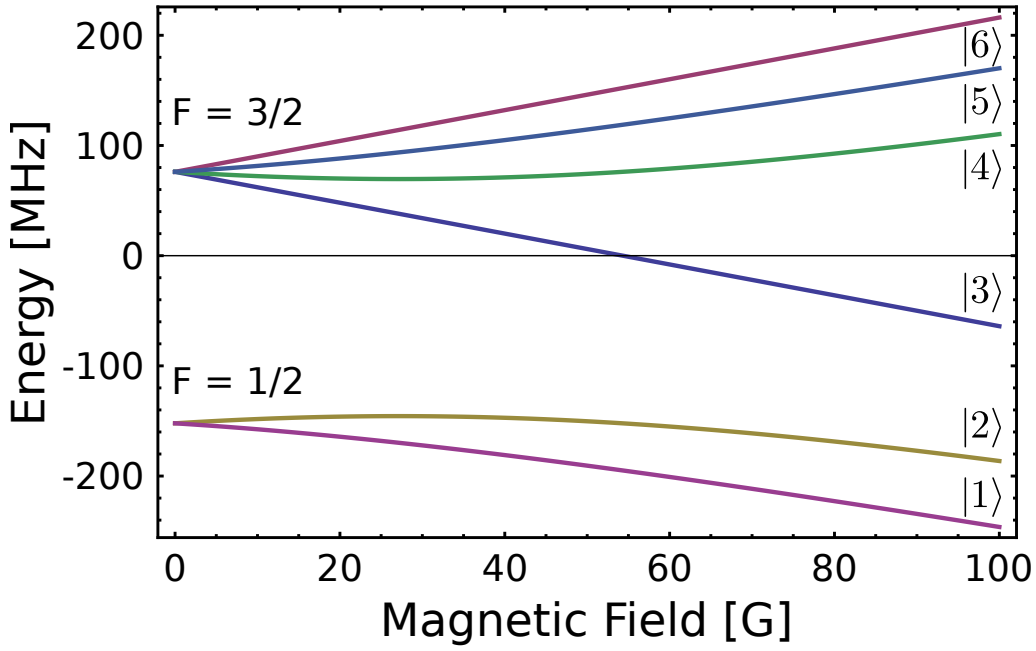


Figure 4.4.: Zeeman splitting of the two hyperfine states for the ground state of ${}^6\text{Li}$. In the low field limit ($B < 10$ G) the hyperfine term in equation 4.8 is a small perturbation. The momenta are still coupled. For the ground state $l = 0$ which leads to a coupling of the spin s and nuclear spin i and the total quantum number for the total angular momentum f represents a good quantum number with basis $|f, m_f\rangle$. For higher magnetic fields this coupling bursts and f is not a good quantum number anymore. The new basis is $|i, m_i\rangle|s, m_s\rangle$. This Zeeman sub-levels are labeled as states $|1\rangle$ to $|6\rangle$, see table 4.1.

bound state. In this regime the states $|1\rangle = |1, -1/2\rangle$ and $|2\rangle = |0, -1/2\rangle$ generate a stable mixture. During the whole collision process the total angular momentum must be conserved, which means that

$$m_N + m_L + m_S + m_I = m'_N + m'_L + m'_S + m'_I \quad (4.9)$$

where m_N is the projection of the orbital angular momentum of the two body state. Note that the quantum numbers mentioned in equation 4.9 refer to the total quantum numbers $\vec{X} = \vec{x}_A + \vec{x}_B$, where A and B describes two colliding atoms. For a s-wave collision the quantum number of the total molecular momentum $N = 0$, which also means $m_N = 0$.

Furthermore, for 2-body collisions, the spin angular momentum projection is conserved, which dictates the dominant rule of this kind of collisions. Underlying this rule only the states $|1\rangle$, $|2\rangle$ and $|3\rangle$ are going to produce stable mixtures [55]. However, assuming a collision of the states $|1\rangle$ with $|3\rangle$ ends up as a product of state $|2\rangle$ and $|2\rangle$ plus an additional energy corresponding to a change of angular momentum since the energy difference of these states are not equal. Or in other words $E_1 + E_3 \rightarrow E_2 + E_2 + \Delta E$. A collision of the states $|1\rangle$ with $|2\rangle$, however, ends up

State	High Field $ m_i, m_s\rangle$	Low Field $ f, m_f\rangle$
$ 1\rangle$	$ 1, -1/2\rangle$	$ 1/2, 1/2\rangle$
$ 2\rangle$	$ 0, -1/2\rangle$	$ 1/2, -1/2\rangle$
$ 3\rangle$	$ -1, -1/2\rangle$	$ 3/2, -3/2\rangle$
$ 4\rangle$	$ -1, 1/2\rangle$	$ 3/2, -1/2\rangle$
$ 5\rangle$	$ 0, 1/2\rangle$	$ 3/2, 1/2\rangle$
$ 6\rangle$	$ 1, 1/2\rangle$	$ 3/2, 3/2\rangle$

Table 4.1.: Zeeman sub-levels of the ground state of ${}^6\text{Li}$. This states occur for a high magnetic field $B > 10$ G. In the low field limit the basis is $|f, m_f\rangle$. For high fields the basis is $|i, m_i\rangle|s, m_s\rangle$. Note that the electronic spin is $s = 1/2$ with $m_s = \pm 1/2$ and the nuclear spin is $i = 1$ with $m_i = -1, 0, 1$.

with the same product of the state. For a fully mathematical expression, we can write this two states as [54].

$$|1\rangle = \sin \Theta_+ |1/2, 0\rangle - \cos \Theta_+ |-1/2, 1\rangle \quad (4.10)$$

$$|2\rangle = \sin \Theta_- |1/2, -1\rangle - \cos \Theta_- |-1/2, 0\rangle \quad (4.11)$$

with

$$\sin \Theta_{\pm} = \frac{1}{\sqrt{1 + (Q^{\pm} + R^{\pm})/2}} \quad (4.12)$$

$$Q^{\pm} = \frac{(\mu_N + 2\mu_e)B}{a_{hf}} \pm \frac{1}{2} \quad (4.13)$$

$$R^{\pm} = \sqrt{(Q^{\pm})^2 + 2} \quad (4.14)$$

For zero magnetic field ($B = 0$) $\sin \Theta_+ = \cos \Theta_- = \sqrt{1/3}$ and $\sin \Theta_- = \cos \Theta_+ = \sqrt{2/3}$. However, for high magnetic field $\sin \Theta_{\pm} = 0$ and $\cos \Theta_{\pm} = 1$. Equation 4.8 was the interaction Hamiltonian for one atom. We can extend this equation for two non-interacting atoms [54, 56]. Therefore we introduce the total electronic spin $\vec{S} = \vec{s}_1 + \vec{s}_2$ and total nuclear spin $\vec{I} = \vec{i}_1 + \vec{i}_2$ [54].

$$H_{int} = \frac{a_{hf}}{\hbar^2} (\vec{s}_1 \vec{i}_1 + \vec{s}_2 \vec{i}_2) + \vec{B} \frac{2\mu_e \vec{S} - \mu_N \vec{I}}{\hbar} \quad (4.15)$$

Since ${}^6\text{Li}$ atoms are Fermions, the two atom scattering states is asymmetric under exchange of the atoms and the open channel of the hyperfine mixture $|12\rangle$ is [54]

$$|12\rangle = \frac{1}{\sqrt{2}} (|1\rangle_1 |2\rangle_2 - |2\rangle_1 |1\rangle_2) \quad (4.16)$$

The total spin of the molecule is given by $\vec{S} = \vec{s}_1 + \vec{s}_2 = 0, 1$ which means, that the collisional state has singlet ($S = 0$) and triplet ($S = 1$) character. The scattering state mentioned in 4.16 can be rewritten in the $|S, m_S; I, m_I\rangle$ basis which

diagonalize the second term of the interaction Hamiltonian in equation 4.15 [21, 54]. The quantum numbers m_S and m_I represents the projection of the total electronic and total nuclear spin to the quantized axis in direction of the magnetic field [54].

$$|12\rangle_B = \sin \Theta_+ \sin \Theta_- |1, 1; 1, -1\rangle \quad (4.17)$$

$$+ \sin \Theta_+ \cos \Theta_- \left(\sqrt{\frac{1}{3}} |0, 0; 0, 0\rangle - \sqrt{\frac{2}{3}} |0, 0; 2, 0\rangle \right) \quad (4.18)$$

$$+ \cos \Theta_+ \sin \Theta_- \left(\sqrt{\frac{1}{3}} |0, 0; 0, 0\rangle + \sqrt{\frac{1}{6}} |0, 0; 2, 0\rangle - \sqrt{\frac{1}{2}} |1, 0; 1, 0\rangle \right) \quad (4.19)$$

$$+ \cos \Theta_+ \cos \Theta_- |1, -1; 1, 1\rangle \quad (4.20)$$

Already mentioned above we can make following assumptions for zero magnetic field ($B = 0$ G) $\sin \Theta_+ = \cos \Theta_- = \sqrt{1/3}$ and $\sin \Theta_- = \cos \Theta_+ = \sqrt{2/3}$ which leads to [54]

$$|12\rangle_{B=0} = \sqrt{\frac{2}{9}} (|1, 1; 1, -1\rangle + |1, -1; 1, 1\rangle - |1, 0; 1, 0\rangle) + \sqrt{\frac{1}{3}} |0, 0; 0, 0\rangle \quad (4.21)$$

From this equation we can extract the singlet state with $S = 0$, $m_S = 0$ and the triplet state $S = 1$, $m_S = -1, 0, 1$. At high magnetic fields (near the Feshbach resonance) m_S and m_I are good quantum numbers and the hyperfine part of the Hamiltonian 4.8 is just a small perturbation. Referring to equations 4.12 we can see that $\sin \Theta_{\pm} \rightarrow 0$. The spin mixture 4.17 shows then a pure triplet character [54].

$$|12\rangle_{800 \leq B \leq 900} = |1, -1; 1, 1\rangle \quad (4.22)$$

near the Feshbach resonance of $B \approx 834$ G energy of the open channel is near the vibrational molecular bound state energy $v = 38$ of the closed channel which has singlet character. This results in a broad Feshbach resonance shown in figure 4.5. The overlap of the wave functions describes the coupling of the open and closed channel which is given by the matrix element of the singlet and triplet state of the hyperfine Hamiltonian [54]

$$\langle 0, 0; 0, 0 | H_{hf} | 1, -1; 1, 1 \rangle \quad (4.23)$$

Furthermore, it is interesting to mention that a simple square-well method can model Feshbach resonances in an analytical solvable way. This model also gives some information about the resonance strength s_{res} and defines Feshbach resonances as 'narrow' when they are closed channel dominated and 'broad' if they are open channel dominated. For a more detailed theoretical description of this model the reader is referred to [15, 21, 57].

4.3. Feshbach resonances in ${}^6\text{Li}$

The previous two sections gave a short theoretical overview of Feshbach resonances. It is interesting to know that ${}^6\text{Li}$ has a very broad Feshbach resonance at a magnetic field of around 834 G. Houbiers first predicted this field strength in 'Elastic and inelastic collisions of ${}^6\text{Li}$ atoms in magnetic and optical traps' published in 1998 [58]. The width ΔB of the Feshbach resonance at $B \approx 834$ G is several hundreds Gauss. An experimental proof for this broad resonance is given by Bourdel [59] and is shown in figure 4.5.

${}^6\text{Li}$ is a Fermion, which means that s-wave scattering occurs only for atoms in distinguishable hyperfine states [15]. For a collision with an orbital quantum number $l > 0$ a potential barrier must be overcome. For ultracold gases, the thermal energy can be below the potential barrier, for example for a p-wave. This ensures that only s-wave collisions can occur. For p-wave scattering another Feshbach resonance for a $|12\rangle$ hyperfine ${}^6\text{Li}$ mixture was found near $B_0 \approx 185$ G [15]. Another narrow s-wave Feshbach resonance was discovered near a magnetic field of ~ 540 G with a width of ~ 100 mG. For an experimental discussion of this narrow Feshbach resonance, the reader is referred to Stecker [50] since our experiment focuses on the broad resonance at ~ 834 G invariably.

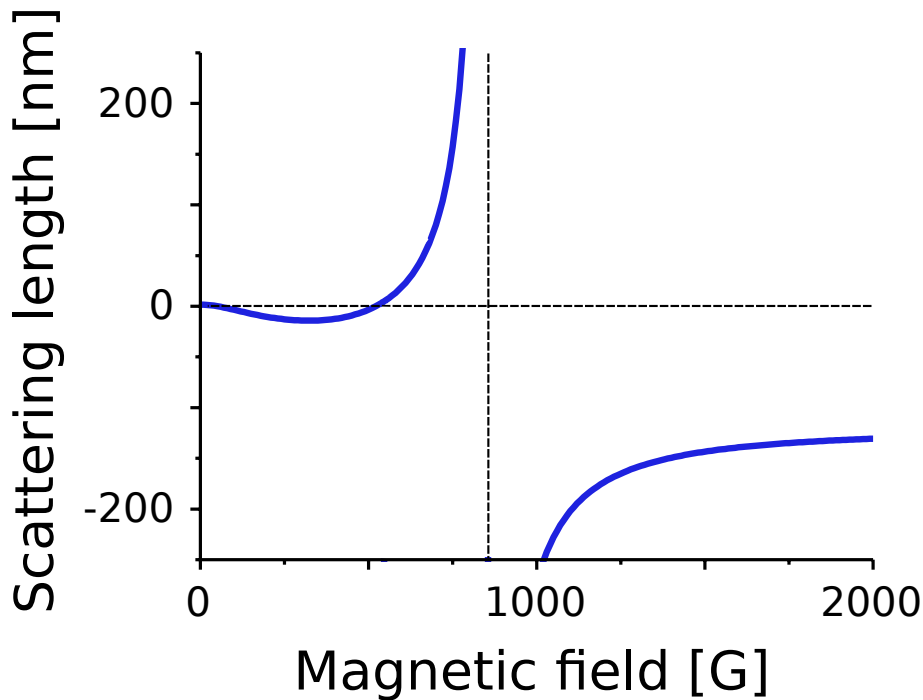


Figure 4.5.: Broad Feshbach resonance in ${}^6\text{Li}$. To see is the scattering length vs. the magnetic field. Taken and adapted from [59].

A valid question is *why does ${}^6\text{Li}$ have two Feshbach resonances for s-wave collisions?* Here we can point out that the two atomic scattering state is a triplet state since $m_s = -1/2$. The singlet potential, however, forms the closed channel. For the singlet potential, the highest vibrational state is the $v = 38$ and couples to the

two atom scattering state. The total nuclear spin of two colliding atoms results into $I = 0, 1, 2$. Since the singlet state has an anti-symmetric character the nuclear spin wave function has to be symmetric. Therefore, the spin singlet cannot be combined with $I = 1$, which has an antisymmetric character. For the total angular momentum we have therefore two possibilities, $F = 0, m_F = 0$ and $F = 2, m_F = 0$. These two hyperfine states are the reason for the two Feshbach resonances. The reason for its width is the near threshold resonance which lies slightly above zero energy [60]. For a fully experimental description of the broad resonance I refer to Abraham, 'Triplet s-wave resonance in ${}^6\text{Li}$ collisions and scattering lengths of ${}^6\text{Li}$ and ${}^7\text{Li}$ ' published in 1997 [60].

As a summary, table 4.2 provides properties for a s-wave scattering ($l = 0$) of our $|12\rangle$ mixture used in the experiment for both Feshbach resonances, $B \approx 834$ G and $B \approx 543$ G.

channel	B_0 [G]	ΔB [G]	a_{bg}/a_0
$ 12\rangle$	834.1	-300	-1405
$ 12\rangle$	543.2	0.1	60

Table 4.2.: S-wave Feshbach resonance properties for a hyperine mixture of ${}^6\text{Li}$ of the states $|1\rangle$ and $|2\rangle$. Numbers are from [15]

4.4. Experimental realization of Feshbach Molecules

In our experiment we generate Feshbach molecules without sweeping the magnetic field over the resonance but by evaporating the gas near the resonance. Most of our experiments are done at a magnetic field of $B = 755$ G. This value is still within the width of the broad resonance at $B \approx 834$ G. One might ask *how do we create these molecules when we are off-resonance?* To answer this question I would refer again to figure 4.2 and 4.5. The information we get out of both figures, is, that at a field of $B = 755$ G the binding energy E_b is small and the scattering length $a(755)$ is large.

Due to energy and momentum conservation it is not possible for two atoms to collide and 'stick' together. This behavior is also visualized in figure 4.1.

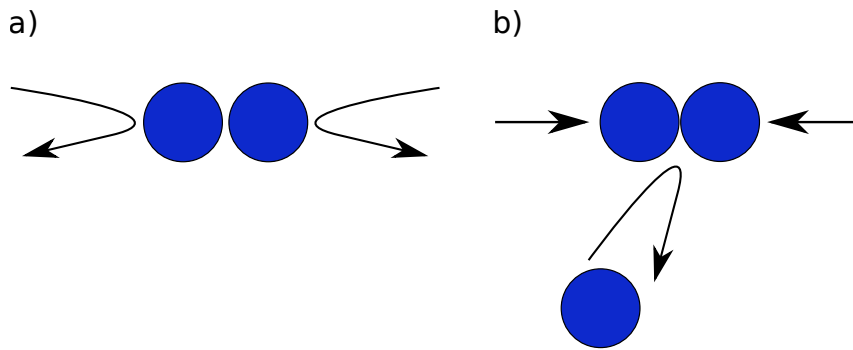


Figure 4.6.: Picture of a two- and three-body collision. a) Two-body collision of two atoms in the $|1\rangle$ and $|2\rangle$ state. Due to conservation of energy the collision energy remains in the system and both atoms carry away the same energy as they had before the collision. b) Three-body collision of two atoms in the $|1\rangle$ state and one atom in the $|2\rangle$ state.

To end up into a molecular bound state we therefore need a third particle which carries the binding energy away while conserving the momentum. A classical picture is imaged in 4.6 b). Here, three atoms, two in the $|1\rangle$ (each labeled with the subscript 1) and one in the $|2\rangle$ state (labeled with the subscript 2) colliding together (3-body collision). The energies before and after the collision are

$$E_1 + E_1 + E_2 \rightarrow E_{FM} + E'_1 \quad (4.24)$$

Due to energy conservation two atoms of two different species are bound as a Feshbach molecule whereas the third atom remains unbound and carries away the kinetic energy. E_{FM} describes the energy of the Feshbach molecule in the state $|12\rangle_{FM}$. In the later chapters of this thesis this state is described as the initial state $|i\rangle$. The reason why we end up with a Feshbach molecule can be described with the help of figure 4.2, b). Our magnetic field $B = 755$ G is near the Feshbach resonance where our binding energy E_b is larger than on resonance. If the thermal energy E_{th} of the atoms is smaller than the binding energy, $k_B T < E_b$, we start to form molecules. From here, we proceed to generate deeply bound molecules for different vibrational quantum levels v .

How do we know that we produced Feshbach molecules in our system? We capture around $2 \cdot 10^7$ ${}^6\text{Li}$ atoms in our MOT. Then, we transfer them into the ODT where we evaporate down to a final trapping power of 150 mW. This number is not arbitrary but can be found experimentally. Therefore, we ramp the trap depth down at $B = 755$ G and take an absorption picture of the remaining atoms in the ODT. The picture can be taken without a magnetic field which we call 'zero field imaging' (ZFI) or with a magnetic field present called 'high field imaging' (HFI). The result of a final trapping power scan (scan of the ODT trap depth) is shown in figure 4.7.

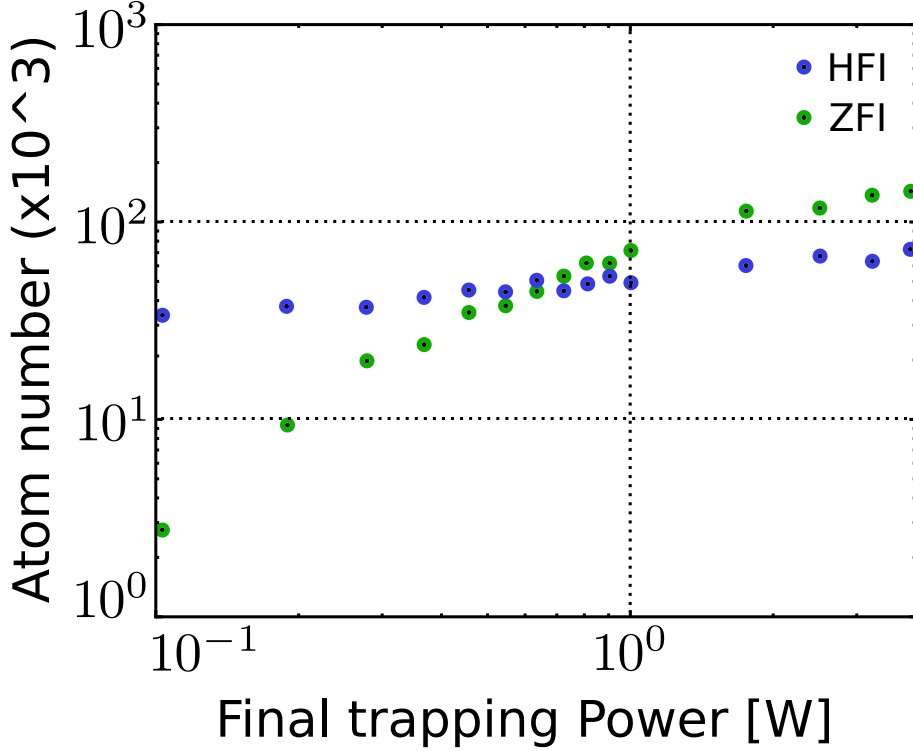


Figure 4.7.: Imaged atoms in the initial state $|i\rangle$ after evaporation. The decreasing slope of the zero field images (ZFI) is an indicator that Feshbach molecules are formed due to three body collisions. For images taken with an magnetic field near the Feshbach resonance $B = 755$ G (HFI) we are able to see atoms. A more detailed discussion can be found in this chapter.

To understand the result in figure 4.7 we should know the difference between HFI and ZFI. Imaging at zero field means imaging without the presence of the magnetic field ($B = 0$ G). In other words, the magnetic field ramps down to zero before taking the absorption image. We image on the MOT pump transition $f = 1/2 \rightarrow {}^2P_{3/2}$. This excitation from the ground to the ${}^2P_{3/2}$ state hits all hyperfine manifolds ($f = 1/2, 3/2, 5/2$) since the natural linewidth of the transition is larger than the hyperfine splitting. Due to the decay back to the ground state a repump beam is necessary. While ramping the magnetic field down, the Feshbach molecules stay at the same energy. The MOT light is not resonant to these molecular transitions. As a result we see the atom number in the ODT dropping for trap depths where $E_{th} < E_b$. For HFI the magnetic field is kept at $B = 755$ G. Here, we are driving hyperfine transitions

from the ${}^2S_{1/2}$ ground state to the ${}^2P_{3/2}$ excited state. The ground state splits into three levels corresponding to $|m_j = -1/2, m_i = 0, \pm 1\rangle$. These states were introduced previously as $|1\rangle$, $|2\rangle$ and $|3\rangle$. We excite these states to the $m'_j = -3/2$ manifold of the excited state. This state splits into three states $|m'_j = -3/2, m_i = 0, \pm 1\rangle$. Even though the separation of the $m'_j = -3/2$ manifold is much smaller than the natural linewidth, the selection rules $\Delta m_j = 0, \pm 1$ and $\Delta m_i = 0$ allows just one specific transition for each state $|1\rangle$, $|2\rangle$ and $|3\rangle$. This also means that the binding energy E_b at a magnetic field near the Feshbach resonance is small. This allows the molecules to absorb the same light as the atoms. When these molecules absorb the imaging light, they get excited and the molecular binding breaks. This enables us to image atoms which were molecules before. The measurement in 4.7 shows the final trapping power when we start to form molecules (where $E_{th} \approx E_b$) which happens around a trapping power of 1 W. Since our molecules have a temperature of 200-300 nK at 150 mW trapping power we can estimate the binding energy to roughly 2.5-3 μK at 1 W trapping power (linear dependence). At a trapping power of 150 mW almost all atoms are paired as Feshbach molecules. The binding energy is plotted in figure 4.2. The next step was to measure the lifetime. Due to collision effects, we can determine the loss in our ODT after evaporation. To measure the lifetime of the molecules after evaporation a holding time was introduced and scanned. The data is shown in figure 4.8.

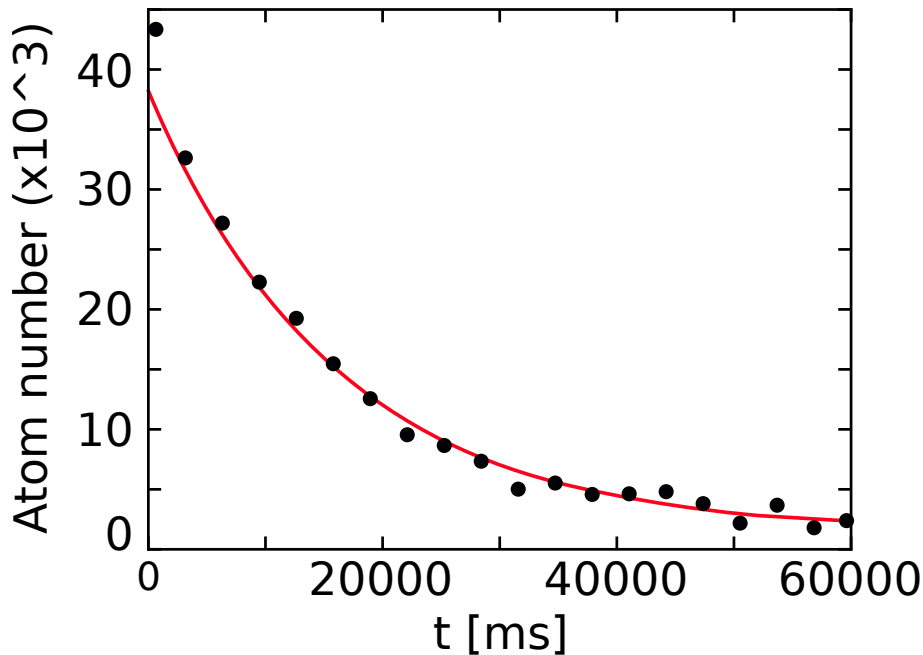


Figure 4.8.: Lifetime of Feshbach molecules in the ODT. With an exponential fit (red line) we can extract the lifetime $\tau = 16045$ ms. The trap power of the ODT was 150 mW which corresponds to a temperature of roughly 200-300 nK.

We used an exponential fit to extract the lifetime of the molecules which are in order of several seconds.

4.5. Quantum Numbers and Selection Rules of the ${}^6\text{Li}_2$ Bound Molecular State

This section gives an introduction to the quantum numbers, properties of the molecule states and the selection rules for the ${}^6\text{Li}_2$ molecule. ${}^6\text{Li}_2$ is a homo nuclear diatomic molecule and has therefore a linear characteristic. Hund's coupling features 5 different cases, labeled from (a) to (e), which are describing different possibilities to couple the spin and orbital momenta of a molecule and characterize it. Compared to atoms, molecules perform rotations and vibrations which has an impact to the molecular energy states and leads also to an additional set of quantum numbers. In this section we will focus on the most relevant Hund's coupling cases (a) and (b). A more detailed discussion can be found in [21, 61].

4.5.1. Hund's Coupling Case (a)

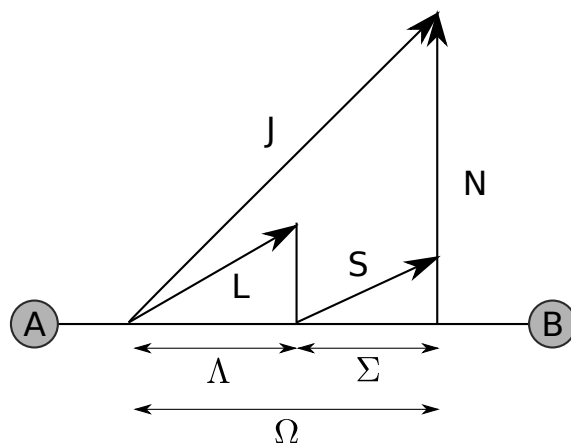


Figure 4.9.: Hund's Coupling Case (a). Taken and adapted from [61]

For small interaction between the rotation of the molecule and the movement of the electrons Hund's coupling case (a) is valid. Here, the total electronic angular momentum $\vec{L} = \vec{l}_1 + \vec{l}_2$ and the total spin $\vec{S} = \vec{s}_1 + \vec{s}_2$ are coupled to the internuclear axis individually and this is stronger compared to the $\vec{L}\vec{S}$ coupling. The \vec{L} and \vec{S} projections on the internuclear axis are labeled by Λ and Σ . Their projections along a quantized axis are denoted by m_L and m_S . The possible quantum numbers are as follow [21]:

$$\Lambda = |m_L|, \quad \Lambda = 0, 1, 2, 3, \dots, L \quad (4.25)$$

$$\Sigma = |m_S|, \quad \Sigma = S, S - 1, S - 2, \dots, -S \quad (4.26)$$

The vector $\vec{\Omega} = \vec{\Lambda} + \vec{\Sigma}$ points along the internuclear axis and represents its projection of the total electronic angular momentum. With this assumption the total angular momentum of the molecule ² can be written as [21]

²excluding the nuclear spin

$$\vec{J} = \vec{N} + \vec{\Omega} \quad (4.27)$$

where \vec{N} is the rotational angular momentum of the nuclei. Note that \vec{N} points perpendicular to the molecular axis. For Hund's coupling case (a) the set of good quantum numbers is therefore $(n, J, S, \Lambda, \Sigma, \Omega)$. The quantum number n represents all electronic and vibrational states [21].

4.5.2. Hund's Coupling Case (b)

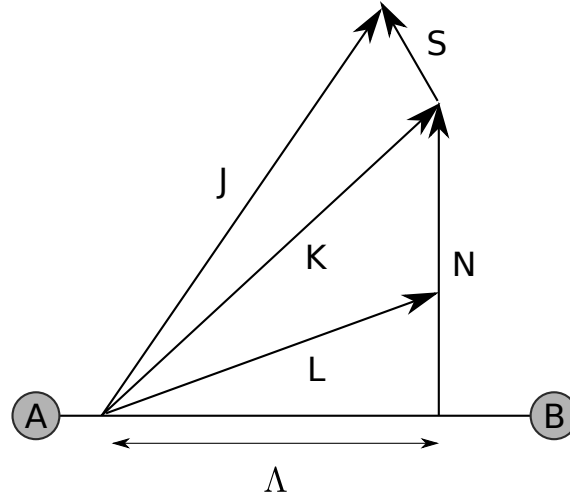


Figure 4.10.: Hund's Coupling Case (b). Taken and adapted from [61]

The main aspect in Hund's Coupling case (b) is that the coupling of the spin \vec{S} to the internuclear axis is not valid anymore. The spin-orbit coupling $\vec{L}\vec{S}$ is therefore weak or even non-existent (for $\Lambda = 0$). In comparison to Hund's Coupling case (a) this means that there is no projection Σ and Ω . These are no longer good quantum numbers. Instead, we find the angular momentum \vec{K} which is a combination of the rotational angular momentum of the nuclei \vec{N} and the projection of \vec{L} on the internuclear axis labeled as Λ , so [21]

$$\vec{K} = \vec{N} + \vec{\Lambda} \quad (4.28)$$

The total angular momentum is

$$\vec{J} = \vec{S} + \vec{K} \quad (4.29)$$

The set of good quantum numbers consists (n, K, J, Λ) . Again, n represents all electronic and vibrational states [21].

4.5.3. State Selection and Preparation for Photoassociation

Similar to atoms the molecular potential curves are labeled as follow

$${}^{2S+1}\Lambda_{\Omega,(g/u)}^{+/-} \quad (4.30)$$

here, \vec{S} is the total electronic spin quantum number. Equivalent to the orbital momentum L for atoms this quantum number for molecules is called Λ . The idea is the same. If $\Lambda = 0$ the state is called Σ (not to be confused with the Σ in Hund's rule discussion). Additional to the atomic potentials, molecular potentials are preceded by a letter. The ground singlet state has a preceded X , where A is the next state where an optical transition is possible from the ground singlet state (followed by B and so on...). Other states which are not accessible from the singlet ground state (like triplet states) are labeled with a lower-case like a, b, c, \dots . The parity of the electronic wave function is represented by the superscript $+/-$ due to reflexions regarding the internuclear axis. The symmetry of the molecular wave function itself is represented by the subscript u/g where u (ungerade) means an odd and g (gerade) an even parity. For a further discussion of the rotational levels of the molecule and its symmetries I refer to [21, 61, 62]. An interesting point is that the two-atom scattering state at 0 G is a superposition of the singlet and triplet state. Therefore it is possible to access both, the singlet and triplet potential in the excited state by the absorption of a photon [21]. The values for the excited molecular states for ${}^6\text{Li}$ are noted in table 4.3.

Potential	$A(1^1\Sigma_u^+)$ [G]	$c(1^3\Sigma_g^+)$	$B(1^1\Pi_u)$	$C(2^1\Sigma_g^+)$	$b(1^3\Pi_u)$
v	29-35	20-26	0-4	0-4	32-38

Table 4.3.: Vibrational states accessible to us given our Ti:Sapphire lasers of the excited molecular ${}^6\text{Li}_2$ potentials. This states are mainly used for our photoassociation and STIRAP experiment described later in this thesis. Numbers from [21]

For the selection rules of an electric dipole transition we can summarize

Quantum Number	Selection Rule
parity	$g \leftrightarrow u$
N	$\Delta N = \pm 1$
S	$\Delta S = 0$
I	$\Delta I = 0$
J	$\Delta J = 0, \pm 1$
F	$\Delta F = 0, \pm 1$
m_F	$\Delta m_F = 0, \pm 1$

Table 4.4.: Selection rules for $\Sigma \rightarrow \Sigma$ transitions for ${}^6\text{Li}_2$. Numbers from [21]

A discussion for molecular selection can be red in [21].

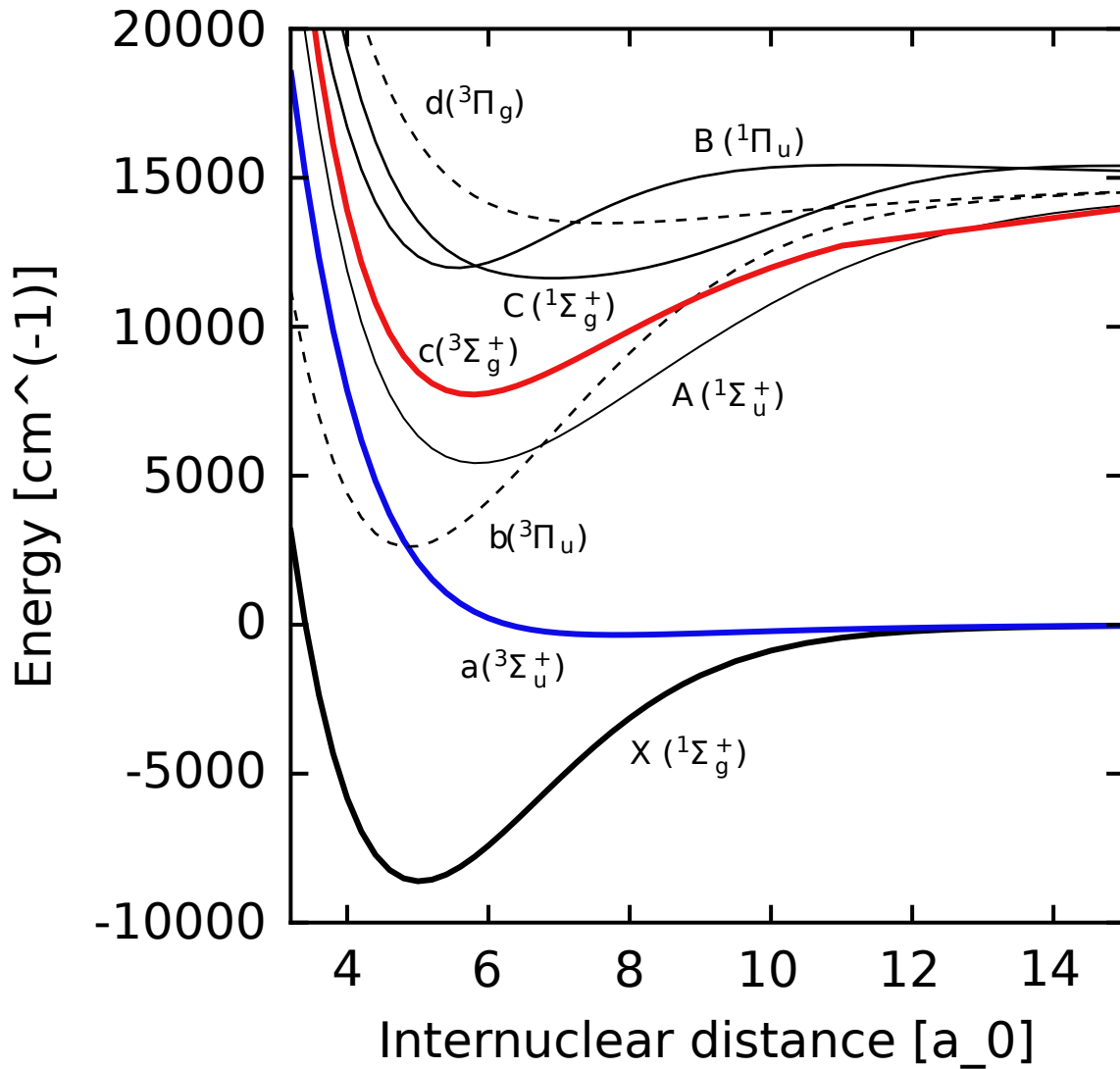


Figure 4.11.: ${}^6\text{Li}_2$ potentials. These potentials are accessible for our photoassociation experiments and STIRAP sequence. The blue (triplet potential) and black (singlet potential) curves are showing the potential of our initial state $|i\rangle$. For the triplet spectroscopy and later for STIRAP we use an excited state $|e\rangle$ in the red potential curve (triplet). Taken and adapted from [21]

5. Photoassociation and Spectroscopy of Ultracold ${}^2\text{Li}_6$ Molecules

The goal of this masters project is to create deeply bound ground state ultracold Feshbach molecules. To achieve this one has to think about which initial quantum states we can populate and to which quantum state we can transfer. In this work, we investigate the transfer of molecules from an initial Feshbach molecular state $|i\rangle$ into the lowest triplet potential, labeled with $|g\rangle$. Molecules exhibit hyperfine structure in the ground state [63] as well as in the excited state [64]. Therefore it is crucial to know about the structures, properties and energies of these quantum states. For the excited state, it would be good to ensure a direct coupling to the lowest hyperfine state $|g\rangle$ without any intermediate steps [65]. The fact that the hyperfine splitting of the excited state can be smaller than the linewidth of the excitation laser leads to another challenge. Here, coupling of several hyperfine levels occurs. This can affect the efficiency which is required for STIRAP due to different coupling abilities of those hyperfine states [23, 66–68]. To enable a coherent coupling for the states $|i\rangle$ and $|g\rangle$ via coupling to the excited state $|e\rangle$ the hyperfine structure must be resolvable and known. A detailed characterization of the used triplet molecular potentials is discussed in [21]. One limitation of the transition $|i\rangle \rightarrow |e\rangle$ is the knowledge of the transition frequency with a precision of the natural linewidth (around 10 MHz). The excitation of molecules into an excited molecular potential via laser light is called photoassociation. Photoassociation experiments where a cold ${}^6\text{Li}_2$ was captured into a MOT were already successfully implemented [69, 70]. However, the temperature of the atomic gas in those experiments was in the order of mK. In this regime limitations caused by the Doppler broadening occurs in order of tens of MHz which is larger than the natural linewidth.

In our experiment, we implemented photoassociation after evaporative cooling of our atom ensemble down to hundreds of nK in an ODT. The Doppler broadening is in a regime of hundreds of kHz which is compared to the natural linewidth smaller by a factor of ~ 100 . The outline of this chapter is to do spectroscopy of the states. The transition frequencies were already roughly known. In the iteration of this chapter we will discuss spectroscopy step-by-step:

1. **Single Color Spectroscopy (SC):** Spectroscopy, to find and characterize the transition from the ground molecular state $|g\rangle$ to the excited molecular state $|e\rangle$. For our study of we focus on the excited molecular state with rotational state $N' = 1$ and the vibrational state $v' = 20$ of the $c(1^1\Sigma_g^+)$ triplet potential.
2. **Two Color Spectroscopy (TC):** Spectroscopy, to find a lower or the lowest molecular state. We call this the $|e\rangle \rightarrow |g\rangle$ transition. Here, the ground state

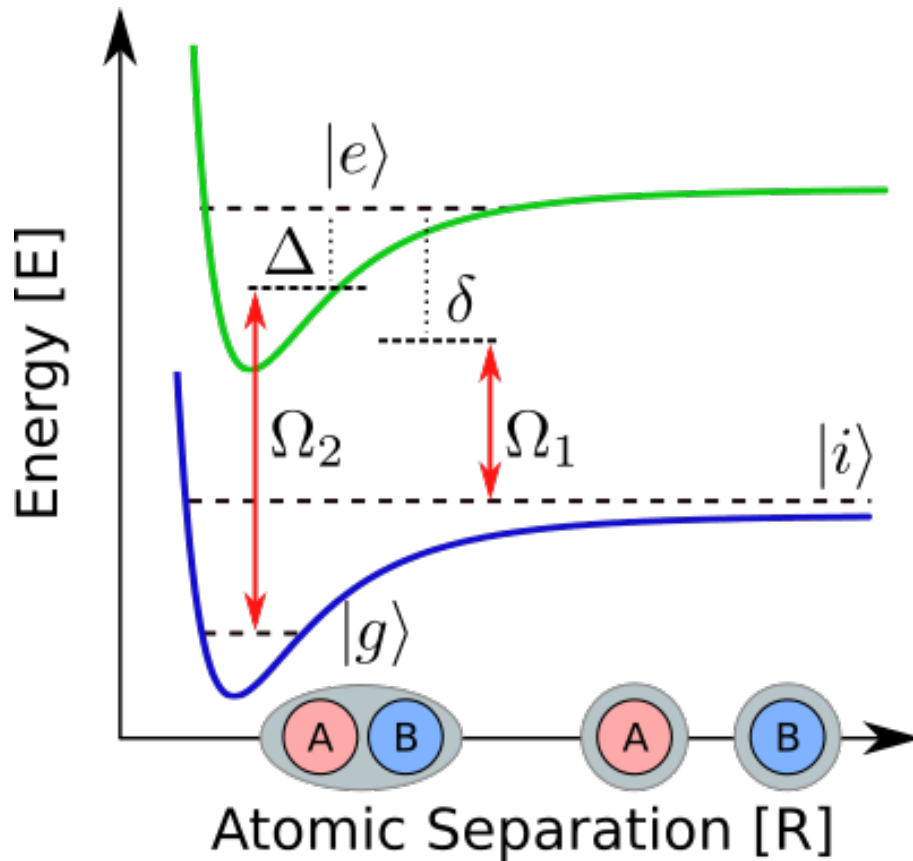


Figure 5.1.: Three level system with molecular potentials. The long lived initial state $|i\rangle$ contains both, free colliding atoms or Feshbach molecule pair. $|e\rangle$ represents the intermediate or excited molecular state, $|g\rangle$ the ground molecular state. The pump field ω_1 couples the states $|i\rangle$ and $|e\rangle$ with a strength Ω_1 and a single photon detuning δ . The Stokes field ω_2 couples the states $|e\rangle$ and $|g\rangle$ with the strength Ω_2 and a two photon detuning $\Delta - \delta$.

$|g\rangle$ is in the lowest triplet potential $a(1^3\Sigma_u^+)$. The rotational state can be $N'' = 0, 2$. We chose the $N = 0$ state to operate.

3. **Autler-Townes Splitting (AT):** Due to the energy splitting of the excited molecular state $|e\rangle$ we can extract the Rabi frequency of the $|e\rangle \rightarrow |g\rangle$ transition. This is done with the excited triplet potential $c(1^1\Sigma_g^+)$ and $v' = 20$ (corresponding to $|e\rangle$) and the lowest triplet potential $a(1^3\Sigma_u^+)$ (corresponding to $|g\rangle$).
4. **Dark State Spectroscopy (DS):** The dark state revival peak gives us insight of the population transfer for the states $|i\rangle \rightarrow |g\rangle$. The position of the revival peak is a good starting point to introduce STIRAP. Moreover, the height of the revival peak is linked to the Rabi frequency of the states. The excited state potential is again the $c(1^1\Sigma_g^+)$ triplet potential and $v' = 20$ and the lowest triplet potential is $a(1^3\Sigma_u^+)$. A dark state spectroscopy is just possible when the two photon detuning is zero and the excitation light is coherent.

For the state selection it is essential that a good Franck-Condon overlap of the states is given. This principle describes the theory of the transition between vibrational states (also called vibronic transitions). If two wave functions of two different vibrational states overlap significantly the transition is more likely. Therefore, we chose the $v' = 20$ state since this state showed the largest Franck-Condon overlap. Xuan Li calculated the values and as far as we know never published. However, we measured the Rabi-frequency of the $v' = 21$ state and confirmed a lower coupling strength compared to the $v' = 20$ state. For a more detailed discussion about the Franck-Condon factor, the reader is referred to [71].

Our experimental setup contains two Ti:Sapphire lasers, a probe and a Stokes laser (labeled TS1 and TS2) with Ω_1, ω_1 and Ω_2, ω_2 . The transitions are shown in figure 5.1 and an overview of the setup can be extracted from the previous chapter. In general, this two lasers couple to an excited molecular state $|e\rangle$. For a good review about a general concept of photoassociation, the reader is referred to [72]. Depending on the magnetic field strength out initial state $|i\rangle$ is either a two atom scattering state ($B = 0$ G) or a Feshbach molecular state ($B \sim 834$ G). Our evaporative cooling is done at $B = 755$ G which is still within the range of the broad Feshbach resonance around ~ 834 G. With this settings, we want to produce ultracold ${}^6\text{Li}_2$ triplet dimers by STIRAP. The vibrational states we characterized in the lowest triplet potential $a(1^3\Sigma_u^+)$ are in the range of $v'' = 0$ to 9.

5.1. Single Color Spectroscopy

Finding the excited molecular state $|e\rangle$ of the $c(1^1\Sigma_g^+)$ potential with $v' = 20$ is the first step towards a controlled population transfer into a ground molecular quantum state. Therefore, we perform a single color scan for identification and localization of the excited state. In a single color experiment, we simply detune the probe laser TS1 and scan over a region where the resonance is expected. Since the calculated resonance frequency is not accurate, a wide range scan is necessary. The result can be seen in figure 5.2. Populating the excited molecular state $|e\rangle$ will cause loss due to spontaneous emission. Since our imaging technique only allows us to image the initial state $|i\rangle$ we see atom loss in the form of a dip near a resonance. Due to interferences while imaging, an unstable dipole trap, air fluctuations and also misalignments and temperature fluctuations the detected atom number is not stable. The step size of 25 MHz was chosen arbitrarily. Compared to the natural linewidth of tens of MHz we assume to be in the frame of hitting most resonances which are widened by power broadening.

For ${}^6\text{Li}_2$ we expect to see 27 states and therefore 27 absorption peaks. Though having a closer look to figure 5.2 we see six absorption dips. There are multiple reasons why we do not see 27 dips. One of them can be power broadening (40 mW) or high exposure time (10 μs) of the excitation laser. Both effects lead to a much more broaden resonance feature and therefore making other transitions closed by unresolvable. The second reason can be the step size of 25 MHz for scanning the pump frequency. Consequently, we might have missed some of the narrower states with a width of \approx 25 MHz. A third reason might be that selection rules prevents driving several transitions. By probing this transition we 'jump' between Σ states, where the selection rule for the rotational quantum number shows $\Delta N = \pm 1$. The initial molecular quantum state has $N = 0$ which means that the rotational level of the excited molecular potential must have $N' = 1$.

Since our measurement shows multiple resonances to chose we should ask the question, *which state is the best?* Using an excited molecular state that is close to another state could be a problem for STIRAP because of associated de-coherence mechanisms. We should therefore aim to find a state that is far away from other states unless we can rotate the polarization to 'switch off' the undesired states close by. In fact, the narrow adsorption dips in figure 5.2 occurs when the polarization of the probe beam was set to 45 degrees. With this polarization our light contains of σ^+ , σ^- and π light. So any transitions which don't infringe the selection rules can be driven. When the same scan was done with pure π light, the narrow absorption features vanished. Another point we have to consider for STIRAP is that the states have to be coupled strongly. Therefore, we concentrate on the broadest feature which is the first manifold in figure 5.2. For a better resolution of the broader feature, we dropped the pump laser power to 150 μW , and the step size was chosen to be 3 MHz. With this settings, we could resolve three different states which were covered by the power broadening effect within the broad manifold, see figure 5.3. This states corresponds to $J' = 0, 1, 2$. Since the left manifold ($J = 1$) is \sim 125 MHz apart from the other two feature, this transition could be a good candidate. To prove that this is a single state an even narrower scan with a lower probe power and exposure time was done. This figure is not shown in this thesis. However, it proved

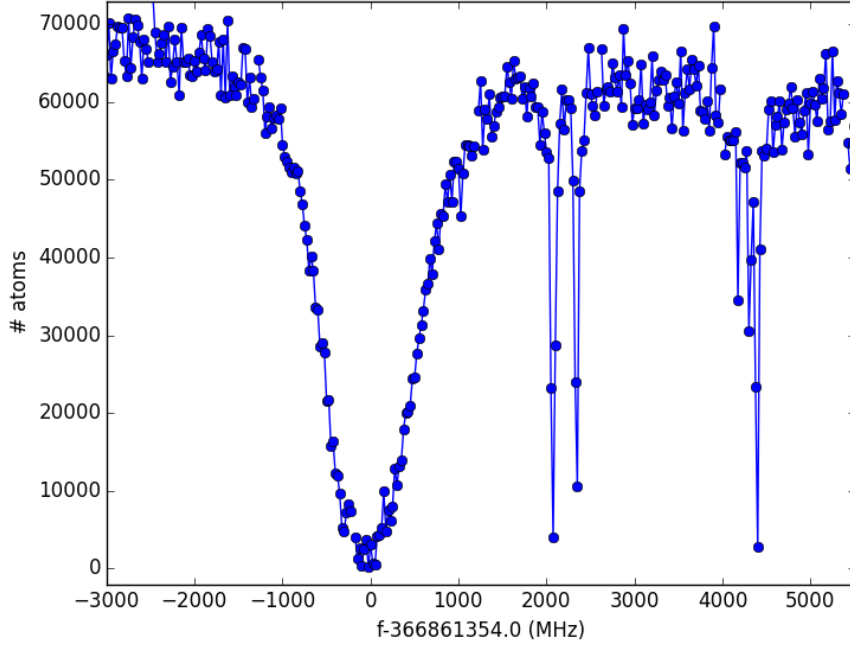


Figure 5.2.: Single-color scan to the $v' = 20$ state of the $c(1^1\Sigma_g^+)$ triplet molecular potential. The result shows the number of the remaining Feshbach molecules in the initial state $|i\rangle$ for different TS1 frequencies. When the frequency of the pump beam ω_1 hits the single-color transition frequency $|i\rangle \rightarrow |e\rangle$ we observe loss in the number of our atoms in the initial state $|i\rangle$. The polarization of the probe beam was set to 45 degrees with respect to the magnetic field direction to simultaneously get σ^+ , σ^- and π light. The probe power was set to 40 mW with an exposure time of 10 μs . The final trapping power of the ODT was 150 mW and the scan had a step size of 25 MHz. The magnetic field was set to $B = 755$ G.

that there is just one absorption dip at the resonance frequency for the $|i\rangle \rightarrow |e\rangle$ transition at roughly 366761.354 GHz.

To measure the natural linewidth of this feature we set our probe laser (TS1) to an intensity where we achieve half loss in atom number on resonance. This intensity setting is just a 'rule of thumb' and has historical roots which are connected to the limits of the old image processor regarding signal to noise ratio and fit accuracy. We found a pump power of $P_p = 105 \mu\text{W}$. With this settings, we can distinguish a natural linewidth of ~ 7 MHz (FWHM of the Gaussian fit) shown in figure 5.4. The next step was to measure the lifetime of our molecules in the excited molecular potential. Therefore, we set the pump laser fix on resonance and excited the molecules from the initial molecular state $|i\rangle$ to $|e\rangle$. There, we switch off the pump light adding a waiting time before measuring the atom number. It is important to mention that the exposure time is chosen relatively high (1000 μs) to decrease the power even more. This ensures again a sequence which is not perturbed by Doppler

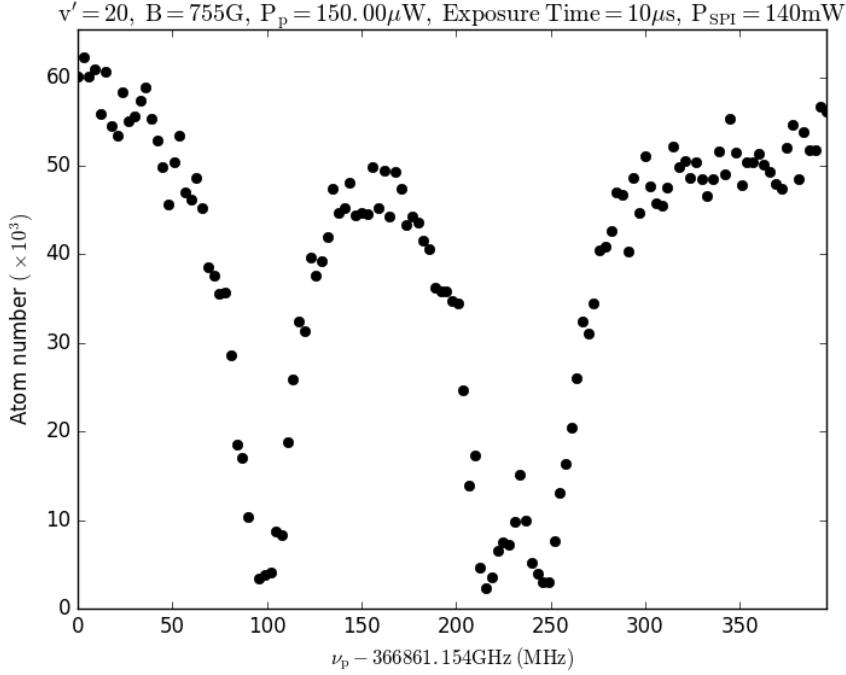


Figure 5.3.: Narrow single-color scan of the broad feature at 366861354 MHz seen in figure 5.2 with reduced power. The excited state $|e\rangle$ is the $v' = 20$ state. While detuning the pump frequency ω_1 three transitions were resolved. Since the electronic spin projection for these states is the same as the initial state ($S = 1$ and $M_S = -1$), and since the nuclear spin projection does not change, the dips correspond to different M_N projections of the rotational quantum number ($N = 1$) of the molecule.

broadening. The remaining atom number in the initial state $|i\rangle$ shows an exponential decay. Via an exponential fit, we extracted a molecular excited state lifetime of $\tau = 1272.93 \mu\text{s}$. The result of this measurement is shown in figure 5.5.

Concerning the coupling strength, we can calculate the Rabi-frequency for the $|i\rangle \rightarrow |e\rangle$ transition. We can model the absorption lines with following equation [73–75].

$$N = N_0 \exp\left(-t_{irr}\Omega_1^2 \frac{\gamma}{\gamma^2 + 4\Delta_p^2}\right) \quad (5.1)$$

In this equation the initial number of Feshbach molecules is given by N_0 , the linewidth of the excited state γ , the irradiation/ holding time t_{irr} , the detuning of the pump light Δ_p and the Rabi-frequency Ω_1 . In general the lifetime of the excited state is given by $\tau_{ex} = 1/\gamma$. In our lifetime experiment we kept the laser frequency on resonance which means that $\Delta_p = 0$. With this assumption equation 5.1 simplifies to the exponential decay

$$N = N_0 \exp\left(-t_{irr} \frac{\Omega_1^2}{\gamma}\right) \quad (5.2)$$

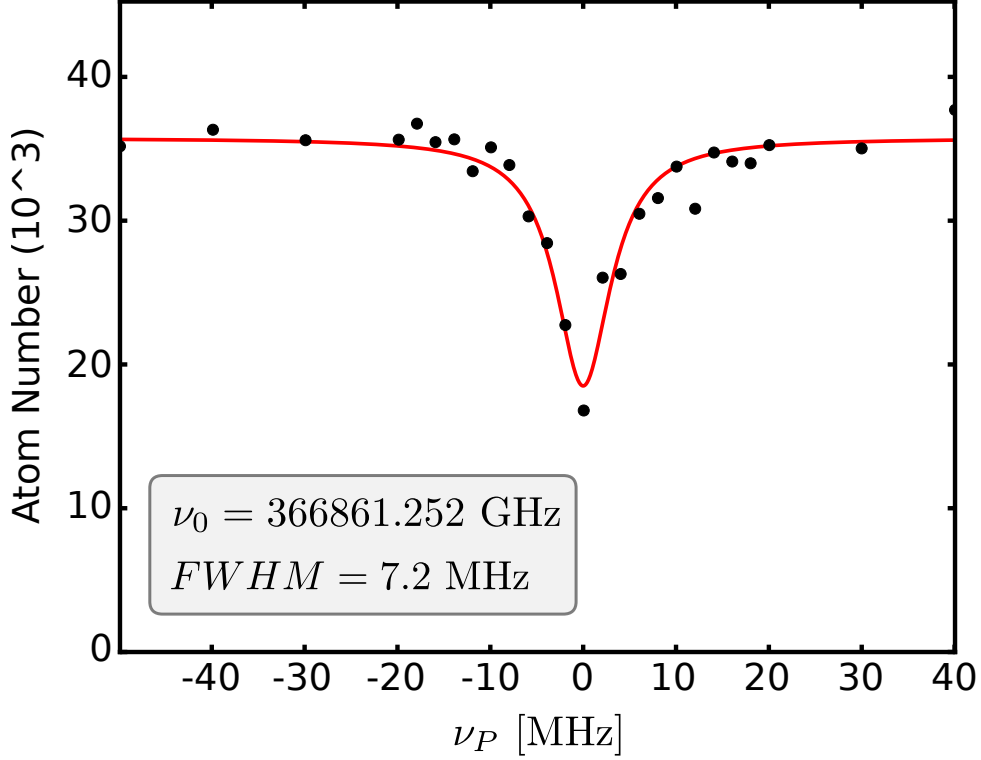


Figure 5.4.: Result of the single-color scan to the $v' = 20$ state of the 'c' potential. This corresponds to the left most dip in figure 5.3. The resonance of the $|i\rangle \rightarrow |e\rangle$ transition was hit by scanning the pump frequency ω_1 at $\nu_P^0 = 366861.252$ GHz. With this settings we achieved around half loss of the atoms by exciting them to $|e\rangle$ on resonance. The natural line width is 7.2 MHz. The probe power was set to $P_p = 80 \mu\text{W}$ and an exposure time was 1000 μs at $B = 755$ G. The final ODT power was 150 mW.

Comparing equation 5.2 with the exponential decay of a state we can state out that $\tau = \gamma/\Omega_1^2$. This expression is valid as long as $\tau \gg \tau_{ex}$ [74]. Furthermore, by comparing we can find

$$\exp\left(-\frac{t}{\tau}\right) = \exp\left(-\frac{\Omega_1^2}{\gamma} t\right) \quad (5.3)$$

$$\Omega_1 = \sqrt{\frac{\gamma}{\tau}} = \sqrt{\frac{2\pi FWHM_{SC}}{\tau}} \quad (5.4)$$

where $\gamma = 2\pi FWHM_{SC}$ and $FWHM_{SC}$ is the FWHM of the single color dip shown in figure 5.4. With equation 5.3 we can obtain a Rabi-frequency of $\Omega_1 \approx 28$ kHz for a probe power of $P_p = 80 \mu\text{W}$ and an exposure time of 1000 μs at $B = 755$ G.

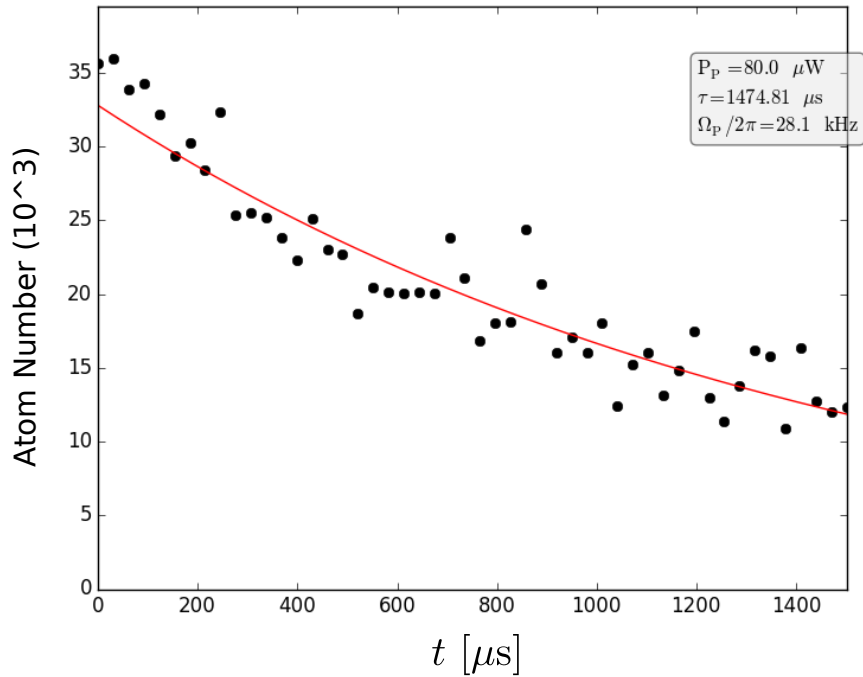


Figure 5.5.: Number of Feshbach molecules remaining after exposing them to light from TS1 at the resonance frequency from the initial state to the $v = 20$ state of the 'c' potential (the resonance corresponds to the dip in figure 5.4. This lifetime provides the Rabi frequency for the transition. The exponential fit gives an approximate value of the lifetime $\tau = 1474.81 \mu\text{s}$ of the initial state $|i\rangle$. The probe power was set to $P_p = 80 \mu\text{W}$, the final ODT power was 150 mW.

5.2. Two Color Spectroscopy

The goal of the two color spectroscopy is to find a molecular ground state $|g\rangle$. This state is either in the lowest lying triplet $a(1^3\Sigma_u^+)$ molecular potential. To characterize the transition of this state a second laser called Stokes laser (TS2) is introduced. For this experiment the frequency of the pump laser is held fix on the single color transition frequency $|i\rangle \rightarrow |e\rangle$. The Stokes laser is detuned and scans over the expected transition frequency $|e\rangle \rightarrow |g\rangle$. The selected power of the Stokes light P_s is much higher compared to the pump light. Furthermore, the Stokes laser the power of the Stokes laser is selected much higher than the pump laser. Therefore, the coupling of the $|e\rangle \rightarrow |g\rangle$ states is much higher than the coupling of the $|i\rangle \rightarrow |e\rangle$ states. Which means that $\Omega_2 \gg \gamma_e \gg \Omega_1$. The strong interaction of two states leads to an energy splitting (dressed state). The resonant coupling and prevention of absorption of an excited state are well known under the name electromagnetically induced transparency (in short EIT) [73]. Studies in this field made pioneering studies like light speed reduction to 17 m per second (slow light) [76]. A theoretical discussion of this effect can be found in [73] based on a three-level system. This theoretical work can also be used for the two-photon spectroscopy we are introducing in this chapter. The Hamiltonian in the rotating frame picture can be described as follows.

$$H = \frac{\hbar}{2} \begin{bmatrix} 0 & \Omega_2 \\ \Omega_2 & 2\delta \end{bmatrix} \quad (5.5)$$

where Ω_2 is the Rabi-frequency for the $|e\rangle \rightarrow |g\rangle$ transition and δ is the detuning of the Stokes light. The eigenstates of this Hamiltonian are

$$|+\rangle = \sin \psi |g\rangle + \cos \psi |e\rangle \quad (5.6)$$

$$|-\rangle = \cos \psi |g\rangle - \sin \psi |e\rangle \quad (5.7)$$

with eigenenergies

$$E_{\pm} = \frac{\delta \pm \sqrt{\delta^2 + \Omega_2^2}}{2} \quad (5.8)$$

If the Stokes field hits the transition frequency $\delta = 0$, an energy split of $E_{\pm} = \pm\Omega_2/2$ for the excited molecular state occurs (dressed state). We are using this splitting to find the ground molecular state. The idea is to excite molecules from the initial molecular state $|i\rangle$ to the excited molecular state $|e\rangle$. As described in the section before this leads to loss. Applying the Stokes laser splits excited molecular state $|e\rangle$ when it hits the resonance frequency for the transition. In this case, the frequency of the probe laser is no longer on resonance with respect to the $|i\rangle \rightarrow |e\rangle$ transition. The loss of the molecules is suppressed and we detect atoms in the initial molecular state $|i\rangle$. The rotational quantum number for the excited state is $N' = 1$. For the lowest lying triplet $a(1^3\Sigma_u^+)$ molecular potential, just the states with a rotational quantum number of $N'' = 0, 2$ are accessible. The results for the $v'' = 6$ state is shown in figure 5.6. The two color resonance frequency for the $v' = 20 \rightarrow v'' = 6$ transition is 367898.764 GHz. This resonance frequency can

be used to find the STIRAP revival. However, a much better resolved two-photon resonance peak can be measured with a dark state measurement ¹.

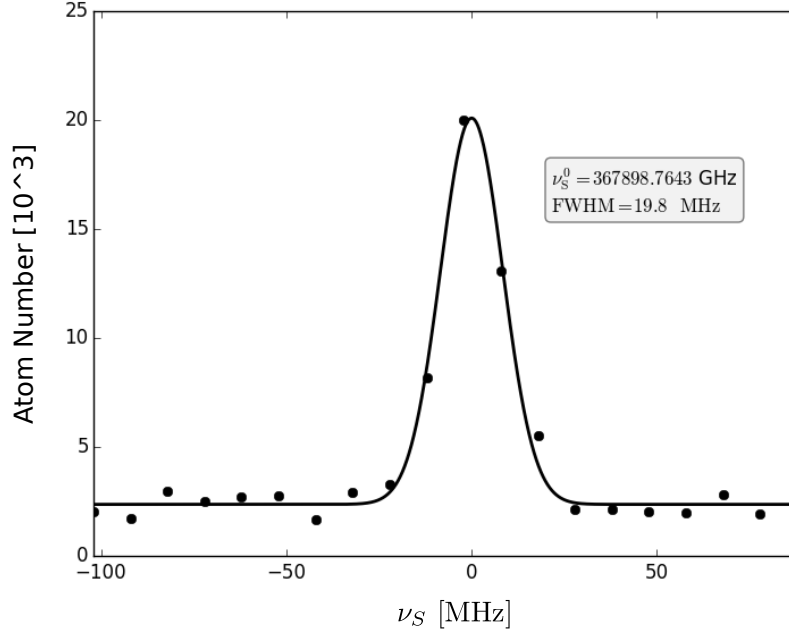


Figure 5.6.: Number of Feshbach molecules after exposing them to two laser fields: the frequency of the pump laser ω_1 is held fixed at the resonance between the Feshbach molecules and the $v' = 20$ state while the Stokes frequency ω_2 is scanned over the $|g\rangle \rightarrow |e\rangle$ transition. Here $|g\rangle$ is the $v'' = 6$ state of the 'a' potential. When ω_2 is on resonance, the loss of Feshbach molecules induced by the pump field is suppressed and the number of Feshbach molecules remaining is large. The two color resonance frequency is $\nu_S^0 = 367898.764$ GHz with a FWHM of 19.8 MHz.

¹Please note, that two color spectroscopy was not done for every state. The dark state measurements shows a much more accurate result in terms of two photon resonance. Therefore, this section contains a measurement for the $v'' = 6$ state

5.3. Autler-Townes Splitting

The Autler-Townes splitting is a simple method to measure the coupling strength of the Stokes field Ω_2 . Characteristic is the double peak structure which was first observed by Autler and Townes [77]. This splitting is also an indicator for the two-photon coherence. The measurement can be done by setting the Stokes laser to a fix resonance of the $|g\rangle \rightarrow |e\rangle$ transition. The probe laser is detuned and scans over the $|i\rangle \rightarrow |e\rangle$ transition. Hitting the resonance transition with the probe laser the excited state splits up (as described in the previous chapter). Therefore, the Hamiltonian of this system is comparable to equation 5.5. The splitting of the states is $\Delta E = \hbar\Omega_2$. This splitting is show in figure 5.7 for the $v'' = 0$ state of the $a(1^3\Sigma_u^+)$ molecular potential. For evaluation the following fit function is used [73, 75].

$$N = N_0 \exp\left(-t_{irr}\Omega_1^2 \frac{4\gamma\delta^2 + \Gamma_{eff}(\Omega_2^2 + \Gamma_{eff}\gamma)}{|\Omega_2^2 + (\gamma + 2i\Delta_P)(\Gamma_{eff} + 2i\delta)|^2}\right) \quad (5.9)$$

In this equation t_{irr} represents the irradiation time. A decay term due to decoherences between the transfer from $|i\rangle \rightarrow |g\rangle$ labeled as Γ_{eff} was added phenomenologically. With this equation all three level couplings can be described and shows also the line shapes. This fit method gives us also a value for the Rabi-frequency Ω_2 which can be directly seen by the splitting of the two states. For the $v'' = 0$ sate in the $a(1^3\Sigma_u^+)$ potential we find a $\Omega_2(v'' = 0) = 14.11$ MHz.

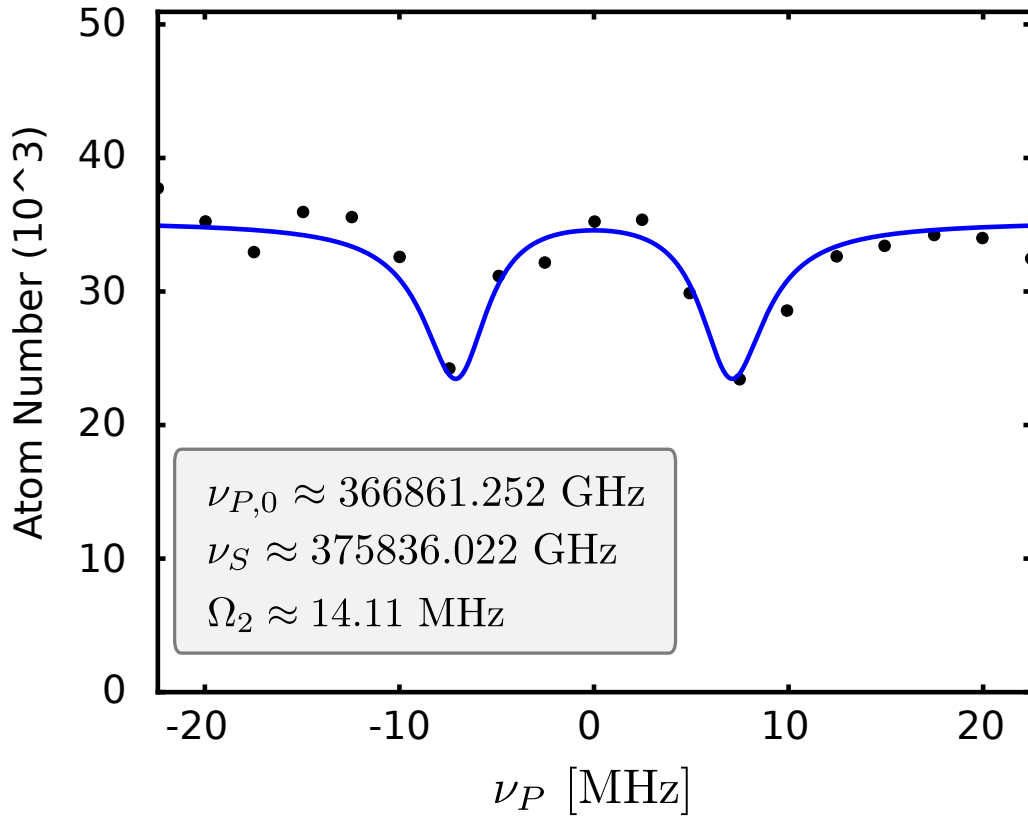


Figure 5.7.: The number of Feshbach molecules observed after exposing them to two laser fields: the frequency of the Stokes laser ω_2 is fixed to the $|g\rangle \rightarrow |e\rangle$ transition (here $|g\rangle$ is the $v'' = 0$ state in the $a(1^3\Sigma_u^+)$ potential and $|e\rangle$ is the $v' = 20$ state in the $c(1^1\Sigma_g^+)$ potential) while the pump laser ω_1 was scanned over the single color resonance $|i\rangle \rightarrow |e\rangle$. Two loss dips are observed instead of a single loss dip because the excited state is split by the Stokes field. This Autler-Townes splitting between the two dips indicates the coupling strength of the Stokes laser, and we extract the Rabi frequency for the Stokes field Ω_2 from the Autler-Townes splitting. The power setting was $P_p = 300 \mu\text{W}$, $P_s = 10 \text{ mW}$ with an exposure time of $40 \mu\text{s}$ and a final ODT trapping power of 150 mW at $B = 755 \text{ G}$.

5.4. Dark State Spectroscopy

STIRAP is a method to transfer the population between different quantum states. These states may have the same parity and are therefore dipole forbidden transitions. Many groups successfully implemented this technique for homonuclear molecules like [18, 19, 78]. In our case we produced ${}^6\text{Li}_2$ molecules in the triplet potential $a(1^3\Sigma_u^+)$ due to population transfer to the lowest triplet state $|g\rangle$. In the previous chapters, we successfully achieved two-color spectroscopy which is the base for dark state spectroscopy. With this spectroscopy, we can extract a sharp two-photon resonance peak. Another advantage is that the resonance relies only on the energy difference between the two lasers, TS1 and TS2. Therefore, it is relatively insensitive to single photon detunings. The uncertainty of the frequency between the two locked TS is in order of several kHz [21]. For the dark state, we are using a square pulse sequence. For the population transfer we can assume that our wave function is a superposition of both coherent states, $|i\rangle$ and $|g\rangle$, multiplied by an amplitude c_x where x describes the different states [21].

$$|\psi\rangle = c_i|i\rangle + c_g|g\rangle \quad (5.10)$$

The transfer to the excited state $|e\rangle$ should be avoided. The excited state shows loss mechanism. In terms of keeping the population this state should not be populated. However, the probability of populating the excited state $|e\rangle$ is as followed [79]:

$$A = \langle e|\vec{d} \cdot \vec{\epsilon}|\psi\rangle = c_i\langle e|d|i\rangle\epsilon_i + c_g\langle e|d|g\rangle\epsilon_g \quad (5.11)$$

$$= c_i\Omega_1 + c_g\Omega_2 \quad (5.12)$$

In equation 5.12 we see the coupling of the states $|i\rangle$ and $|e\rangle$ due to the Rabi frequency of the probe field Ω_1 as well as the coupling of the $|e\rangle$ and $|g\rangle$ states induced by the Rabi frequency of the Stokes field Ω_2 . At a specific point in time, we can set the amplitudes $A = 0$ which results in a 'dark' state [79].

$$c_g = -\frac{\Omega_1}{\Omega_2}c_i \quad (5.13)$$

For the time evolution of this state we must think that the amplitudes, as well as the Rabi frequencies, can evolve in time.

$$A(t) = c_i e^{\frac{-iE_i t}{\hbar}} \Omega_1 e^{-i\omega_1 t} + c_g e^{\frac{-iE_g t}{\hbar}} \Omega_2 e^{-i\omega_2 t} \quad (5.14)$$

It is important to mention that E_i and E_g describing the energies of the state $|i\rangle$ and $|g\rangle$ and $\omega_{P/S}$ are the optical frequencies of the pump and Stokes field. Again, in order to consider the states as 'dark' we set $A(t) = 0$ [79].

$$c_g = -c_i \cdot \frac{e^{\frac{-iE_i t}{\hbar}} \Omega_1 e^{-i\omega_1 t}}{e^{\frac{-iE_g t}{\hbar}} \Omega_2 e^{-i\omega_2 t}} \quad (5.15)$$

It is easy to see that to consider the states as 'dark', the exponents must be the same at all times [79].

$$\frac{-iE_it}{\hbar} - i\omega_1 t = \frac{-iE_g t}{\hbar} - i\omega_2 t \quad (5.16)$$

$$\omega_g - \omega_i = \frac{E_i - E_g}{\hbar} \quad (5.17)$$

which is the two-photon resonance [79].

The interaction of the atomic system with the external laser field is described by the Hamiltonian matrix $H(t)$. The rotating-wave approximation (RWA) allows us to neglect fast oscillations. The Hamiltonian matrix $H(t)$ in the RWA can therefore be written as [79]:

$$H = \frac{\hbar}{2} \begin{bmatrix} 0 & \Omega_1(t) & 0 \\ \Omega_1(t) & 2\Delta & \Omega_2(t) \\ 0 & \Omega_2(t) & 2\delta \end{bmatrix} \quad (5.18)$$

with the Rabi frequency $\Omega_{P/S}(t) = \frac{-d_{i,j}\varepsilon_{P/S}(t)}{\hbar}$ and $\delta = \Delta_P - \Delta_S$. Note, that the phenomenological decay rates are neglected. The Hamiltonian is written in the dressed picture of the atom. The condition of the population transfer is that the single photon detuning and two photon detuning are zero, $\Delta = \delta = 0$. Therefore, we can calculate three eigenstates [79]

$$|i^+\rangle = \frac{1}{\sqrt{2}}(\sin\Theta|i\rangle + |e\rangle + \cos\Theta|g\rangle) \quad (5.19)$$

$$|i^0\rangle = \cos\Theta|i\rangle + \sin\Theta|g\rangle \quad (5.20)$$

$$|i^-\rangle = \frac{1}{\sqrt{2}}(\sin\Theta|i\rangle - |e\rangle + \cos\Theta|g\rangle) \quad (5.21)$$

In this section we focus on the dark state which is given by $|i^0\rangle = \cos\Theta|i\rangle + \sin\Theta|g\rangle$. As a side note, the two remaining states are the so-called 'bright states'. The eigenenergy for the dark state is $E^0 = 0$. If we take a closer look at equation 5.21 we see that it is independent of the excited state. The interpretation of this eigenstate gives us a direct connection from the initial atomic or Feshbach state $|i\rangle$ to the molecular ground state $|g\rangle$. Furthermore, we define the mixing angle Θ [79].

$$\tan\Theta = \frac{\sin\Theta}{\cos\Theta} = \frac{\Omega_1}{\Omega_2} \quad (5.22)$$

With this expression, we can rewrite and normalize equation 5.21.

$$|Dark\rangle = |i^0\rangle = \frac{\Omega_2|i\rangle - \Omega_1|g\rangle}{\sqrt{\Omega_1^2 + \Omega_2^2}} \quad (5.23)$$

The bright state is a superposition of the eigenstates $|i^+\rangle$ and $|i^-\rangle$. We can write the bright state as follows [21]:

$$|Bright\rangle = \frac{1}{2}(|i^+\rangle + |i^-\rangle) = \frac{\Omega_1|i\rangle + \Omega_2|g\rangle}{\sqrt{\Omega_1^2 + \Omega_2^2}} \quad (5.24)$$

For the experimental realization the probe and Stokes lasers are turned on at the same time. The pulses are rectangular, where the Stokes field is turned off slightly before (μs) the probe field. The result is that the initial state $|i\rangle$ is projected on the bright and dark state. If the field is turned off, the population is projected back to the initial state $|i\rangle$. With the expectation value we can calculate the height of the revival peak.

$$|\langle i|Dark\rangle|^2 \times |\langle Dark|i\rangle|^2 = \frac{\Omega_2^4}{(\Omega_1^2 + \Omega_2^2)^2} \quad (5.25)$$

From this equation we can see that the coupling strength Ω_2 plays a major role. For a narrow dark state feature we have to satisfy the requirement $\Omega_2 \gg \gamma_e$. This also prevents us from acting in the Autler-Townes regime where a doublet due to the excited state splitting would appear. Furthermore, to suppress loss $\Omega_2 \gg \Omega_1$. A dark state measurement for the $v'' = 0$ is shown in figure 5.8

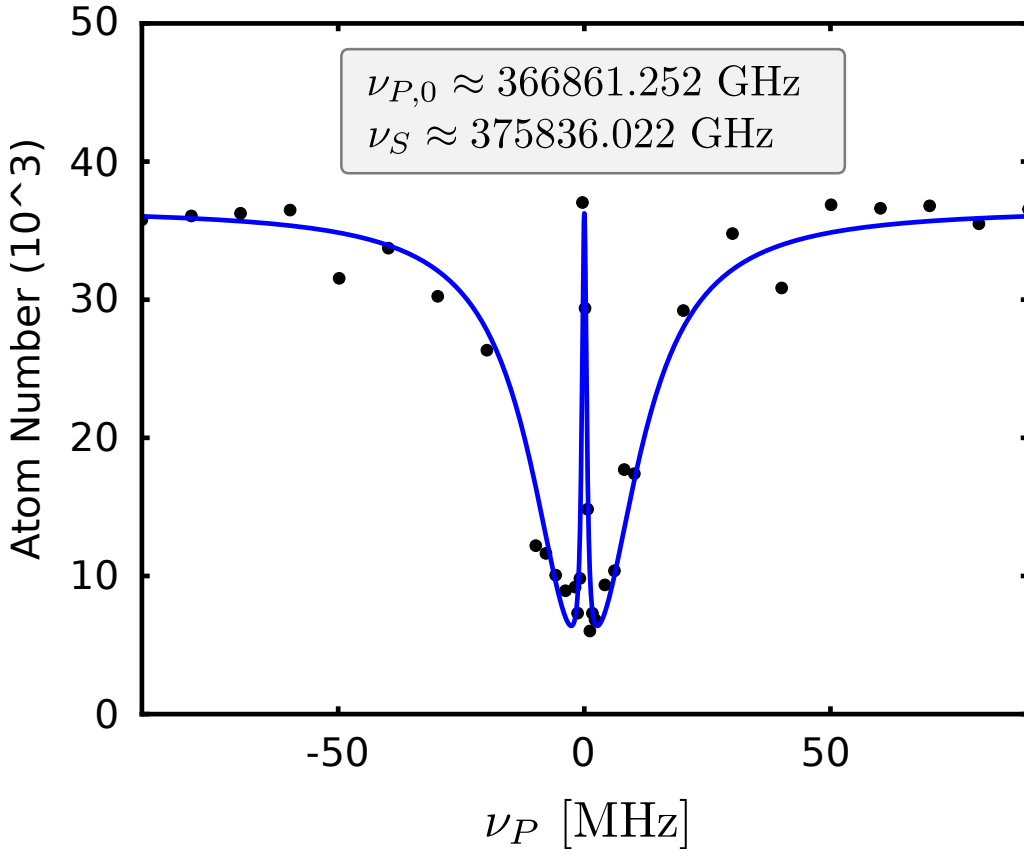


Figure 5.8.: The number of Feshbach molecules observed after exposing them to two laser fields: the frequency of the Stokes laser ω_2 is fixed to the $|g\rangle \rightarrow |e\rangle$ transition (here $|g\rangle$ is the $v'' = 0$ state in the $a(1^3\Sigma_u^+)$ potential and $|e\rangle$ is the $v' = 20$ state in the $c(1^1\Sigma_g^+)$ potential) while the pump laser ω_1 was scanned over the single color resonance $|i\rangle \rightarrow |e\rangle$. The probe power is set to $P_p = 100$ mW and the Stokes power is $P_s = 10$ mW. The data was taken at $B = 755$ G and a final ODT trapping power of 150 mW.

6. STIRAP of Ultracold Feshbach Molecules

The final step in this thesis is to produce ultracold Feshbach molecules in the lowest triplet potential. Due to spectroscopy, we characterize the vibronic states. Now, the next challenge for is to control the population transfer of quantum states. Or in other words, we want to populate the ground state of the lowest triplet potential. The so-called Stimulated Raman Adiabatic Raman Passage (STIRAP) allows an efficient and selective population transfer between quantum states without loss due to spontaneous emission. The idea is to couple two discrete quantum states ($|i\rangle$ and $|g\rangle$) via an intermediate/excited state $|e\rangle$, which is usually a radiatively decaying state. Note, that the direct population transfer is forbidden due to selection rules (see the previous chapter). However, using the excited state for coupling, it won't get populated in the STIRAP sequence. Therefore, spontaneous emission from the excited state is suppressed and, ideally, no loss in the population should be seen. Due to this reason the lifetime of the excited state $|e\rangle$ can be short and the STIRAP efficiency should not be affected. The method of a coherent population transfer is already known for two decades [23, 80]. First acquisitions of transferring molecules between different vibrational states in molecular beam experiments were proposed in [81, 82]. An important point to realize STIRAP is the adiabatic condition, which is discussed later in this chapter. Other to this, a theoretical treatment will be discussed in the following section. Later, a successfully implemented experimental measurement is shown and evaluated for the $v'' = 0$ and $v'' = 9$ state of the 'a' triplet potential. Additionally, lifetime measurements for the deeply bound Feshbach molecules were taken showing an interesting behavior.

6.1. Theory behind STIRAP - The 3-Level Model

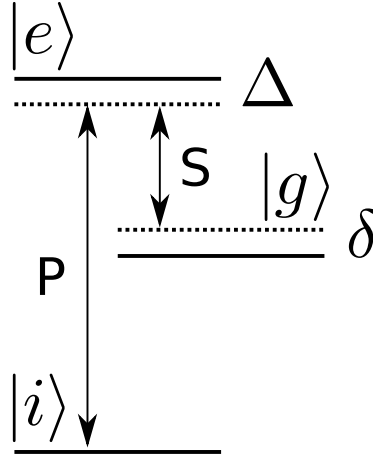


Figure 6.1.: Three level linkage of quantum states. The initial state $|i\rangle$ and the intermediate/excited state $|e\rangle$ are coupled via the P -field (pump laser). The intermediate/excited state $|e\rangle$ and the ground state $|g\rangle$ are coupled through the S -field (Stokes laser). (a) Λ linkage: The single photon detuning Δ is the detuning of the P -field Δ_P . Therefore, the two photon detuning δ is the difference both, the pump and Stokes detuning $\Delta_P - \Delta_S$. The optical frequencies we found after spectroscopy are for $v' = 20$, $v'' = 9$: probe laser frequency 366861.2522 GHz, Stokes laser frequency: 366885.6354 GHz. For $v'' = 0$ we find a Stokes laser frequency of 375836.0223 GHz.

The simplest description of the STIRAP process is the population transfer of three quantum states. More precisely, the speech is about the transfer of the population from the initial quantum state $|i\rangle$ to a target quantum state (or ground state) $|g\rangle$. Since the direct population transfer from $|i\rangle$ to $|g\rangle$ is forbidden due to selection rules coupling requires an intermediate quantum state or excited state $|e\rangle$. Coupling those three states, the so-called 3-level system, can be achieved by to coherent laser, the pump (P) and Stokes (S) laser. In the following, we are using the Λ scheme to describe our system.

The time-dependent Schroedinger equation describes the dynamics of this atomic 3-level system.

$$i\hbar \frac{d}{dt} \Psi(t) = H(t) \Psi(t) \quad (6.1)$$

In equation 6.1 the interaction of the atomic system with the external laser field is described by the Hamiltonian matrix $H(t)$. The rotating-wave approximation (RWA) allows us to neglect fast oscillations. The Hamiltonian matrix $H(t)$ in the RWA can therefore be written as [79]:

$$H = \frac{\hbar}{2} \begin{bmatrix} 0 & \Omega_1(t) & 0 \\ \Omega_1(t) & 2\Delta & \Omega_2(t) \\ 0 & \Omega_2(t) & 2\delta \end{bmatrix} \quad (6.2)$$

with the Rabi frequencies for the pump and Stokes field Ω_1 and Ω_2

$$\Omega_{1/2}(t) = \frac{-d_{i,j}\varepsilon_{1/2}(t)}{\hbar} \quad (6.3)$$

and the single and two color detuning $\delta = \Delta_1 - \Delta_2$. The dipole transition moments for the transition $|i\rangle \rightarrow |e\rangle$ is given by d_{ie} and for the transition $|e\rangle \rightarrow |g\rangle$ by d_{eg} . In the RWA the optical frequencies ω_1 and ω_2 are the frequencies of the electric fields P and S . It is important to mention that their amplitudes in the RWA are given by ε_1 and ε_2 which are slowly varying. As already mentioned the excited state $|e\rangle$ underlies spontaneous emission. This can be described in equation 6.2 by adding phenomenological off-diagonal terms which are imaginary and not stated in this thesis. There is a probability that the population loss from the excited state $|e\rangle$ decays into another quantum state, for example, $|i\rangle$ or $|g\rangle$. These transitions are not coherent transitions and thus not desirable for STIRAP. For a study of incoherences in the STIRAP process, please have a look at reference [74]. The energies can be written concerning the detuning [66].

$$\hbar\Delta_P = E_e - E_i - \hbar\omega_1 \quad (6.4)$$

$$\hbar\Delta_S = E_e - E_g - \hbar\omega_2 \quad (6.5)$$

For STIRAP it is necessary that the two photon detuning $\delta = 0$. This means that the two single photon detuning for the $|i\rangle \rightarrow |e\rangle$ and $|e\rangle \rightarrow |g\rangle$ transitions are equal $\Delta_1 = \Delta_2$. The eigenstates of the Hamiltonian 6.2 are given by

$$|a^0\rangle = \cos \Theta(t)|i\rangle - \sin \Theta(t)|g\rangle \quad (6.6)$$

$$|a^+\rangle = \sin \Theta(t) \sin \phi(t)|i\rangle + \cos \phi(t)|e\rangle + \cos \Theta(t) \sin \phi(t)|g\rangle \quad (6.7)$$

$$|a^-\rangle = \sin \Theta(t) \sin \phi(t)|i\rangle - \cos \phi(t)|e\rangle + \cos \Theta(t) \sin \phi(t)|g\rangle \quad (6.8)$$

We can see that equation 6.7 and 6.8 contain every state. Therefore, these eigenstates are going to populate the excited state $|e\rangle$. However, our goal is to transfer the population without any loss. Therefore, the only solution we are interested in is shown in equation 6.6. This solution shows no connection to the excited state $|e\rangle$ and is therefore immune against spontaneous emission. Similar to the previous chapter, this solution is the so-called 'dark state' or 'coherent population trapping' state [79]. And here we need to do things differently to the Two-Color spectroscopy we did in the previous chapter. Here, we need to ensure that the set of eigenstates changes slowly. This ensures that the whole quantum system remains in the dark state adiabatically following the $|i\rangle \rightarrow |g\rangle$ transition. This can be understood with the mixing angle which relates the ratio of the Rabi-frequencies to a time-dependent angle $\Theta(t)$ [79].

$$\tan \Theta(t) = \frac{\Omega_1(t)}{\Omega_2(t)} = \frac{\sin \Theta(t)}{\cos \Theta(t)} \quad (6.9)$$

The behavior of the population during the STIRAP sequence is shown in figure 6.2 d). At the beginning of the STIRAP sequence the population is in the initial state $|i\rangle$ which means for equation 6.6 that $\sin \Theta(t)$ must vanish. This happens for $\Theta(t) = 0$

and concluding $\Omega_1(t)/\Omega_2(t) = 0$. By the end of the sequence the population should end in the ground state $|g\rangle$. With the same thoughts we find that $\Omega_2/\Omega_1 = 0$ and $\Theta(t) = \pi/2$ [79]. The evolution of the mixing angle is shown in figure 6.2 c). To achieve this a counterintuitive pulse sequence is necessary, which means that the first laser which couples two states is the Stokes laser with coupling strength Ω_2 which is imaged in 6.2 a). How the states behave can be seen by the time evolution of their energies ϵ :

$$\epsilon_{\pm}(t) = \frac{1}{2} \left[\Delta \pm \sqrt{\Delta^2 + \Omega_{eff}(t)^2} \right] \quad (6.10)$$

$$\Omega_{eff}(t) = \sqrt{\Omega_1^2 + \Omega_2^2} \quad (6.11)$$

We can see that for zero detuning $\Delta = 0$ and large or very short times $\Omega_{eff} = 0$ the energy is zero. If the Rabi-frequencies $\Omega_1(t)$ and/or $\Omega_2(t)$ are nonzero, $\Omega_{eff}(t) \neq 0$ and an energy splitting of ϵ_{\pm} occurs. This splitting is related to the Autler-Townes splitting which was discussed previously. The energy of the dark state ϵ_0 stays zero though. We can assume that at the beginning ϵ_0 is related to the initial state $|i\rangle$. By the end of the sequence, ϵ_0 is related to the ground state $|g\rangle$. The behavior of the energies is shown in figure 6.2 b). To get a zero eigenvalue, it is crucial that the two-photon resonance $\delta = 0$. For any other detunings we start to populate the excited state $|e\rangle$ which leads to loss of population [83].

6.2. The Adiabatic Approximation

There are certain conditions for an adiabatic evolution during STIRAP, or in other words, there are conditions for the state vector to follow the dark state. Several conditions to achieve an adiabatic evolution are described for example in [68, 84]. If the evolution is not adiabatic, then the state will not follow the dark state perfectly and will be coupled to the bright state leading to a loss of molecules through spontaneous emission. When we assume that the population is completely in the initial state $|1\rangle$, a complete population transfer is given under the following condition:

$$\frac{\Omega_1(t)}{\Omega_2(t)} \rightarrow 0 \quad \text{for } t \rightarrow -\infty \quad (6.12)$$

$$\frac{\Omega_2(t)}{\Omega_1(t)} \rightarrow 0 \quad \text{for } t \rightarrow +\infty \quad (6.13)$$

In the experiment this means that the Stokes laser with the Rabi-frequency $\Omega_2(t)$ must be turned on before the probe laser starts to interact with the system, which means $\Omega_2(t) \neq 0$ and $\Omega_1(t) = 0$ for $t \rightarrow -\infty$. For $t \rightarrow +\infty$ the Stokes laser must be turned off before the probe laser. In other words $\Omega_2(t) = 0$ and $\Omega_1(t) \neq 0$. This is the counterintuitive pulse sequence which was already mentioned in the previous section. The local adiabatic condition is as follows [84]

$$\Omega_{eff}(t) \gg |\dot{\Theta}(t)| = \frac{|\Omega_2(t)\dot{\Omega}_1(t) - \Omega_1(t)\dot{\Omega}_2(t)|}{\Omega_1(t)^2 + \Omega_2(t)^2} \quad (6.14)$$

This means that the change of the mixing angle $\dot{\Theta}(t)$ (which was introduced in the previous section) should be smaller compared to the splitting of the eigenvalues $\Omega_{eff}(t)$ which prevents a non adiabatic coupling [84]. This condition is local since it must be valid during the whole population transfer sequence [79]. The integration over the time of the Rabi-frequencies gives us the pulse area A and therefore the global adiabatic condition [79]

$$A = \int_{-\infty}^{\infty} \Omega_{eff}(t) dt \quad (6.15)$$

Comparing this to the local adiabatic condition in equation 6.14 we can rewrite the integral for A . Using the mixing angle instead [79].

$$A \gg \frac{\pi}{2} \quad (6.16)$$

Now, we can assume that every part of the pulse area A has a peak Rabi-frequency Ω_{max} . The minimal pulse area A_{min} depends on the transfer efficiency and the pulse shape itself. With this assumptions, we can multiply with the pulse duration T and find [79]

$$A_{min} > \Omega_{max} T \quad (6.17)$$

A rule of thumb is to have a pulse area of $A_{min} \simeq 10$. This factor ensures an efficient population transfer [79]. The two lasers must be mutually phase coherent

during the pulse sequence, that is for a time given by T . If our Rabi-frequencies are not large, then T must be long in order for the STIRAP pulse to be adiabatic. But if T is longer than the phase coherence time of the lasers, then this leads to a problem since phase jumps of the lasers also transfer population out of the dark state.

6.3. STIRAP Experiment and Lifetime of Ultracold Feshbach Molecules

Having the right pulse sequence is mandatory to succeed STIRAP. Or in other words, the evolution of the pulse sequence must be adiabatic. Loss can be eliminated when the excited state $|e\rangle$ is not populated. Which means that the state vector $\psi(t)$ must be aligned to the dark state $|a^0\rangle$ for all times. Fulfilling this requirement we introduced a Gaussian pulses sequence. As showed in figure 6.2 the whole pulse sequence can be divided into 5 sections [79].

1. *S induced Autler-Townes phase:* At the beginning of the sequence we find our population in the state $|i\rangle$. However, the Stokes laser is turned on adiabatically first while the pump laser is still off. This is known as the counterintuitive pulse order. The effect is that the S field couples the $|g\rangle \rightarrow |e\rangle$ transition with a strength of the Rabi frequency $\Omega_S(t)$. This coupling splits the excited state $|e\rangle$ while the population is remaining in state $|i\rangle$ is untouched yet. In terms of Rabi frequencies this means that $|\Omega_S(t)| > 0$ while $\Omega_P(t) = 0$ or in other words $|\Omega_S(t)| \gg |\Omega_P(t)|$. This can be achieved when the mixing angle $\Theta = 0$. The state vector is still equal to ψ_i or $|i\rangle$.
2. *S induced CPT phase:* At the peak of the S field (strong S field) the P field is turned on adiabatically. At this stage the P pulse is still much weaker than the S pulse. In terms of Rabi frequencies this means that $|\Omega_S(t)| \gg |\Omega_P(t)|$ but $|\Omega_S(t)| \neq 0 \neq |\Omega_P(t)|$. Due to this fact the excited state is still divided which suppress the population transition from $|i\rangle \rightarrow |e\rangle$. One can also describe this effect that destructive interference cancels out the transition rate. Since the pulses are adiabatic the state vector can still be described as ψ_i or $|i\rangle$.
3. *Adiabatic passage phase:* The S field starts to decrease while the P field is constantly increasing. However, at this stage, both fields are considered as strong. Presumably, the Rabi frequencies of both fields are equal $|\Omega_S(t)| = |\Omega_P(t)|$ and both fields coupling to each other. The mixing angle changes from 0 towards $\pi/2$. Since the state vector changes from ψ_i or $|i\rangle$ towards $-\psi_g$ or $-|g\rangle$ it shows a linear combination of both states.
4. *P induced CPT phase:* The P field strong compared to the S field. In terms of Rabi frequencies this means that $|\Omega_P(t)| \gg |\Omega_S(t)|$ but $|\Omega_P(t)| \neq 0 \neq |\Omega_S(t)|$. Therefore, the much stronger P field couples the $|i\rangle \rightarrow |e\rangle$ transition and splits the excited state $|e\rangle$ (Autler-Townes splitting) and suppress population transfer of the weakly coupled $|g\rangle \rightarrow |e\rangle$ transition. Therefore, the state vector can be described as $-\psi_g$ or $|g\rangle$.

5. *P induced Autler-Townes phase:* The Stokes laser is turned off while the pump laser is at its maximum. Due to a strong coupling of the $|g\rangle \rightarrow |e\rangle$ transition the Autler-Townes splitting of the excited state $|e\rangle$ is at its maximum. The population are remaining in state $|e\rangle$ and are 'isolated' from any other transitions. In terms of Rabi frequencies this means that $|\Omega_P(t)| > 0$ while $\Omega_S(t) = 0$ or in other words $|\Omega_P(t)| \gg |\Omega_S(t)|$. The mixing angle $\Theta = \pi/2$. The state vector is equal to ψ_g or $|g\rangle$.

These 5 steps are describing a one-way STIRAP sequence. However, since our experimental setup allows us to image the initial state $|i\rangle$, we need to initialize this pulse sequence twice to transfer the population back to the initial state $|i\rangle$. In our experiment we scan the pump detuning Δ_P over the resonance frequency of the $|i\rangle \rightarrow |e\rangle$ transition. After successfully initializing a STIRAP round trip we can image the initial state for every detuning resulting in a high atomic or molecular revival in case of hitting the resonance frequency $\Delta_1 = 0$. As an example we see this revival peaks in figure 6.3¹ for the $v'' = 6$ rotational state. By comparing the number of atoms or molecules in the initial state $|i\rangle$ with and without executing the STIRAP pulse sequence we gain a STIRAP round-trip efficiency of roughly 70 %. Additionally, we measured the lifetime of our deeply bound molecules for all the rotational stages between $v'' = 0$ and $v'' = 9$. An example is shown in figure 6.4. To measure the lifetime we enlarged the time between the make and unmake pulse sequence. By imaging the initial state $|i\rangle$ we note a loss in atom number. We assume a two body loss and therefore we could use an exponential function to fit the data. One interesting thing is that the $v'' = 9$ state shows a longer lifetime ($\tau = 2949.17 \mu\text{s}$) than the $v'' = 0$ ($\tau = 1585.36 \mu\text{s}$) state, which is unexpected. Note, that the $v'' = 6$ state is right in between of both values with $\tau = 2813.61 \mu\text{s}$. Currently, we are about to study this phenomenon. To ensure, that we are not handling a BEC we measured the trap frequency of the ODT recently. The ODT trap frequency is related to the temperature of the sample. Also, it allows us to measure the density of our sample, which wasn't done at an earlier experimental stage, yet. However, this measurements showed, that we are far under the critical temperature T_c and therefore into the BEC regime. The same lifetime measurements should be done with higher temperatures. This can be easily implemented via tuning the magnetic field down and decreasing the ODT trap depth. So at the stage where this data was measured we assumed to have a diluted gas but created a deeply bound molecular BEC in the lowest triplet state instead.

¹The dataset for the $v'' = 6$ state is shown since this data set was complete. The idea is the same for the $v'' = 0$ and $v'' = 9$ state

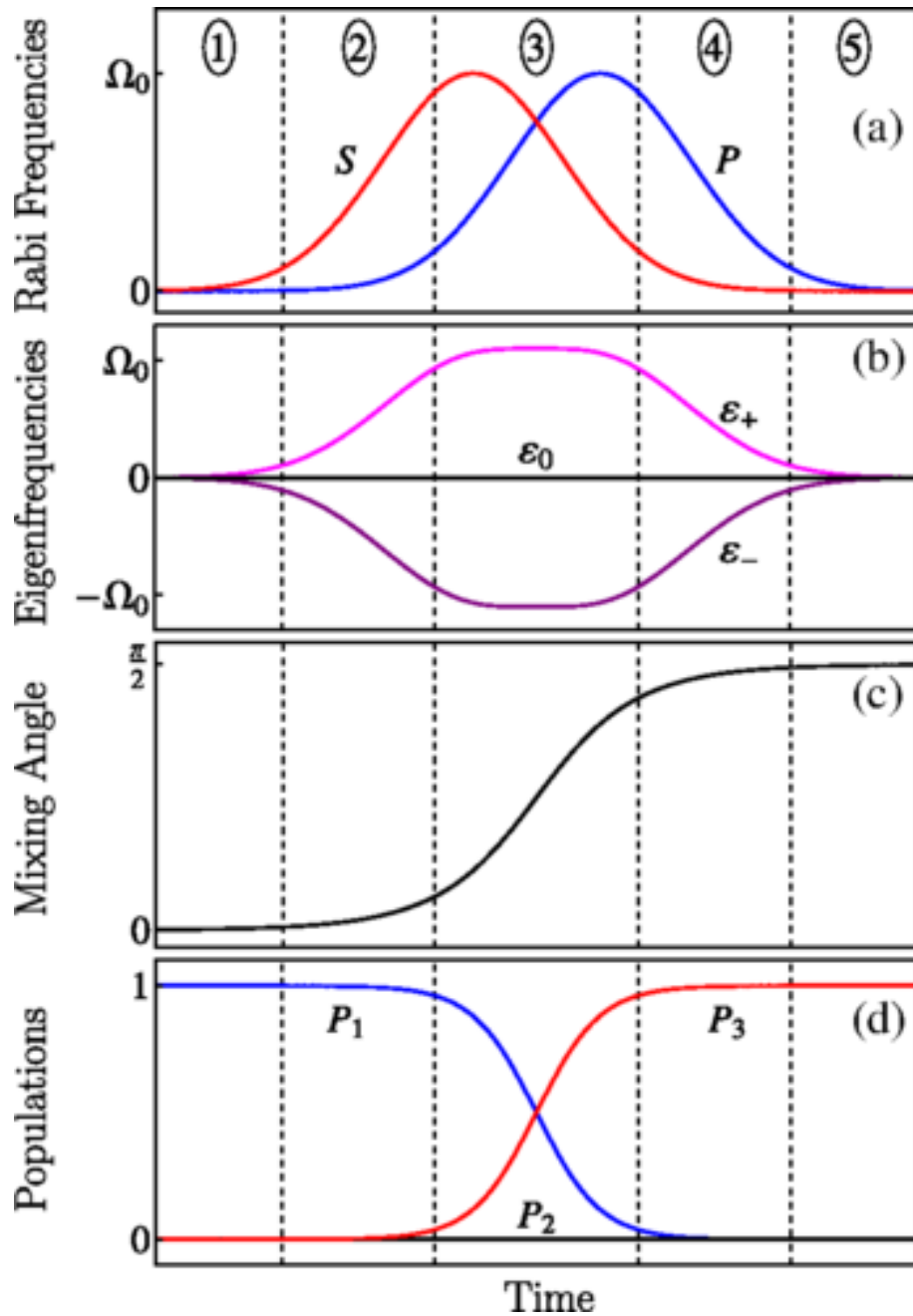


Figure 6.2.: STIRAP experiment for two Gaussian pulses tuned on the single-photon resonance $\Delta_P = \Delta_S = 0$. The whole STIRAP procedure can be segmented into five different regimes (see numbers 1-5, separated by the dotted lines). (a) Time evolution of the Rabi frequencies for the pump (P) and Stokes (S) field $\Omega_P(t)$ and $\Omega_S(t)$. Both Rabi-frequencies are equal and have therefore the same peak value Ω_0 . The pulse sequence counterintuitive in that the Stokes field turned on before the pump field. (b) Adiabatic time dependence of the Eigenvalues $\epsilon_0(t)$, $\epsilon_{\pm}(t)$. (c) Time evolution of the mixing angle $\Theta(t)$. (d) Time dependence population behavior P_i , P_e , P_g for the three different quantum states described by the three-level system. Adapted from [79].

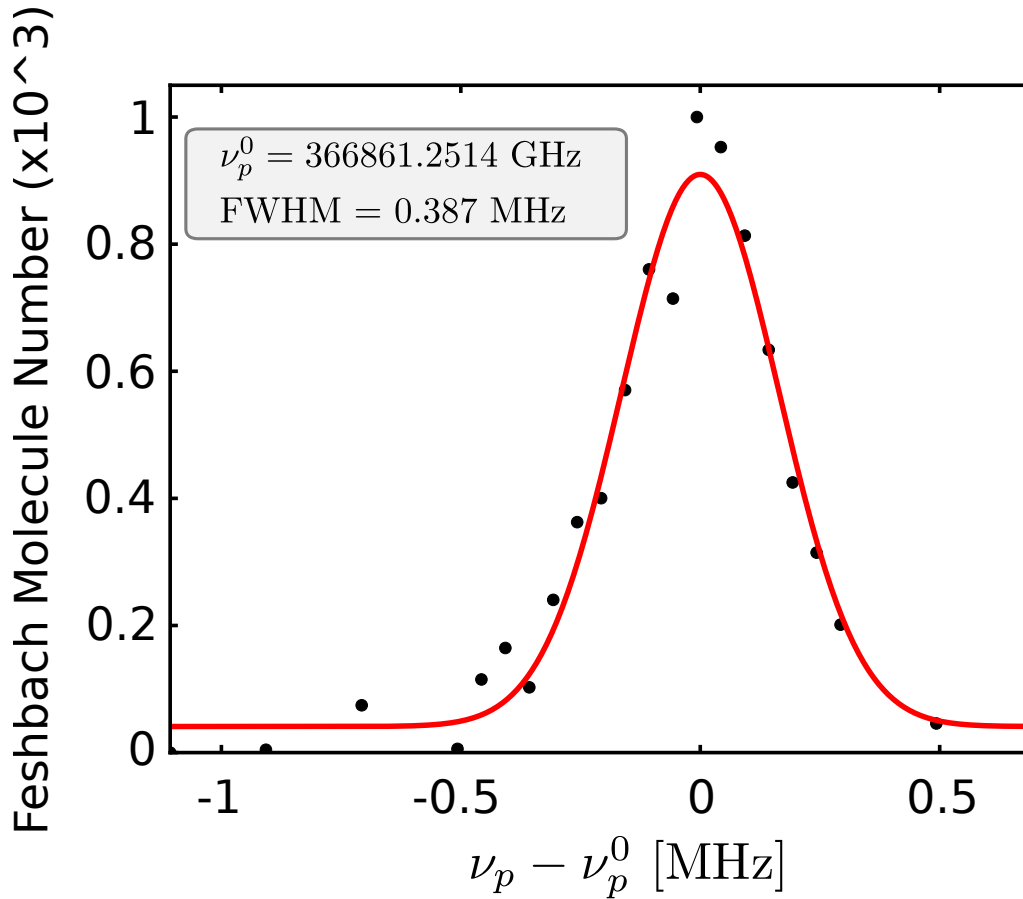


Figure 6.3.: Number of Feshbach molecules after exposing them to a STIRAP pulse sequence that moves them into the ground state and back to the Feshbach molecule state as a function of the two photon detuning. The $|e\rangle$ state was the $v = 20$ level of the $c(1^1\Sigma_g^+)$ potential and the $|g\rangle$ was the $v'' = 6$ level of the $a(1^3\Sigma_u^+)$ potential. The frequency of the probe field ν_p was scanned by ± 1 MHz around the single-photon resonance frequency $\nu_p^0 = 366861.25$.

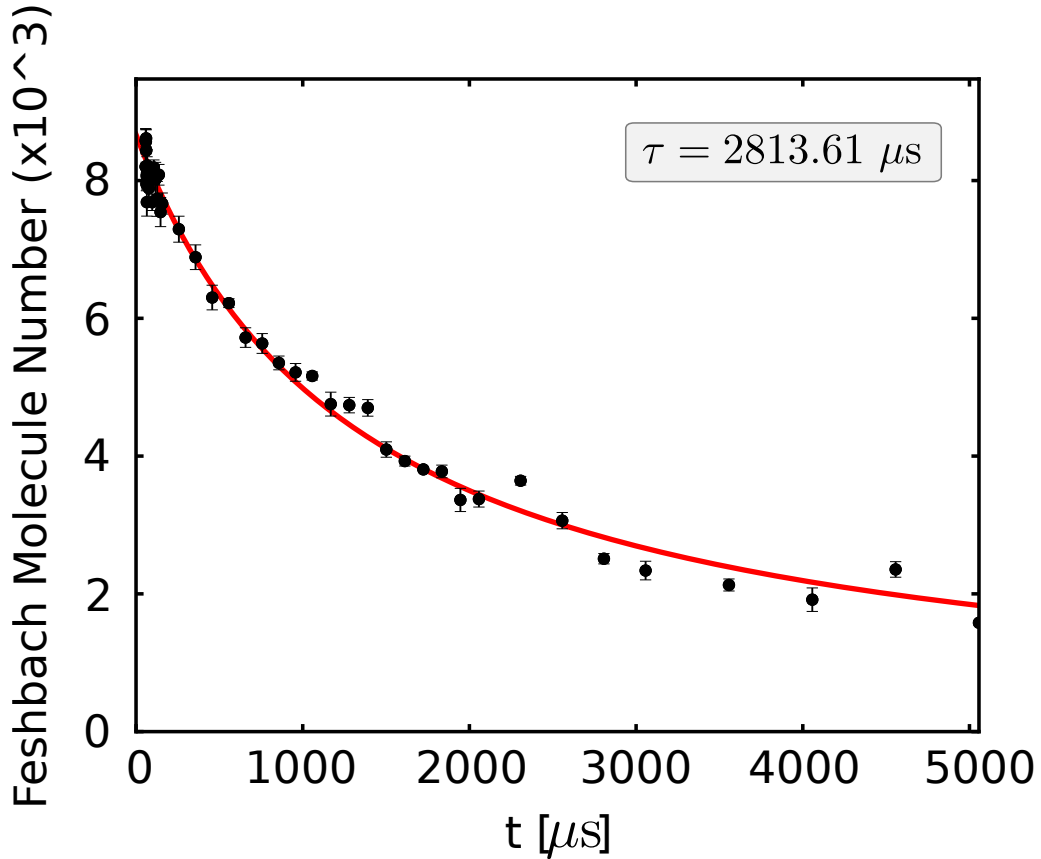


Figure 6.4.: Lifetime for molecules in the $v'' = 6$ level of the 'a' state. Shown is the number of Feshbach molecules after exposing them to a STIRAP pulse sequence that moves them into the $v'' = 6$ level of the 'a' state where they are held for a variable time and then transformed back to the Feshbach molecule state as a function of the hold time. The $|e\rangle$ state was the $v' = 20$ level of the $c(1^1\Sigma_g^+)$ potential and the $|g\rangle$ was the $v'' = 6$ level of the $a(1^3\Sigma_u^+)$ potential. The lifetime data is the average of 4 measurements. The exponential fit extracts a lifetime of $\tau = 2813.61 \mu\text{s}$ ².

7. Conclusion & Outlook

With the photoassociation method we succeeded in converting a population of Li Feshbach dimers from a weakly bound Feshbach molecular state to a deeply bound molecular state. This transition was driven by a 2-photon coupling of the two states through a third state and then adiabatically altering the quantum state by controlling the Raman laser powers (a process known as Stimulated Raman adiabatic passage, STIRAP [23, 81]). Before the implementation of the STIRAP method we characterized the used quantum states. Starting from the collision channel $2S_{1/2} + 2S_{1/2}$ which forms our initial state $|i\rangle$ and have singlet and triplet character¹. This gives us the freedom to successfully make deeply bound molecules with singlet or triplet character. Both experiments were successfully done. However, in this thesis we set the focus on molecules with triplet character. The excited triplet molecular potential $a(1^3\Sigma_u^+)$, especially the vibrational state $v' = 20$, shows a good Franck-Condon overlap and forms from now on our excited state $|e\rangle$. The natural linewidth of the $|i\rangle \rightarrow |e\rangle$ transition is in order of 7 MHz. The transition frequency of these states is $\nu_p^0 = 366861.25$ GHz with a Rabi-frequency of $\Omega_1 \approx 28$ kHz for $P_p = 80 \mu\text{W}$. The lifetime of the Feshbach molecules in $|e\rangle$ is $\tau = 1273 \mu\text{s}$. To create deeply bound Feshbach molecules we need to find a ground state which can be found via two-color spectroscopy. We found every vibronic state between $v'' = 0$ and 9, named as the ground state $|g\rangle$ of the lowest lying triplet potential $a(1^3\Sigma_u^+)$. The Autler-Townes splitting of the excited state $|e\rangle$ gave us an information about the Rabi-frequency $\Omega_2 \approx 14$ MHz for the $|e\rangle \rightarrow |g\rangle$ transition and a Stokes power of $P_s = 10$ mW. For a more detailed characterization of the two photon resonance we successfully showed a dark state revival. This revival peak gives us an insight of the coupling of the states as well as the detuning of the two-photon transition and coherence of the excitation lasers.

This characterization of the used quantum states lead to successfully transfer the population from the initial state $|i\rangle$ to the ground state $|g\rangle$ of the lowest lying triplet molecular potential $a(1^3\Sigma_u^+)$. Therefore, we generated deeply bond triplet molecules. Additional lifetime measurements of these molecules in the ground state showed, that the $v'' = 9$ state is longer lived than the $v'' = 0$ state. We found a lifetime of $2949.17 \mu\text{s}$ for the $v'' = 9$ state, and $1585.36 \mu\text{s}$ for the $v'' = 0$ state. This phenomenon is not fully understand and is part of our current studies. On top of this an ODT trap frequency and time of flight measurement gave us insight about the temperature of the sample lately. With a sample temperature of around 200-300 nK we already crossed the critical temperature for a BEC. Therefore, all the measurements in this thesis are the results of a molecular BEC. One of the following

¹Since ^6Li shows a broad Feshbach resonance around $B = 834$ G, all of our experiments were done with a static magnetic field of $B = 755$ G. The value was used since the transition frequencies were already known to a precision of 1-2 GHz. In this regime the scattering length is still large since the width of the broad Feshbach resonance is ~ 300 G.

steps is to reproduce these measurements with a higher temperature which gives us a diluted quantum gas.

In general this thesis shows that Feshbach resonances play an important role in such experiments since they allow for the inter-atomic interactions to be controlled by the application of a magnetic field [85]. A long term goal is to create an ensemble of deeply bound RbLi molecules (Bose-Fermi pairing) which can have both a magnetic and an electric dipole moment. The combination of these two ingredients of these molecules allows for a wider variety of many-body systems to be realized than with just the cold atoms. We can also think about studying the interaction of Fermi gases (sea of ${}^6\text{Li}$ atoms) with impurities provided by a dilute bosonic gas like ${}^{87}\text{Rb}$. This system might help to study the Kondo effect [86], a many-body phenomenon of electronic conduction with magnetic impurities. In the Kondo effect, scattering of conduction electrons with the impurity leads to a spin dependent interaction and can modify the dependence of the resistivity at low temperatures. There are many outstanding questions and ideas about this effect including the properties and nature of the Kondo screening cloud (as proposed by Ian Affleck [87]).

A. Bibliography

- [1] Vassiliki Kalogera and Albert Lazzarini. LIGO and the opening of a unique observational window on the universe. *Proceedings of the National Academy of Sciences*, 114(12):3017–3025, 2017. ISSN 0027-8424. doi: 10.1073/pnas.1612908114. URL <http://www.pnas.org/lookup/doi/10.1073/pnas.1612908114>. 1
- [2] F. Jelezko and J. Wrachtrup. Single defect centres in diamond: A review. *Physica Status Solidi (A) Applications and Materials Science*, 203(13):3207–3225, 2006. ISSN 18626300. doi: 10.1002/pssa.200671403. 1
- [3] J. B. Fixler, G. T. Foster, J. M. McGuirk, and M. A. Kasevich. Atom interferometer measurement of the newtonian constant of gravity. *Science*, 315(5808):74–77, 2007. ISSN 00368075. doi: 10.1126/science.1135459. 1
- [4] P. G H Sandars. Measurability of the proton electric dipole moment. *Physical Review Letters*, 19(24):1396–1398, 1967. ISSN 00319007. doi: 10.1103/PhysRevLett.19.1396.
- [5] Eric R. Hudson, H. J. Lewandowski, Brian C. Sawyer, and Jun Ye. Cold molecule spectroscopy for constraining the evolution of the fine structure constant. *Physical Review Letters*, 96(14):1–4, 2006. ISSN 00319007. doi: 10.1103/PhysRevLett.96.143004. 1
- [6] D. DeMille. Quantum Computation with Trapped Polar Molecules. *Physical Review Letters*, 88(6):4, 2002. ISSN 10797114. doi: 10.1103/PhysRevLett.88.067901. 1
- [7] S. F. Yelin, K. Kirby, and R. Cote. Schemes for robust quantum computation with polar molecules. pages 2–5, 2006. ISSN 1050-2947. doi: 10.1103/PhysRevA.74.050301. URL <http://arxiv.org/abs/quant-ph/0602030><http://dx.doi.org/10.1103/PhysRevA.74.050301>. 1
- [8] G. Pupillo, A. Micheli, H. P. Büchler, and P. Zoller. Condensed Matter Physics with Cold Polar Molecules. 2008. URL <http://arxiv.org/abs/0805.1896>. 1
- [9] A. Micheli, G. K. Brennen, and P. Zoller. A toolbox for lattice-spin models with polar molecules. *Nature Physics*, 2(5):341–347, 2006. ISSN 17452473. doi: 10.1038/nphys287. 1
- [10] M. H. Anderson, J. R. Ensher, M. R. Matthews, C. E. Wieman, and E. A. Cornell. Observation of Bose-Einstein Condensation in a Dilute Atomic Vapor. *Science*, 269(5221):198–201, 1995. ISSN 0036-8075. doi: 10.1126/science.269.5221.198. URL <http://www.sciencemag.org/cgi/doi/10.1126/science.269.5221.198>. 1

-
- [11] K. B. Davis, M. O. Mewes, M. R. Andrews, N. J. Van Druten, D. S. Durfee, D. M. Kurn, and W. Ketterle. Bose-Einstein condensation in a gas of sodium atoms. *Physical Review Letters*, 75(22):3969–3973, 1995. ISSN 00319007. doi: 10.1103/PhysRevLett.75.3969. 1
- [12] C. C. Bradley, C. A. Sackett, J. J. Tollett, and R. G. Hulet. Evidence of Bose-Einstein condensation in an atomic gas with attractive interactions. *Physical Review Letters*, 75(9):1687–1690, 1995. ISSN 00319007. doi: 10.1103/PhysRevLett.75.1687. 1
- [13] B. De Marco, J. L. Bohn, J. P. Burke, M. Holland, and D. S. Jin. Measurement of p-wave threshold law using evaporatively cooled fermionic atoms. *Physical Review Letters*, 82(21):4208–4211, 1999. ISSN 10797114. doi: 10.1103/PhysRevLett.82.4208. 1
- [14] Andrew G Truscott, Kevin E Strecker, William I McAlexander, Guthrie B Partridge, G Hulet, and Randall G Hulet. in a Gas of Trapped Atoms. *Science*, 291(5513):2570–2572, 2001. 1
- [15] Cheng Chin, Rudolf Grimm, Paul Julienne, and Eite Tiesinga. Feshbach resonances in ultracold gases. *Reviews of Modern Physics*, 82(2):1225–1286, 2010. ISSN 00346861. doi: 10.1103/RevModPhys.82.1225. 1, 19, 20, 27, 28, 29
- [16] Immanuel Bloch, Jean Dalibard, and Wilhelm Zwerger. Many-body physics with ultracold gases. *Reviews of Modern Physics*, 80(3):885–964, 2008. ISSN 00346861. doi: 10.1103/RevModPhys.80.885. 1
- [17] Johann G. Danzl, Manfred J. Mark, Elmar Haller, Mattias Gustavsson, Russell Hart, Jesus Aldegunde, Jeremy M. Hutson, and Hanns Christoph Nägerl. An ultracold high-density sample of rovibronic ground-state molecules in an optical lattice. *Nature Physics*, 6(4):265–270, 2010. ISSN 17452473. doi: 10.1038/nphys1533. URL <http://dx.doi.org/10.1038/nphys1533>. 1
- [18] Johann Danzl, Elmar Haller, Mattias Gustavsson, Manfred Mark, Russell Hart, Nadia Bouloufa, Olivier Dulieu, Helmut Ritsch, and Hanns-christoph Nägerl. Quantum Gas of Deeply Bound Ground State Molecules. 321(August):1062–1067, 2008. 1, 49
- [19] F. Lang, K. Winkler, C. Strauss, R. Grimm, and J. Hecker Denschlag. Ultracold triplet molecules in the rovibrational ground state. *Physical Review Letters*, 101(13):1–4, 2008. ISSN 00319007. doi: 10.1103/PhysRevLett.101.133005. 1, 49
- [20] Peter K. Molony, Philip D. Gregory, Zhonghua Ji, Bo Lu, Michael P. Köppinger, C. Ruth Le Sueur, Caroline L. Blackley, Jeremy M. Hutson, and Simon L. Cornish. Creation of ultracold Rb 87 Cs 133 molecules in the rovibrational ground state. *Physical Review Letters*, 113(25):1–5, 2014. ISSN 10797114. doi: 10.1103/PhysRevLett.113.255301. 1
- [21] Will Gunton. Photoassociation and Feshbach Resonance Studies in Ultra-Cold Gases of 6Li and Rb Atoms. (April), 2016. 1, 2, 5, 8, 9, 10, 11, 12, 13, 14, 15, 27, 33, 34, 35, 36, 37, 49, 50

-
- [22] M. D. Di Rosa. Laser-cooling molecules: Concept, candidates, and supporting hyperfine-resolved measurements of rotational lines in the A-X(0,0) band of CaH. *European Physical Journal D*, 31(2):395–402, 2004. ISSN 14346060. doi: 10.1140/epjd/e2004-00167-2. [2](#)
- [23] K Bergmann, H Theuer, and B W Shore. Coherent population transfer among quantum states of atoms and molecules. *Rev. Mod. Phys.*, 70(3):1003–1023, 1998. ISSN 0034-6861. doi: 10.1103/RevModPhys.70.1003. [2](#), [37](#), [53](#), [63](#)
- [24] Mariusz Semczuk. Photoassociation Spectroscopy of a degenerated Fermi gas of 6Li. (January), 2015. [2](#), [5](#), [8](#), [14](#)
- [25] Gene Polovy. *Thesis is in progress*. PhD thesis, University of British Columbia, 2018. [2](#), [10](#), [16](#)
- [26] Gene Polovy, Julian Schmidt, Denis Umland, Erik Frieling, Kahan Dare, Kirk W. Madison. Phase noise reduction of mutually tunable lasers with an external acousto-optic modulator. *Will be published soon*, pages 1–5, 2018. [2](#), [5](#), [9](#)
- [27] Michael E Gehm. Properties of 6 Li. pages 1–33, 2003. [5](#), [6](#), [7](#), [24](#)
- [28] Keith Ladouceur, Bruce G Klappauf, Janelle Van Dongen, Nina Rauhut, Bastian Schuster, Arthur K Mills, David J Jones, and Kirk W Madison. Compact laser cooling apparatus for simultaneous cooling of lithium and rubidium. 26 (2):210–217, 2009. [8](#)
- [29] Keith Ladouceur. Experimental Advances toward a Compact Dual-Species Laser Cooling Apparatus. 2008. doi: 10.14288/1.0066703.
- [30] Janelle Van Dongen. *Simultaneous cooling and trapping of 6Li and 85/87Rb*. PhD thesis.
- [31] Swati Singh. Progress towards ultra-cold ensembles of rubidium and lithium. *Strategy*, (October), 2007. [8](#)
- [32] William James Bowden. An Experimental Apparatus for the Laser Cooling of Lithium and Rubidium. (October), 2014. [13](#), [14](#)
- [33] M D Jones, J Nute, J Wu, S Warriar, L Hackermüller, M D Jones, J Nute, J Wu, S Warriar, and L Hackermüller. Versatile cold atom source for multi-species experiments Versatile cold atom source for multi-species experiments. 113103(2014), 2016. doi: 10.1063/1.4900577. [14](#)
- [34] William Bowden, Will Gunton, Mariusz Semczuk, Kahan Dare, Kirk W Madison, William Bowden, Will Gunton, Mariusz Semczuk, Kahan Dare, and Kirk W Madison. An adaptable dual species effusive source and Zeeman slower design demonstrated with Rb and Li An adaptable dual species effusive source and Zeeman slower design demonstrated with Rb and Li. 043111, 2016. doi: 10.1063/1.4945567. [14](#)

-
- [35] J Van Dongen, C Zhu, D Clement, G Dufour, J L Booth, and K W Madison. Trap-depth determination from residual gas collisions. 022708:1–11, 2011. doi: 10.1103/PhysRevA.84.022708. 14
- [36] Rudolf Grimm and Matthias Weidem. Optical dipole traps for neutral atoms. 1987. 16
- [37] A V Turlapov and M Yu Kagan. Evaporative cooling of unitary Fermi gas mixtures in optical traps. 2006. doi: 10.1088/1367-2630/8/9/213. 16
- [38] Daniel Adam Steck. Quantum and Atom Optics Author contact information :. 16
- [39] Kenneth Martin O’Hara. *Optical Trapping and Evaporative Cooling of Fermionic Atoms*. PhD thesis, Duke University, 2000. 16
- [40] Herman Feshbach. Unified theory of nuclear reactions. *Reviews of Modern Physics*, 36(4):1076–1078, 1964. ISSN 00346861. doi: 10.1103/RevModPhys.36.1076. 19
- [41] Francesca Ferlaino, Steven Knoop, and Rudolf Grimm. Ultracold Feshbach Molecules. 19, 21, 22, 23
- [42] John L Bohn. Semianalytic theory of laser-assisted resonant cold collisions. 60 (1):414–425, 1999. 20
- [43] P O Fedichev, Yu Kagan, G V Shlyapnikov, and J T M Walraven. Influence of Nearly Resonant Light on the Scattering Length in Low-Temperature Atomic Gases. (1), 1996.
- [44] P O Fedichev, M J Bijlsma, and P Zoller. Extended Molecules and Geometric Scattering Resonances in Optical Lattices. (February):1–4, 2004. doi: 10.1103/PhysRevLett.92.080401. 20
- [45] A. Axelsson A.J. Moerdijk, B.J. Verhaar. Resonances in ultracold collisions of 6Li , 7Li , and 23Na . 51(6):4852–4861, 1995. 20
- [46] Cindy A. Regal, Christopher Ticknor, John L. Bohn, and Deborah S. Jin. Creation of ultracold molecules from a Fermi gas of atoms. *Nature*, 424(6944): 47–50, 2003. ISSN 00280836. doi: 10.1038/nature01738. 23
- [47] J Herbig, Tobias Kraemer, Michael Mark, Tino Weber, Cheng Chin, Hanns-Christoph Na gerl, and Rudolf Grimm. Preparation of a Pure Molecular Quantum Gas. *Science*, 301(5639):1510–1513, 2003. URL <http://www.sciencemag.org/cgi/doi/10.1126/science.1088876>{%}5Cnpapers3://publication/doi/10.1126/science.1088876.
- [48] Stephan Dürr, Thomas Volz, Andreas Marte, and Gerhard Rempe. Observation of Molecules Produced from a Bose-Einstein Condensate. *Physical Review Letters*, 92(2):4, 2004. ISSN 10797114. doi: 10.1103/PhysRevLett.92.020406.

-
- [49] J. Cubizolles, T. Bourdel, S. J.J.M.F. Kokkelmans, G. V. Shlyapnikov, and C. Salomon. Production of long-lived ultracold [formula presented] molecules from a fermi gas. *Physical Review Letters*, 91(24):1–4, 2003. ISSN 10797114. doi: 10.1103/PhysRevLett.91.240401.
- [50] Kevin E. Strecker, Guthrie B. Partridge, and Randall G. Hulet. Conversion of an Atomic Fermi Gas to a Long-Lived Molecular Bose Gas. *Physical Review Letters*, 91(8):6–9, 2003. ISSN 10797114. doi: 10.1103/PhysRevLett.91.080406. 23, 28
- [51] Will Gunton, Mariusz Semczuk, and Kirk W. Madison. Realization of BEC-BCS crossover physics in a compact oven-loaded magneto-optic trap apparatus. 2013. doi: 10.1103/PhysRevA.88.023624. URL <http://arxiv.org/abs/1307.5445><http://dx.doi.org/10.1103/PhysRevA.88.023624>. 24
- [52] S. Simonucci, P. Pieri, and G. C. Strinati. Broad vs. narrow Fano-Feshbach resonances in the BCS-BEC crossover with trapped Fermi atoms. *Europhysics Letters*, 69(5):713–718, 2005. ISSN 02955075. doi: 10.1209/epl/i2004-10412-2.
- [53] G. B. Partridge, K. E. Strecker, R. I. Kamar, M. W. Jack, and R. G. Hulet. Molecular probe of pairing in the BEC-BCS crossover. *Physical Review Letters*, 95(2):8–11, 2005. ISSN 00319007. doi: 10.1103/PhysRevLett.95.020404. 24
- [54] G. M. Falco and H. T.C. Stoof. Dressed molecules in resonantly interacting ultracold atomic Fermi gases. *Physical Review A - Atomic, Molecular, and Optical Physics*, 75(2):25–41, 2007. ISSN 10502947. doi: 10.1103/PhysRevA.75.023612. 24, 26, 27
- [55] T B Ottenstein, T Lompe, M Kohnen, A N Wenz, and S Jochim. Collisional Stability of a Three-Component Degenerate Fermi Gas. 203202(November): 1–4, 2008. doi: 10.1103/PhysRevLett.101.203202. 25
- [56] B. J. Verhaar H. T. C. Stoof, J. M. V. A. Koelman. Spin-exchange and dipole relaxation rates in atomic hydrogen Rigorous and simplified calculations. 38 (7), 1988. 26
- [57] S. J.J.M.F. Kokkelmans, J. N. Milstein, M. L. Chiofalo, R. Walser, and M. J. Holland. Resonance superfluidity: Renormalization of resonance scattering theory. *Physical Review A - Atomic, Molecular, and Optical Physics*, 65(5):14, 2002. ISSN 10941622. doi: 10.1103/PhysRevA.65.053617. 27
- [58] M. Houbiers, H. T. C. Stoof, W. I. McAlexander, and R. G. Hulet. Elastic and inelastic collisions of 6Li atoms in magnetic and optical traps. *Physical Review A*, 57(3):R1497–R1500, 1998. ISSN 1050-2947. doi: 10.1103/PhysRevA.57.R1497. URL <http://link.aps.org/doi/10.1103/PhysRevA.57.R1497>. 28
- [59] T. Bourdel, J. Cubizolles, L. Khaykovich, K. M. F. Magalhães, S. J. J. M. F. Kokkelmans, G. V. Shlyapnikov, and C. Salomon. Measurement of the Interaction Energy near a Feshbach Resonance in a 6Li Fermi Gas. *Physical Review Letters*, 91(2):020402, 2003. ISSN 0031-9007. doi: 10.

- 1103/PhysRevLett.91.020402. URL <https://link.aps.org/doi/10.1103/PhysRevLett.91.020402>. 28
- [60] E R I Abraham, W I McAlexander, J M Gerton, R G Hulet, R Côté, and A Dalgarno. Triplet s-wave resonance in ^6Li collisions and scattering lengths of ^6Li and ^7Li . *Physical Review A*, 55(5):R3299–R3302, 1997. ISSN 1050-2947. doi: 10.1103/PhysRevA.55.R3299. URL <http://link.aps.org/doi/10.1103/PhysRevA.55.R3299>. 29
- [61] C. J. Joachain B. H. Bransden. *Physics of Atoms and Molecules*. 1983. ISBN 0-582-44401-2. 33, 34, 35
- [62] G. Herzberg. *Molecular Spectra and Molecular Structure, I. Spectra of Diatomic Molecules*. New York, 1950. 35
- [63] J Aldegunde and Jeremy M Hutson. Hyperfine energy levels of alkali-metal dimers : Ground-state homonuclear molecules in magnetic fields. pages 1–8, 2009. doi: 10.1103/PhysRevA.79.013401. 37
- [64] Jianmei Bai, E H Ahmed, B Beser, Y Guan, S Kotochigova, and A M Lyyra. Global analysis of data on the spin-orbit-coupled A 1 states of Cs 2. 032514: 1–17, 2011. doi: 10.1103/PhysRevA.83.032514. 37
- [65] S Ospelkaus, K Ni, and G Que. Controlling the Hyperfine State of Rovibronic Ground-State Polar Molecules. 030402(January):2–5, 2010. doi: 10.1103/PhysRevLett.104.030402. 37
- [66] N V Vitanov and S Stenholm. Adiabatic population transfer via multiple intermediate states. 60(5):3820–3832, 1999. 37, 55
- [67] Taiwang Cheng, Hariyanto Darmawan, and Alex Brown. Stimulated Raman adiabatic passage in molecules : The effects of background states. (September 2006):1–11, 2007. doi: 10.1103/PhysRevA.75.013411.
- [68] A Kuhn, G W Coulston, G Z He, S Schiemann, K Bergmann, W S Warren, A Kuhn, G W Coulston, G Z He, S Schiemann, and K Bergmann. Population transfer by stimulated Raman scattering with delayed pulses using spectrally broad light Population transfer by stimulated Raman scattering with delayed pulses using spectrally broad light. 4215(1992), 2015. doi: 10.1063/1.462840. 37, 57
- [69] E R I Abraham, W I McAlexander, H T C Stoof, and R G Hulet. Hyperfine structure in photoassociative spectra of 6Li_2 and 7Li_2 . 53(5):3092–3097, 1996. 37
- [70] E R I Abraham, N W M Ritchie, W I McAlexander, and R G Hulet. Photoassociative spectroscopy of long-range states of ultracold Li_2 and Li_2 . 7773(1995), 2009. doi: 10.1063/1.470296. 37
- [71] Roland L Dunbrack. Calculation of Franck-Condon Factors for Undergraduate Quantum Chemistry. 83(11):953–955, 1986. doi: 10.1021/ed063p953. 39

-
- [72] Kevin M. Jones, Eite Tiesinga, Paul D. Lett, and Paul S. Julienne. Ultracold photoassociation spectroscopy: Long-range molecules and atomic scattering. *Reviews of Modern Physics*, 78(2):483–535, 2006. ISSN 00346861. doi: 10.1103/RevModPhys.78.483. 39
- [73] Michael Fleischhauer, Atac Imamoglu, and Jonathan P. Marangos. Electromagnetically induced transparency: Optics in coherent media. *Reviews of Modern Physics*, 77(2):633–673, 2005. ISSN 0034-6861. doi: 10.1103/RevModPhys.77.633. URL <https://link.aps.org/doi/10.1103/RevModPhys.77.633>. 42, 45, 47
- [74] Markus Debatin. Creation of Ultracold RbCs Ground-State Molecules. (July), 2013. 43, 55
- [75] Markus Debatin, Tetsu Takekoshi, Raffael Rameshan, Lukas Reichso, Francesca Ferlaino, Rudolf Grimm, Romain Vexiau, and Nadia Bouloufa. Molecular spectroscopy for ground-state transfer of ultracold RbCs molecules. pages 18926–18935, 2011. doi: 10.1039/c1cp21769k. 42, 47
- [76] Lene Vestergaard Hau, S E Harris, Zachary Dutton, Cyrus H Behroozi, and Edwin H Land Boulevard. Light speed reduction to 17 metres per second in an ultracold atomic gas. 397(February):594–598, 1999. 45
- [77] C.H. Townes S.H. Autler. Stark Effect in Rapidly Varying Fields. *Physical Review*, 100(2), 1955. 47
- [78] Simon Stellmer, Benjamin Pasquiou, Rudolf Grimm, and Florian Schreck. Creation of Ultracold Sr 2 Molecules in the Electronic Ground State. 115302 (September):1–5, 2012. doi: 10.1103/PhysRevLett.109.115302. 49
- [79] Nikolay V. Vitanov, Andon A. Rangelov, Bruce W. Shore, and Klaas Bergmann. Stimulated Raman adiabatic passage in physics, chemistry, and beyond. *Reviews of Modern Physics*, 89(1):1–66, 2017. ISSN 15390756. doi: 10.1103/RevModPhys.89.015006. 49, 50, 54, 55, 56, 57, 58, 60
- [80] Nikolay V Vitanov, Thomas Halfmann, Bruce W Shore, and Klaas Bergmann. Laser Induced Population Transfer By Adiabatic Passage Techniques. *Annual Review of Physical Chemistry*, pages 763–809, 2001. doi: doi:10.1146/annurev.physchem.52.1.763. 53
- [81] U. Gaubatz, P. Rudecki, S. Schiemann, and K. Bergmann. Population transfer between molecular vibrational levels by stimulated Raman scattering with partially overlapping laser fields. A new concept and experimental results. *The Journal of Chemical Physics*, 92(9):5363–5376, 1990. ISSN 0021-9606. doi: 10.1063/1.458514. URL <http://arxiv.org/abs/1011.1669><http://dx.doi.org/10.1088/1751-8113/44/8/085201><http://stacks.iop.org/1751-8121/44/i=8/a=085201?key=crossref.abc74c979a75846b3de48a5587bf708f><http://scitation.aip.org/content/aip/journal/jcp/92/9/10.1063/1.458514>. 53, 63

-
- [82] U. Gaubatz, P. Rudecki, M. Becker, S. Schiemann, M. Külz, and K. Bergmann. Population switching between vibrational levels in molecular beams. *Chemical Physics Letters*, 149(5-6):463–468, 1988. ISSN 00092614. doi: 10.1016/0009-2614(88)80364-6. 53
- [83] M.P. Fewell, B.W. Shore, and K. Bergmann. Coherent Population Transfer among Three States : Full algebraic solutions and the relevance of non adiabatic processes to transfer by delayed pulses. *Aust. J. Phys.*, 50, 1997. 56
- [84] J.R. Kuklinski, U. Gaubatz, F.T. Hioe, and K. Bergmann. Adiabatic population transfer in a three-level system driven by delayed laser pulses. *Physical Review A*, 40(11):6–9, 1989. 57
- [85] Z. Li, S. Singh, T. V. Tscherbul, and K. W. Madison. Feshbach resonances in ultracold 85Rb-87Rb and 6Li-87Rb mixtures. pages 1–9, 2008. doi: 10.1103/PhysRevA.78.022710. URL <http://arxiv.org/abs/0807.0417><http://dx.doi.org/10.1103/PhysRevA.78.022710>. 64
- [86] Bhuvanesh Sundar and Erich J. Mueller. Proposal to directly observe the Kondo effect through enhanced photoinduced scattering of cold fermionic and bosonic atoms. *Physical Review A*, 93(2), 2016. ISSN 24699934. doi: 10.1103/PhysRevA.93.023635. 64
- [87] Ian Affleck. Conformal field theory approach to the Kondo effect. *Lecture Notes*, pages 1–46, 1995. URL <http://arxiv.org/abs/cond-mat/9512099>. 64

Acknowledgement

- ★ I would like to thank PROF. JOERG WRACHTRUP and PROF. TILMAN PFAU who are co-examiner/ examiner of this thesis and who enabled me doing the experimental work in Vancouver. They both saw the advantage of such a collaboration between two institutes. Working in a foreign country brings much more challenges than just succeeding in the lab.
- ★ I would like to thank PROF. KIRK W. MADISON who supervised my experimental work at UBC. He taught me not only how to survive in a physics lab, but also about life.
- ★ I would like to thank PROF. JEFF YOUNG who gave me an opportunity to work in his lab at UBC. By that, he supported me in my very first weeks in Vancouver.
- ★ I would like to thank DR. ILJA GERHARDT who supported me in every step of my masters and organized the collaboration with UBC from Germany. Without him, this thesis would not exist.
- ★ I would like to thank PROF. TOBIAS SCHAEZT who gave me the chance to work in his group at the University of Freiburg. Also, he understood that writing a master thesis takes time and therefore he supported me.
- ★ I would like to thank GENE POLOVY who taught me everything about the complex experiment in the lab of Kirk Madison at UBC. Without him, none of the presented measurements could have been done.
- ★ I would like to thank PASCAL WAECKESSER, JULIAN SCHMIDT, MARKUS DEBATIN, ERIK FRIELING and FABIAN RICHTER from the University of Freiburg. They supported me during my stay in Freiburg and also made the environment as comfortable as possible during writing this thesis.
- ★ I would like to thank MARY LUPTON, FAMILY LUPTON and MY FAMILY as well. They supported me till the end of my masters, even from the other side of the world. They also showed me, that a distance doesn't mean to be all by myself.